ON THE GENERATION OF PIPELINE ACOUSTIC RESONANCE

By

© RALPH E. HARRIS, B.Sc., M.Eng.

A Thesis

Submitted to the School of Graduate Studies

in Partial Fulfillment of the Requirements

for the Degree

Doctor of Philosophy

McMaster University

August 1987

ON THE GENERATION OF PIPELINE ACOUSTIC RESONANCE

DOCTOR OF PHILOSOPHY
(Mechanical Engineering)

McMASTER UNIVERSITY
Hamilton, Ontario

TITLE: ON THE GENERATION OF PIPELINE ACOUSTIC RESONANCE

AUTHOR: Ralph E. Harris, B.Sc., M.Eng.

SUPERVISOR: M.A. Dokainish, D.S. Weaver

NUMBER OF PAGES: xiii, 160

ABSTRACT

A flow configuration capable of exciting and interacting with the acoustic plane waves modes of a piping system is examined both experimentally and theoretically. The acoustic source is generated by placing two standard geometry orifice plates in the flow. Strong acoustic pressures exceeding 125 dB inside the pipe are generated with the orifice plate separation distance small (<2%) in comparison to the wavelength of the lowest frequency excited. The acoustic source is shown to excite those modes possessing an acoustic pressure node (acoustic velocity anti-node) at or near the source location. The Strouhal number based on mean orifice velocity and orifice plate separation ranges from 0.5 to 1.0, and is sensitive to cavity diameter. Flow visualization photographs examining the fluid mechanics of the phenomenon are provided. The photographs reveal the presence of an oscillating shear layer near the upstream orifice plate, and subsequent roll up into a large scale vortex and propagation to the downstream orifice plate. The effect of mean turbulence levels at the upstream separation plane on the fluid dynamics and coupled acoustic production is studied.

An acoustic model of the piping system is developed using the 4 pole method. The acoustic model, as well as the modelling procedures, are examined and tested in detail. A theoretical model of the coupled fluid/acoustic oscillator is developed by combining published characteristics of separated inviscid sheared flows with the developed acoustic model. The theoretical model predictions compare favorably, both qualitatively, and quantitatively with the experimental results.

ACKNOWLEDGEMENT

The author would like to thank Dr. M.A. Dokainish for his encouragement, financial, and resource support provided during the course of the research program.

The author is happy to express his appreciation to Dr. D.S. Weaver for the numerous insightful, interesting and lively discussions which arose throughout the course of the research effort, many of them related to the work presented in this thesis. Dr. Weaver's persistent demand for better pictures, more physical insight, and perspective was both painful and beneficial.

Finally, I would like to thank Valerie Harris, friend and wife, for her unending patience and understanding.

TABLE OF CONTENTS

TABLE OF CONTENTS (continued)

LIST OF FIGURES

LIST OF FIGURES (continued)

LIST OF FIGURES (continued)

LIST OF FIGURES (continued)

LIST OF TABLES

NOMENCLATURE

c	Sound speed
c( )	Complex conjugate of ( )
dP, dp	Change in acoustic pressure across source
dU, du	Change in acoustic velocity across source
Do	Orifice diameter
Dp	Pipe diameter
Dc	Cavity diameter
G(f)	Feedback transfer function
I(f)	Acoustic intensity
k	Wave number
Kr	k /(1 + M)
Ki	k/(1 – M)
Lt	Total pipe length
Lc	Cavity separation
M	Mach number
OTF	Open loop transfer function
Pi	Incident (right running) waves
Pr	Reflected (left running) waves
R^2	Correlation coefficient
R(f)	Reflective coefficient
s	Microphone separation
S	Pipe area
Vo	Orifice velocity

NOMENCLATURE (continued)

Vp	Upstream pipe velocity
V_{rms}, $(Ve)_{rms}$	rms velocity fluctuations at exit plane of cavity
V_j	Cavity exit plane jet velocity
V_{em}	Mean exit velocity
x1	Distance from unknown termination to microphone 1
x2	Distance from unknown termination to microphone 2
Z(f)	Impedance
δ	Shear layer characteristic dimension
ρ	Air density
ω	Frequency (rad/sec)
γ^2_{ij}	Ordinary coherence function between (i) and (j)
θ_o	Initial separation angle
ζ	Shear layer displacement

CHAPTER 1

THESIS OUTLINE

1.0 Introduction

Significant problems in the field of flow induced vibrations (FIV) have been examined by industry and academic investigators alike. Traditionally, FIV research was limited to the aeroelastic problem of classical flutter and divergence of aircraft wings. More recently, however, the field has expanded to encompass problems ranging from the vibration of hydraulic gate valves to the strumming and singing of overhead power transmission lines. Unquestionably, the nuclear power industry has provided many interesting and important FIV problems, and has been a major contributor (and beneficiary) of conferences concerned solely with the field of flow induced vibrations [1.1,1.2,1.3].

Coupled fluid/elastic vibration is not restricted to problems involving structural motion. Dynamic fluid pressures, and periodic fluid oscillations can arise through the interaction of the flow with the acoustic field. In low damping situations the coincidence of the acoustic resonating frequency with a structural natural frequency can cause significant structural vibration. Without structural motion, operator annoyance and fatigue may still be a concern if only a small fraction of the available flow dynamic head is converted to acoustic energy.

The work presented in this thesis is part of an on going study investigating the fluid mechanics, acoustic source characteristics, and fluid/acoustic interaction of a flow-excited resonance. A flow geometry is examined both experimentally and theoretically which generates a periodic fluid oscillation inherently coupled with a strong acoustic resonance in a pipeline. Low frequency dynamic pressures can be produced where the characteristic dimension of the flow geometry is much smaller than the wavelength of the frequencies excited. The possibility for low frequency acoustic production makes this phenomenon a potential problem for inducing structural vibration. Included in the goals of the research program, and the work presented in this thesis is the desire to provide further insight into resonators of this type, and lead to the development of design guidelines for resonance avoidance.

1.2 Thesis overview

Figure 1.1 summarizes the areas of work and the organization of the research presented in this thesis. The phenomenon under investigation couples the fluid motion with the pipe line acoustics to generate a strong acoustic resonance. For this reason measurements and theoretical model developments separating the piping acoustic contributions and fluid mechanics are required.

In chapter 2 a literature review of previous experimental and theoretical work examining the generation of sound in ducts and pipes is presented. Aspects of a flow geometry capable of exciting the plane wave modes of a piping system which have not been fully investigated by previous research are identified. The experimental facility designed and built by the author for the work presented in this thesis is described. This facility was designed to allow several fundamental aspects of the flow excited resonance to be examined. These include identification of the basic acoustic source characteristics, as well as examination of the effect of cavity geometry on the frequency/velocity relationship. Also included are the results of a study examining the effect of mean turbulence on the acoustic production, as well as photographs from a flow visualization study identifying the main features of the fluid dynamics.

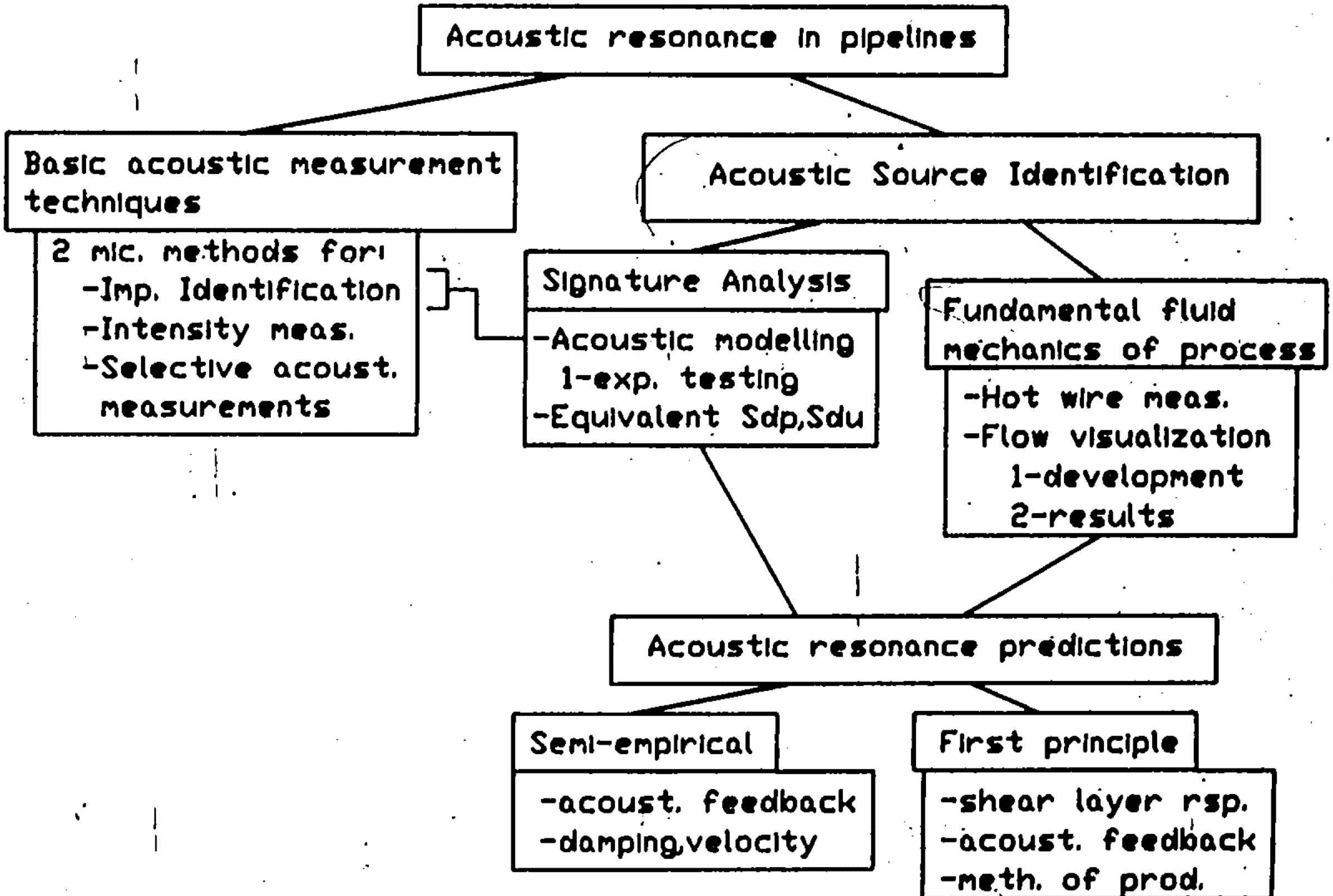

Figure 1.1 : Thesis flow chart identifying major areas of investigation

In chapter 3, fundamental measurement techniques necessary for accurate acoustic modelling of the source environment are examined. A novel measurement technique suitable for source impedance identification is also developed. The feasibility of using a two channel FFT analyser and correspondingly two passes of data acquisition in conjunction with the source impedance identification method is tested in detail.

An acoustic model of the piping system, incorporating model parameters obtained using the techniques presented in chapter 3 is developed in chapter 4. Detailed experimental testing of the model development is made which examines both the modelling approach as well as the required measurements. An acoustic signature analysis is identified and applied to the phenomenon under study.

In chapter 5 the developed acoustic model is utilized to generate a self-excited model of the coupled fluid/acoustic system. The predicted results and general characteristics are compared with the measurements of chapter 2.

Proposals for future work as well as a detailed chapter wise summary of the results and major contributions of the individual areas of study are provided in chapter 6. Also included is a general discussion of the phenomenon under study, as well as conclusions regarding the general applicability of the theoretical model for use in design.

CHAPTER 2

FUNDAMENTAL EXPERIMENTAL MEASUREMENTS

2.0 INTRODUCTION

Significant structural pipeline vibration can be induced by plane wave acoustic resonance inside the pipe as experienced, for example, by Ontario Hydro in the main steam line at their Bruce Nuclear Power Station. The details of this problem were summarized by Hartlên and Jaster at Karlsruhe 1979 [2.1]. The acoustic source, initially forcing a reduction from 791 MW to 625 MW, demonstrated a constant Strouhal number dependency between reactor load (flow velocity) and acoustic frequency. Qualitatively, the acoustic source displayed many of the characteristics typically associated with a cavity type resonance, i.e. a strong periodic fluid oscillation reinforced by a local acoustic resonance. However, the very low frequency generation and interaction with the piping plane wave acoustic modes, combined with the difficulty in identifying both the location of the acoustic source within the main steam pipe line, as well as the appropriate solution (either structural modification or flow modification) demonstrated the need for further study. This chapter presents experimental results of a fundamental study to examine the generation of plane wave acoustic resonance in pipelines. A flow field is generated which interacts strongly with the longitudinal acoustic modes of the piping system. This interaction generates an acoustic source capable of producing very low frequency sound necessary for significant structural excitation of piping loops.

2.1 Selection of acoustic source

The generation of flow induced noise in pipelines (ducting systems) can be broadly categorized as: broad band noise sources which excite (with-out feedback) the plane wave modes, pure tone sources which interact primarily with local or cross modes to produce a lock-in phenomenon, and finally pure tone sources which interact with the longitudinal modes of the piping system and also produce lock-in (signifying strong acoustic feedback). It is primarily the second two categories which display highly organized fluid motions and can generate the significant fluctuating pressures necessary to cause rapid structural failures.

Early experimental results by Parker [2.2,2.3,2.4] illustrated the possible excitation of ducting cross modes by vortex shedding from a flat plate. Cumpsty and Whitehead [2.5] examined the effect of wake length organization by forcing the trailing edge of the plate to vibrate. Archibald [2.6] examined the effect of sound on the vortex production to develop a linear feedback type model to account for the main characteristics of the self excitation. Welsh and Stokes [2.7] have provided clear flow visualization pictures illustrating the convection of large scale vortices from the trailing edge of these type configurations. A successful modelling of the sound production process was achieved in [2.7] which utilized the formulation by Howe [2.8]. Essentially this formulation is based on the rate at which the flow does work on the acoustic field, which is given by:

$$P = -\rho \int [(\omega \times \bar{v}) \cdot u] \, dV \qquad [2.1]$$

where:

P = work rate

ω = vorticity

v = incompressible velocity

u = acoustic particle velocity

ρ = air density

Equation 2.1 implies that no work is done on the acoustic field if the mean convective path of the fluid disturbances are parallel to the acoustic field.

The generation of strong acoustic resonance by flow past cavities is another potential source of noise in ducting systems. Earlier work by Rossiter [2.9] utilized an acoustic feedback model to explain the strong cavity oscillations. Rossiter proposed that the cavity tones were a result of the convection of vortices shed periodically from the upstream lip of the cavity. Upon impingement (interaction) with the downstream edge, acoustic pulses were generated which led in turn to the shedding of new vortices from the upstream lip. A semi-empirical model was proposed which controlled the necessary time of the feedback required for the stable oscillations.

Bilanin and Covert [2.10] improved on the basic approach of Rossiter by relating the instabilities of the free shear layer present in the system to the production of sound. In this model the amplitude of the acoustic disturbances were scaled to the fluctuating mass addition into the cavity. The acoustic characteristics of the cavity beneath the shear layer were modelled in detail, providing the mechanism in which the pressure pulses generated downstream could influence the shear layer at the shear point. A similar approach was used by Elder [2.11] to model the depth mode resonance of flow past a deep cavity. In this instance the shear layer instability equations developed by Michalke [2.12] for an inviscid shear layer were combined with the 1 dimensional impedance characteristics of a closed organ pipe. Again the shear layer was influenced only at the shear point. Measurement of the shear layer motion indicated better correlation of the results near the separation point than near the impingement location.

Tam and Block [2.13] analyzed in detailed the influence of sound on the instability waves of a shear layer in order to predict the relationship between resonant frequencies and velocity over a cavity. In this model a line source was assumed along the downstream edge of the cavity without examining the details in which the sound was produced. Detailed Schlieren photographs by Keller and Escudier [2.14] for a variety of cavity configurations show the control of large scale eddy structures by the wave field within the cavity for high Mach number and high frequency oscillations. Nelson et al [2.15,2.16] examined in detail the flow acoustic interaction for a classical Hemholtz resonator configuration excited by grazing flow by utilizing both flow visualization and laser doppler anemometry. Here the details of the source generation could be examined by calculation of the Reynolds shear stress over the resonator mouth. The photographs clearly show large scale vortices shed periodically from the upstream edge. The vortices were convected to the downstream edge of the cavity at a uniform velocity, at which point the mean speed of the vortices doubled. Significant conclusions regarding the mechanism for energy conversion were made, including the generation of a source/sink pair whose difference accounted for the net flow of acoustic energy to the far field.

Common to all of the described resonant systems and models is the presence of an hydrodynamically unstable shear layer. The characteristics of impinging shear layers has been summarized by Rockwell [2.17]. The sequence of events described by Rockwell necessary for the oscillations to be self-sustained include:

(a) Impingement of organized vorticity fluctuations resulting in an upstream influence,

(b) Conversion of the resulting disturbance to a velocity (and displacement) fluctuation in the vicinity of the separation point,

(c) Initial exponential amplification of this disturbance by the shear layer as it is convected downstream.

(d) Saturation in the growth of the shear layer resulting in a transfer of energy to harmonics of the fundamental frequency.

The generation of an organized shear layer oscillation is not restricted to situations with acoustic reinforced only. In a review paper Rockwell and Naudascher [2.18] summarize the unstable flow past cavities into: fluid dynamic, fluid resonant, and fluid elastic oscillations. The conceptual model for these situation remain the same. A disturbance at the shear point is selectively amplified by the unstable shear layer. The convection and impingement of the larger scale disturbance on the downstream edge in turn effects the upstream shear sensitive point. In the absence of elastic or acoustic vibrations the feed back is solely through incompressible means. The resulting velocity/frequency characteristics of the oscillation will be primarily determined by the shear layer amplification characteristics and the dimensions of the cavity. In the case of fluid elastic oscillations, the impingement of the travelling disturbance excites the local structural environment. The response and corresponding feedback in the form of a relative displacement to the shear sensitive point will be frequency dependent. The frequency dependent response is also present when the environment is excited acoustically. Thus, for fluid resonant and fluid elastic oscillations, the characteristics of the resulting oscillations will depend on the amplification characteristics of the shear layer and the frequency response characteristics of the vibrating system (either acoustic or structural).

The excitation of duct cross modes by vortex shedding, or cavity modes by a shear layer oscillation is generally associated with frequencies much higher than those necessary to interact significantly with the structural modes of a piping system. The generation of lower frequency resonance, where the basic process of the system (shear layer oscillations) interact with the plane wave (longitudinal) modes of the piping system has received considerably less attention in the literature. Rockwell and Schachenmann [2.19,2.20] and Schachenmann and Rockwell [2.21] have experimentally investigated in detail a resonator of this type. The experiments utilized an axisymmetric cavity placed at the end of a pipe. They were able to measure the relative amplitude of the hydrodynamic to acoustic wave amplitude at separation. The clear difference (a factor of 3) in the ratios at resonance was associated with the "Q factor" of each mode. This "Q factor" is, of course a measure of damping related to both the flow and frequency dependent impedance of the system. Other important observations made from the measurements include the clear phase difference of (2 pi n) at resonance between the separation point and the impingement location. As well, the exponential growth predicted using inviscid theory for axisymmetric jets by Plaschko [2.22] is not seen over the entire cavity length. The maximum measured disturbance amplification was in the order of 3. This reduction in expected amplification is attributed to the large disturbances and the associated saturation at the shear point. Although the general process and sequence of events necessary for the sustained oscillation to occur are well understood, the details of the sound production were not investigated in [4.20-4.21].

Nomoto and Culick [4.23] examined the basic characteristic of an acoustic resonator similar to that studied in [4.19-4.21]. The cavity was generated by placing two closely spaced baffles in the duct. However, by placing the resonator inside the duct and not at or near the end of the piping system, they were unable to excite all resonant duct frequencies. A flow visualization study indicated the presence of an integral number of vortices between the baffles. The resulting velocity,cavity separation,frequency data were analyzed by plotting a stability zone diagram.

Clearly Rockwell and Schachenmann [4.19-4.21] and Nomoto and Culick [4.23] were investigating the same basic resonator. However, the results of [4.23] indicate that the shear layer oscillation and roll up is not solely dependent on the damping factor of each acoustic mode. In this chapter, the results of an experimental study investigating further aspects of the resonator examined in [4.19-4.21] and [4.23] are presented. In particular, the experimental program identifies the influence of the piping acoustics, the resonator location within the piping system, and the mean turbulence levels on the fluid mechanics and associated acoustic production of the source.

2.2 Experimental Facility

Figure 2.1 presents a schematic diagram of the rig constructed specifically for this investigation. The entrance bellmouth is designed to reduce entrance flow noise to the rig without significantly altering the open end impedance values in the frequency range studied. The plenum is lined with acoustic foam and is baffled to reduce blower noise transmitted upstream to the test section. Experiments were conducted to measure the acoustic transfer function between microphones located at the blower entrance, and 15 cm upstream of the plenum entrance. Despite modifications to the internal baffle arrangements which reduced transmitted blower noise, peaks in spectrum of the microphone mounted in the test section existed. These peaks were situated at frequencies corresponding to the blade pass frequency of the blower (4 times the rpm) and the first few harmonics. The sound pressure level of these peaks were several orders of magnitude below those produced by the acoustic source. However, in order to eliminate any influence of this sound on the acoustic source under investigation, the experiments were conducted at frequencies far removed from the blower noise. A dissipative muffler was designed and constructed (at the expense of significant pressure drop) which virtually eliminated any blower exhaust noise from entering the test section via the upstream bellmouth. The muffler exhausted outside of the building. This not only removed the smoke particles generated during the flow visualization study, but it also helped to maintain a constant room temperature. The blower itself is a positive displacement multi-vane type blower providing a high suction head,with reduced acoustic pressure pulses. The test section consists of flanged acrylic sections allowing the position of the acoustic source to be moved along the pipe at roughly 1 m intervals. The overall length of the pipe in these

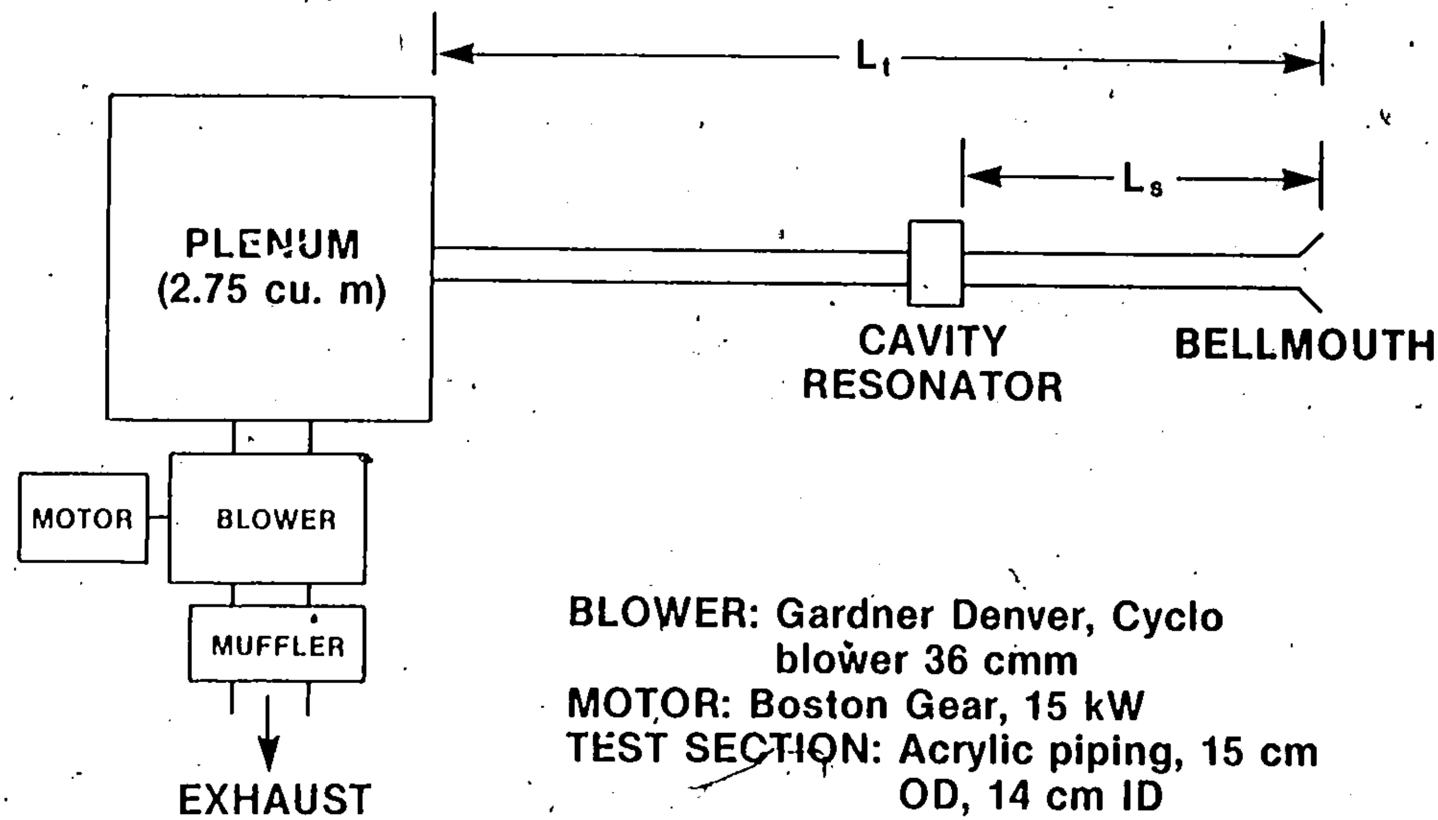

Figure 2.1 : Schematic diagram of experimental facility

experiments was restricted to 9 m. This length effectively separates the blower noise generated at the blade pass frequencies, from the piping acoustic modes excited by the resonator. This clear separation of frequencies removes the need for a more complicated experimental rig or data acquisition procedure necessary to reduce the background noise levels in the acoustic measurements. The flow velocity was measured upstream of the singularity using hotwire anemometry. The acoustic response can be measured at 4 locations in the rig simultaneously using 4 flush mounted B@K 6 mm microphones. Two channels of time domain information can be analyzed on line using a Nicolet 660b FFT analyzer and then down loaded to a VAX 730 for subsequent manipulation. When more than 2 channels of simultaneous information is required, a multi channel A to D board driven by the Vax 730 can be used. A relatively large pipe diameter was chosen for the test section to facilitate detailed velocity measurements across the section, as well as improve the resolution of the flow visualization pictures. Two orifice plates were used to generate the cavity resonator as shown in figure 2.2. Essentially this is the classic "bird call" acoustic source referred to by Rayleigh [2.24].

2.3 Basic Source Characteristics

Figure 2.3 presents a typical plot of measured acoustic frequency versus mean orifice velocity, where the orifice velocity is calculated using the measured upstream centerline velocity and the orifice to pipe area ratio (value 3.93). This experiment was conducted with a total pipe length of 8.04m, cavity length of 4.32 cm, with the upstream orifice located 4.06 m downstream of the entrance bellmouth. Several basic characteristics of the resonator are illustrated in this plot. First, the presence of a very strong lock-on phenomenon is clearly seen, ie., for a wide range of velocities the pure tone generated is centered about a unique frequency. The largest excursion from the frequency of maximum

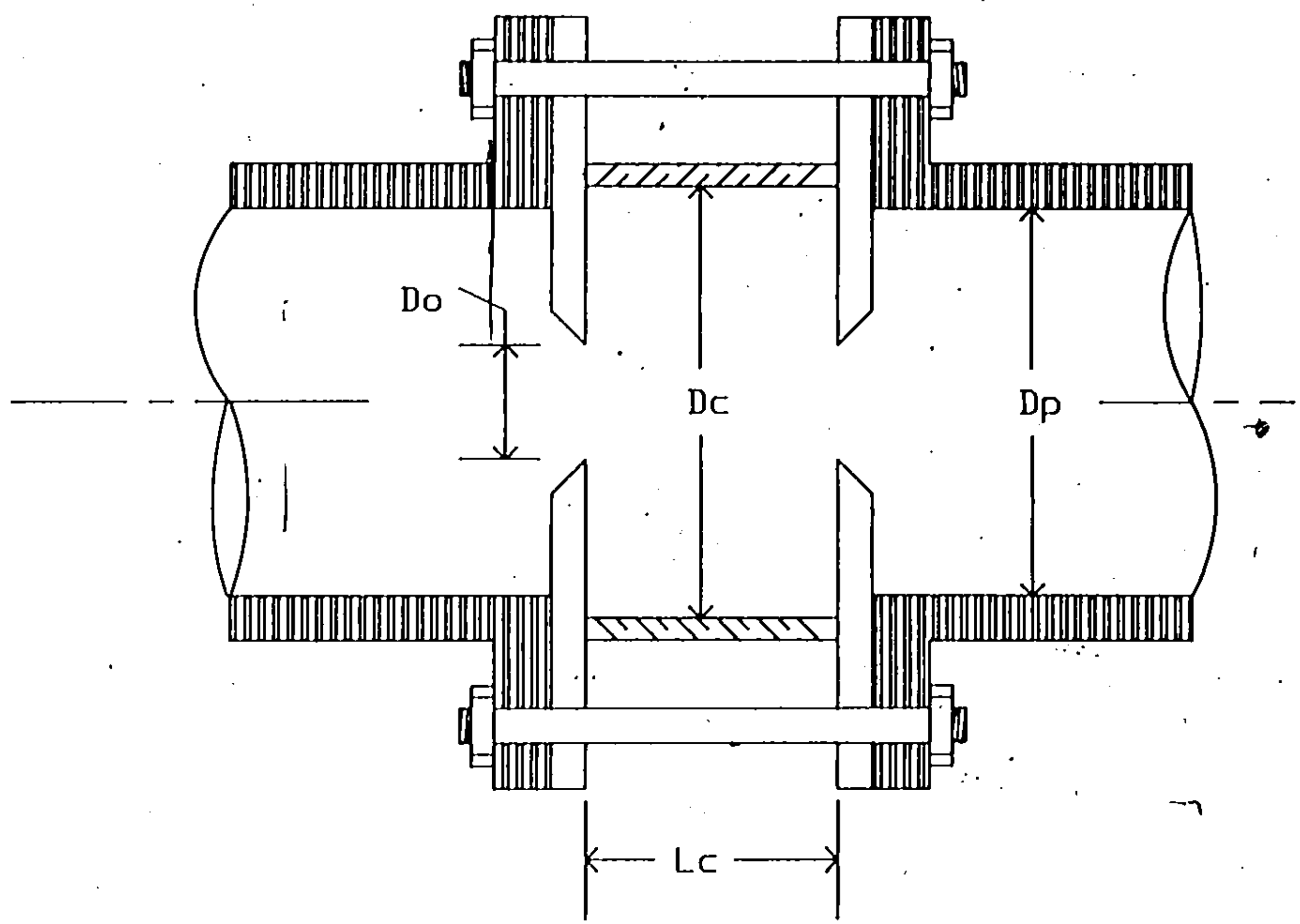

Figure 2.2 : Basic geometry of axisymmetric cavity resonator

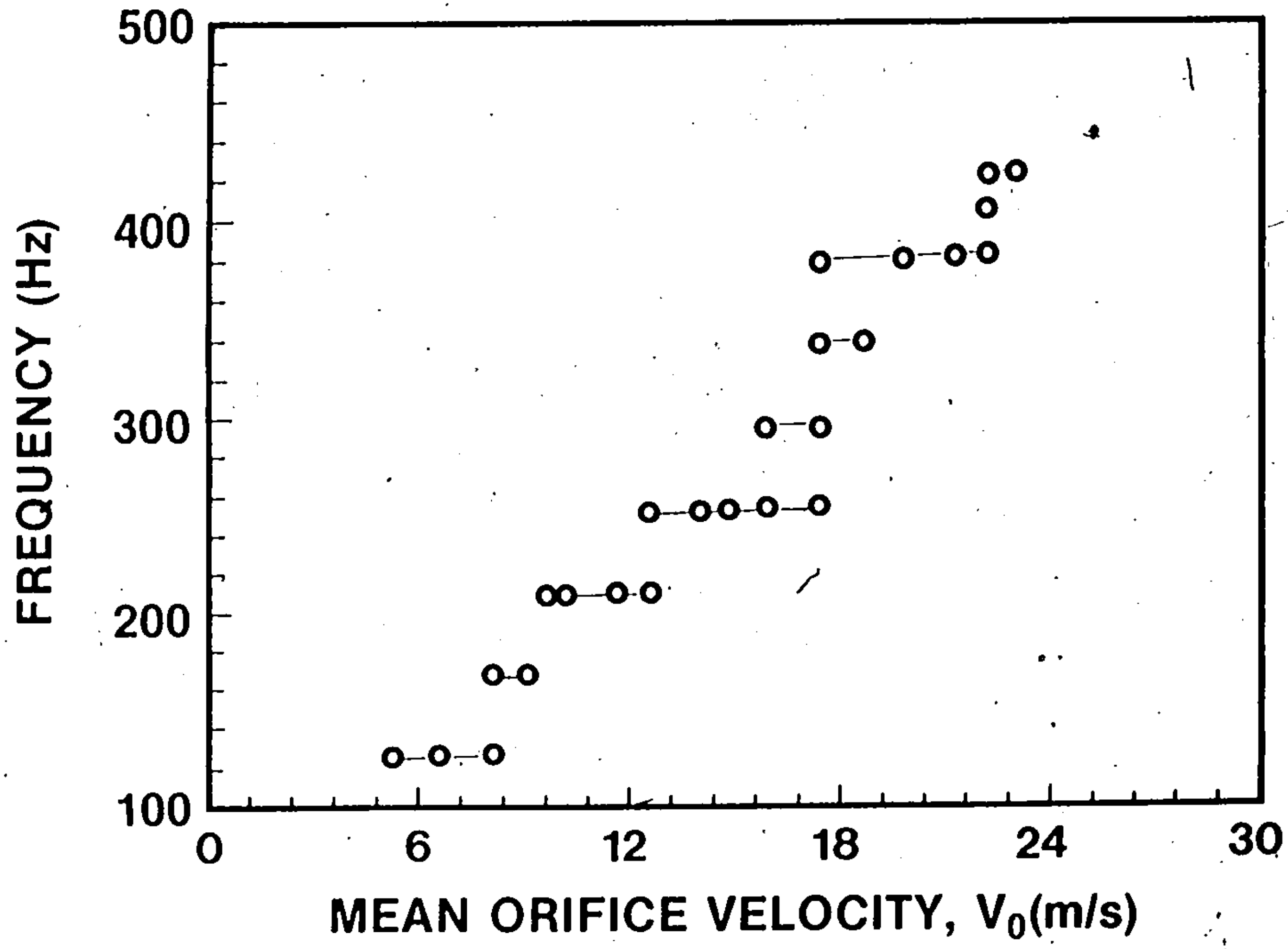

Figure 2.3 : Typical plot of measured acoustic frequency versus mean orifice velocity. (Lt=8.04m, Ls=4.06m, Lc=4.32cm)

output is approximately 2 Hz from the velocity of first occurrence, until the resonator jumps to a different plane wave mode. The possibility of multiple frequency output is also illustrated in this plot. However, this usually occurs at or near the points of frequency jumping where the acoustic output is reduced.

By shifting the singularity throughout the test section it was possible to determine the basic dipole nature of the acoustic source. Figures 2.4 present the frequency velocity plot with the identical cavity geometry located at two other positions in the pipe. Figures 2.5 present plots of the computed acoustic mode shapes corresponding to the resonating frequencies of figures 2.3 and 2.4. The resonant frequencies and corresponding mode shapes were calculated assuming an open pipe of length 8.04 m, and perfect open end boundary conditions. It is clear from examination of the resonating frequencies and location of the double orifice cavity within the rig that the source interacts and excites the modes possessing a pressure node (particle velocity anti-node) at or near the double orifice resonator. For the particular case presented in figure 2.3, positioning the source nominally at the centre of the test section, located it at a pressure node or antinode for all resonant frequencies. Thus, the even valued sequence of resonating modes (6,8,10..) are those preferred by a dipole type source. The deviation from this sequence at frequencies less than 125 Hz, or at 402 Hz (mode 19) will be discussed in chapter 5.

The sound pressure levels measured just outside of the bellmouth entrance (nominally a pressure node at all frequencies) varied from 90 dBA at the lowest sounding frequency of 125 Hz, to 115 dBA at the higher frequencies. The peak RMS sound pressure level measured in the test section, or outside the bellmouth did not necessarily increase with available dynamic head. In figure 2.6 the peak acoustic pressures in each of the sounding modes are plotted against flow velocity. This data is taken from the same experiment which produced figure 2.3. The peak modal pressures are calculated as:

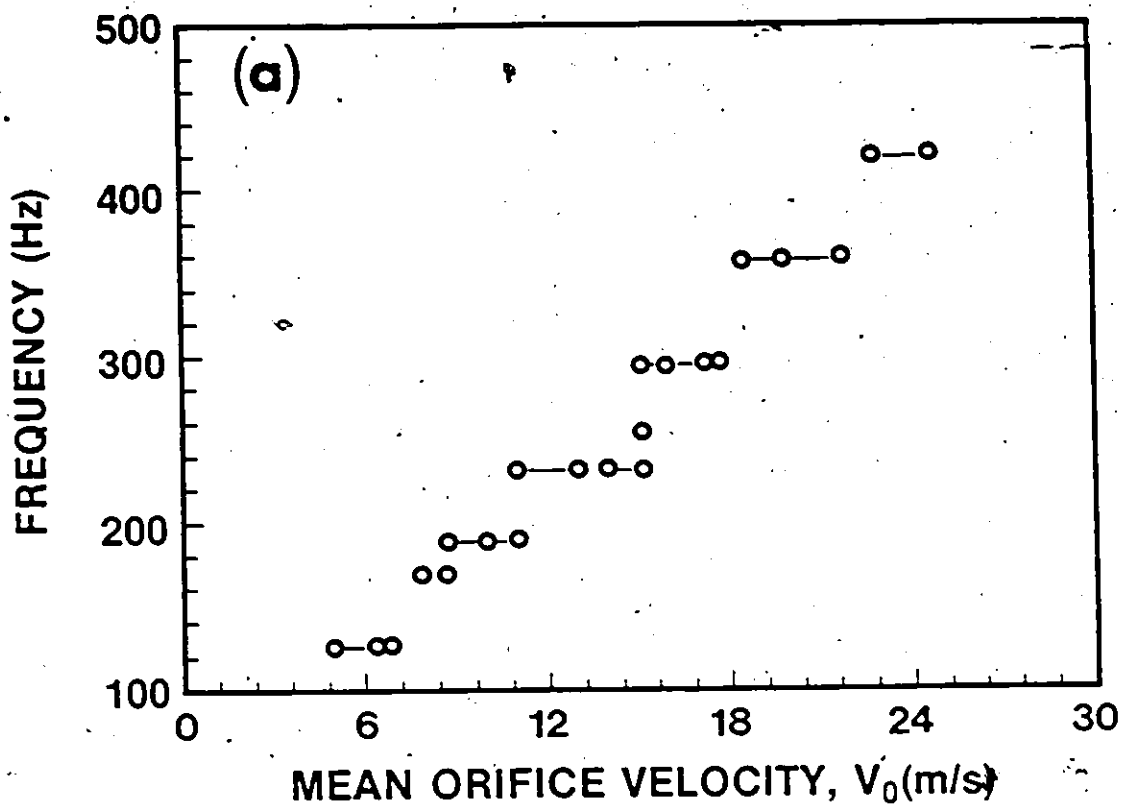

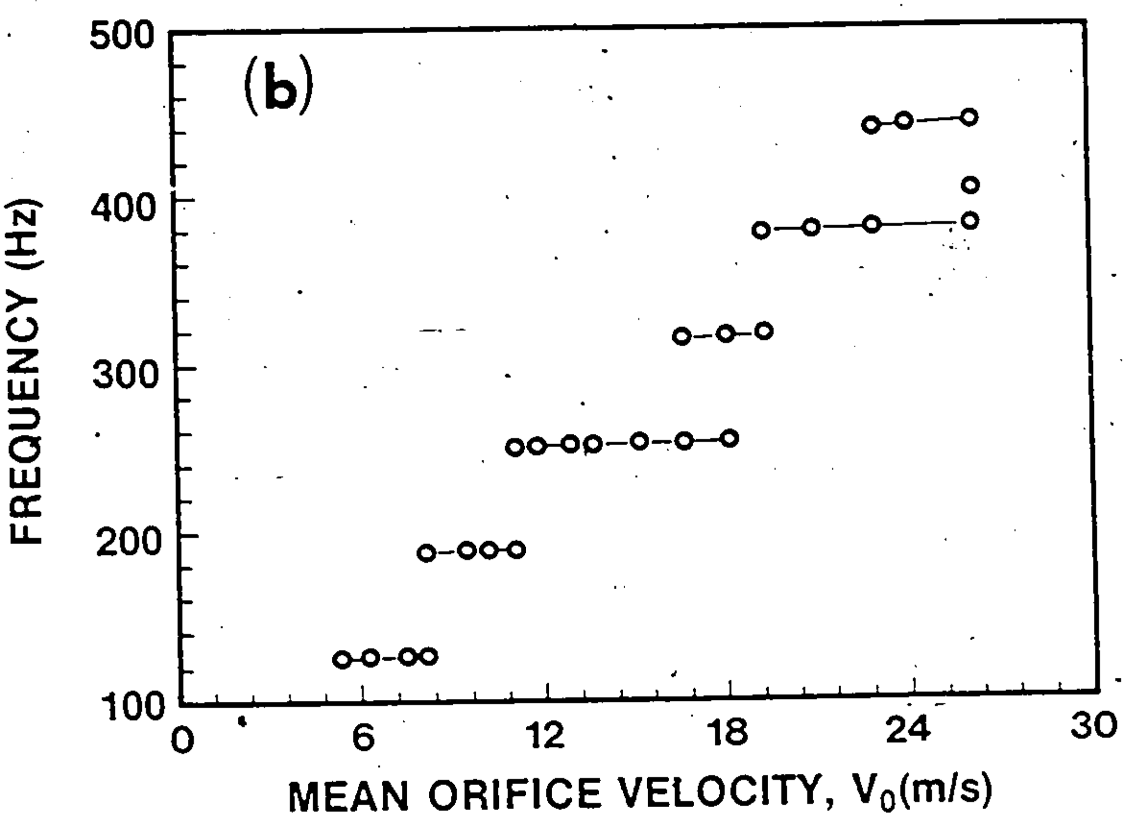

Figure 2.4 : Plot of measured acoustic frequency versus mean orifice velocity. (a: Lt=8.04m, Ls=2.78m, Lc=4.32cm),(b: Lt=8.04m, Ls=5.33m, Lc=4.32cm)

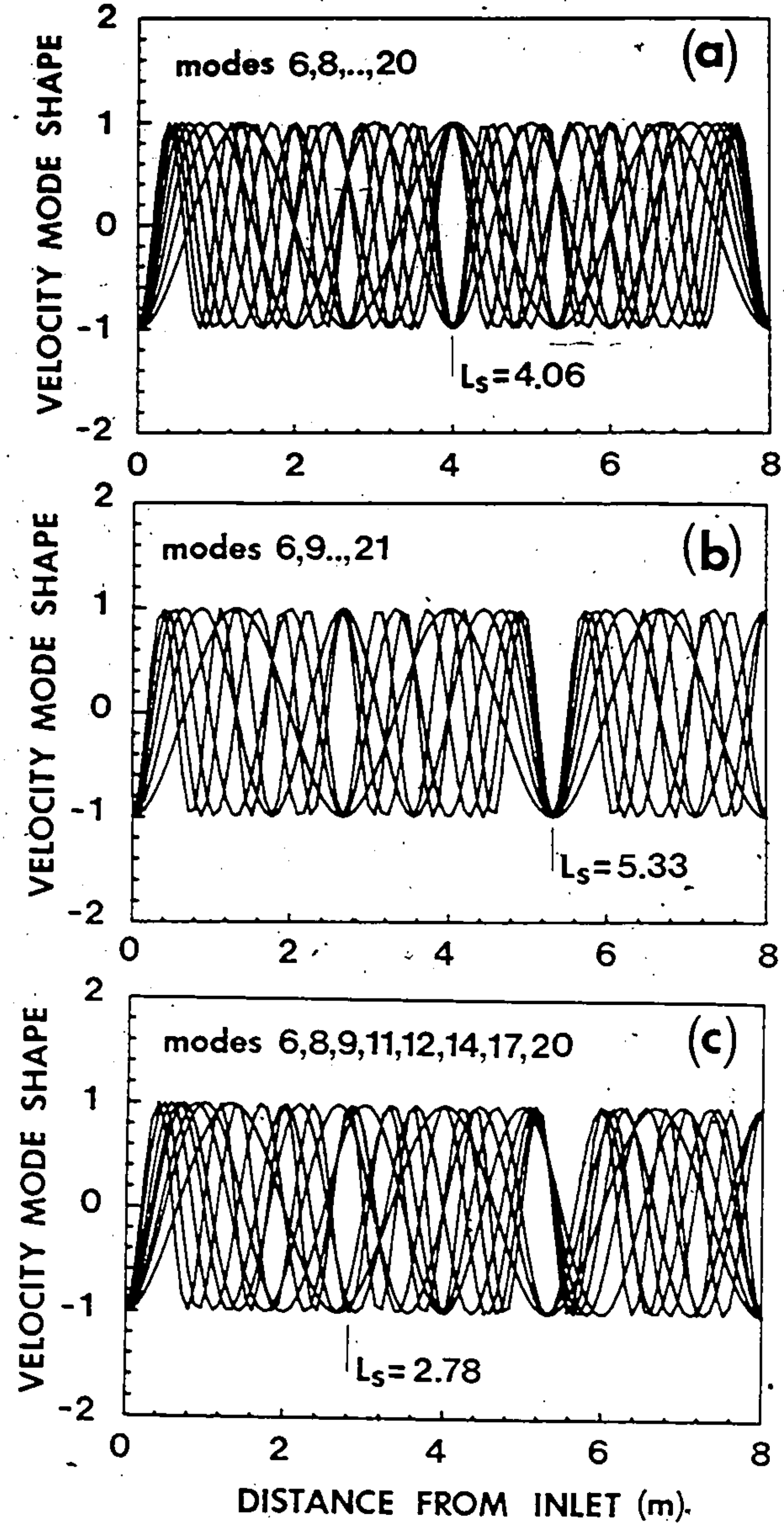

Figure 2.5 : Acoustic particle velocity mode shape for resonating modes. (a:Lt=8.04m, Ls=4.06m), (b:Lt=8.04m, Ls=5.33m), (c:Lt=8.04m, Ls=2.78m)

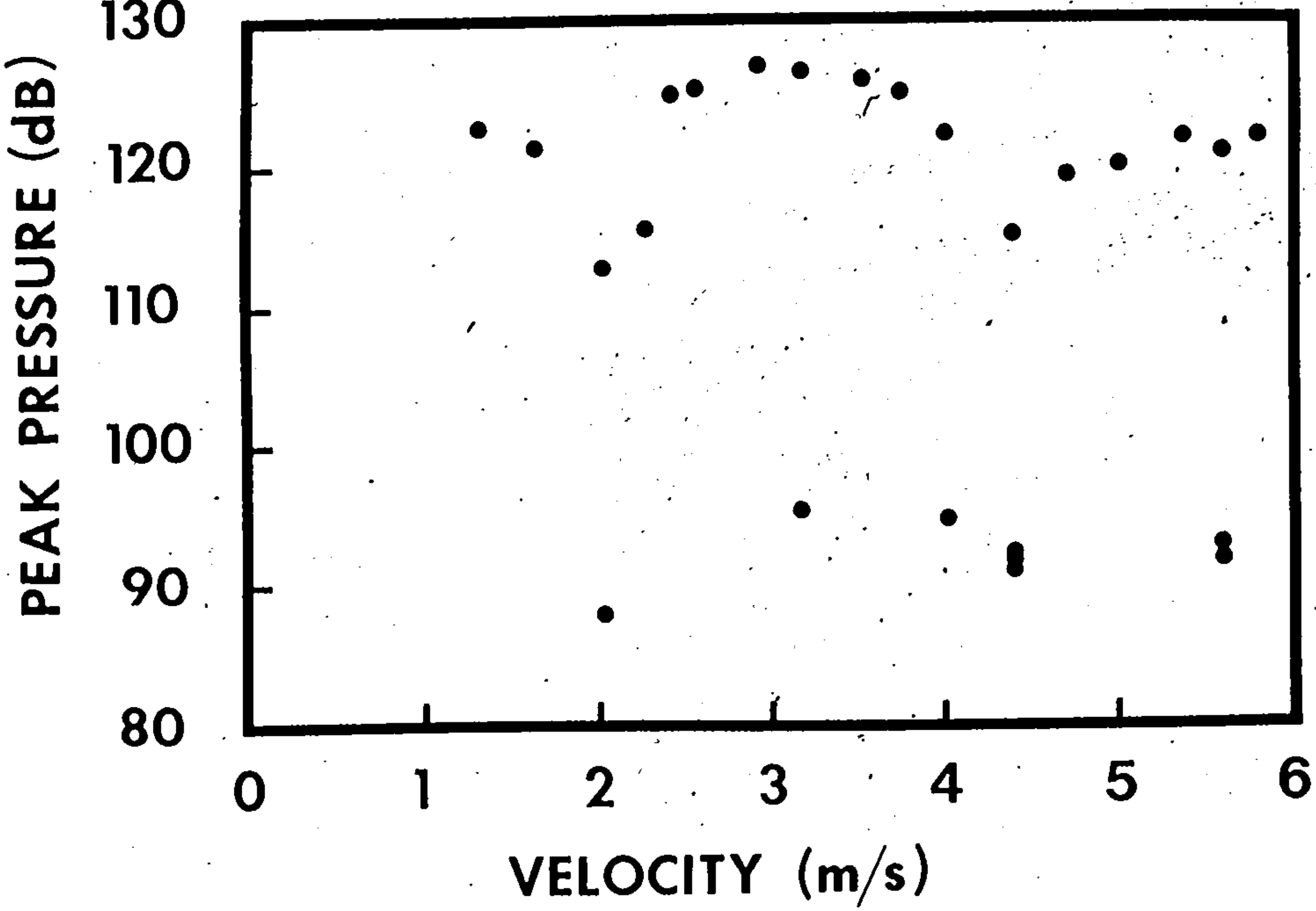

Figure 2.6 : Calculated peak modal acoustic pressure versus upstream velocity. (Lt=8.04m, Ls=4.06m, Lc=4.32cm, Lm=1.04m)

$$P_p = \frac{P_m}{\sin\left(n * pi * \frac{X_m}{l_t}\right)} \qquad [2.2]$$

where:

P_p = peak modal pressure

P_m = acoustic pressure at mic. location

n = mode number

X_m = microphone location (1.04m from bellmouth)

l_t = total pipe length (8.04m)

The values lying below 95dB occur at the velocities where multiple tones are produced. For this particular case the peak modal pressures occur at 210 Hz and not at the highest frequency of 420 Hz excited in the test.

In figure 2.7 the frequency of maximum acoustic output times the cavity separation is plotted against mean orifice velocity. This data was obtained by varying Lc from 4 cm to 9 cm. In earlier models of cavity resonance [2.10] the slope of this line represents the ratio of free stream velocity to the velocity at which the fluid disturbance propagates downstream. A best fit line through this data does not pass through zero (this slope would represent a Strouhal number) since a dependance of Strouhal number on Mach number clearly exists. If the data for any individual cavity separation is plotted, the scatter about the straight line is virtually eliminated. Thus the scatter seen in the data of figure 2.7 about the best fit line represents a variation in the slope from 0.67 (R^2 = 0.998) to 0.77 (R^2 = 0.999). The Strouhal number based on the mean orifice velocity and the cavity separation varies from approximately 1.0 at the lower flow velocities to 0.8 at the upper ranges of the velocities tested. The absence of a flow conditioner immediately upstream of the resonator, and the corresponding variation in velocity profile, and angle of separation with mean flow will contribute to some of the variation in Strouhal number.

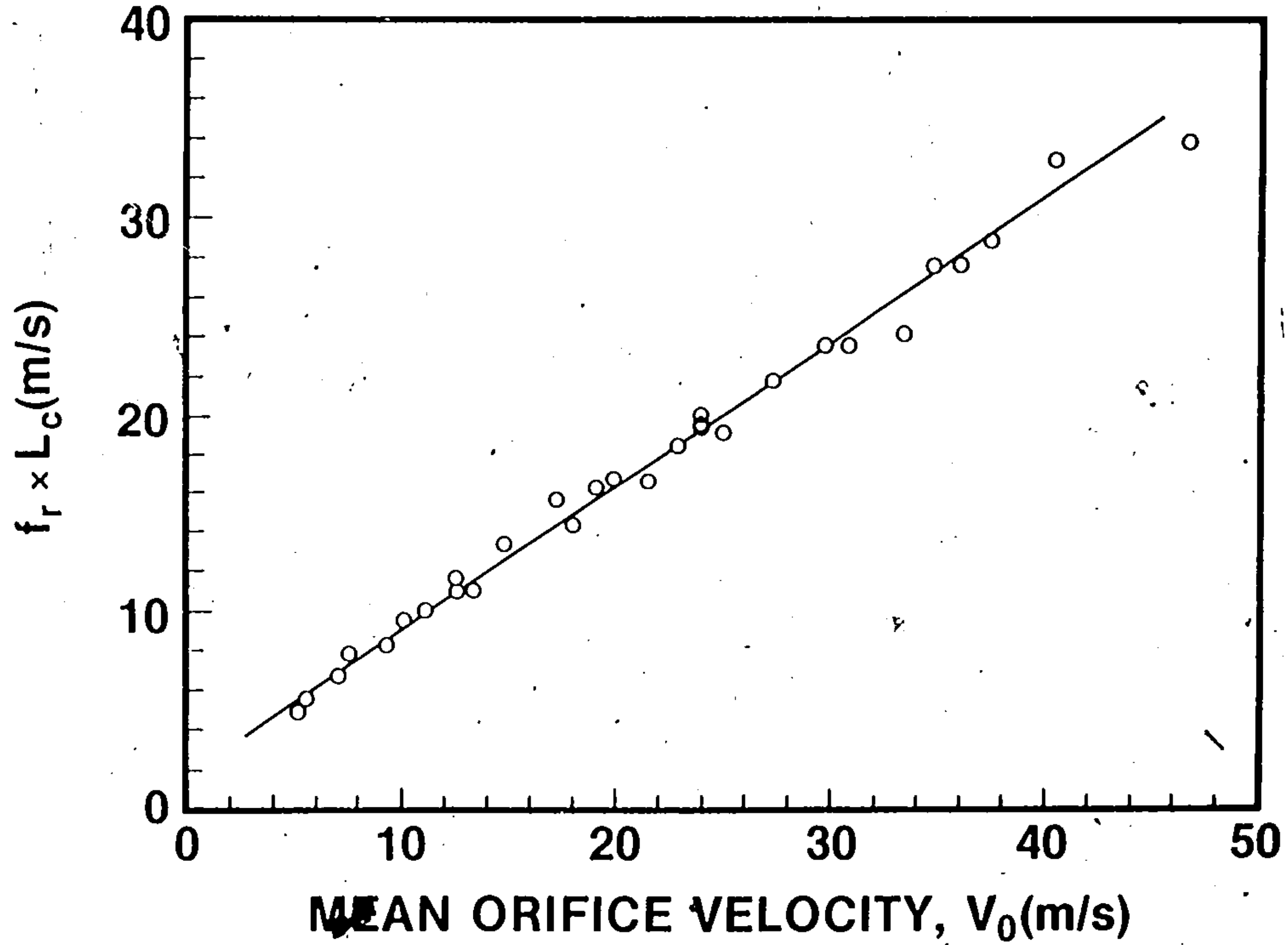

Figure 2.7 : Frequency of maximum acoustic output times cavity separation versus mean orifice velocity.
(43mm <= Lc <= 87mm, Ls=5.33m, Lt=8.04m)

If periodic components (ie vortex shedding) exist in the flow in the absence of any elastic (either structural or acoustic) response, the calculation of a Strouhal number from the frequency/velocity data taken at resonance will usually cause an under estimation of the value necessary to predict the onset of the resonance. In the case of vortex shedding from bluff bodies, the coincidence of the vortex shedding frequency with the elastic resonant frequency can cause sufficient structural motion to completely control the fluid mechanics. It is known that the ability of a shear layer (which is the initial stage of a large scale vorticity development) to amplify disturbances is significantly reduced if the amplitude of the disturbance at the separation point approaches or exceeds the fundamental dimension (thickness) of the shear layer. If a significant displacement at the separation point exists resulting from large amplitude motion, then saturation in the resulting displacement itself will occur. It is this saturation in the response of the elastic system arising from the saturation in the shear layer amplification characteristics which can cause the under estimation in the Strouhal number evaluated using the velocity and frequency at maximum amplitude. In the case of the acoustic resonance under study, the scale of the acoustic fluid particle displacements at the separation point during maximum acoustic output are significantly smaller than what is easily measured if the response is in the form of a structural vibration. This allows dynamic response measurements to be made well before complete saturation in the shear layer and resulting acoustic response occurs. In figure 2.8, the frequency and velocity data at first occurrence of any measured acoustic output, rather than at peak acoustic output are used in the identical fashion as figure 2.6. While data taken at resonance in structural motion environments may be suspect, the use of first occurance data for the acoustic phenonenon is clearly not correct.

A series of experiments were conducted to examine the effect of cavity diameter on the resonator characteristics. Figure 2.9 presents a summary of this data. The mode selection

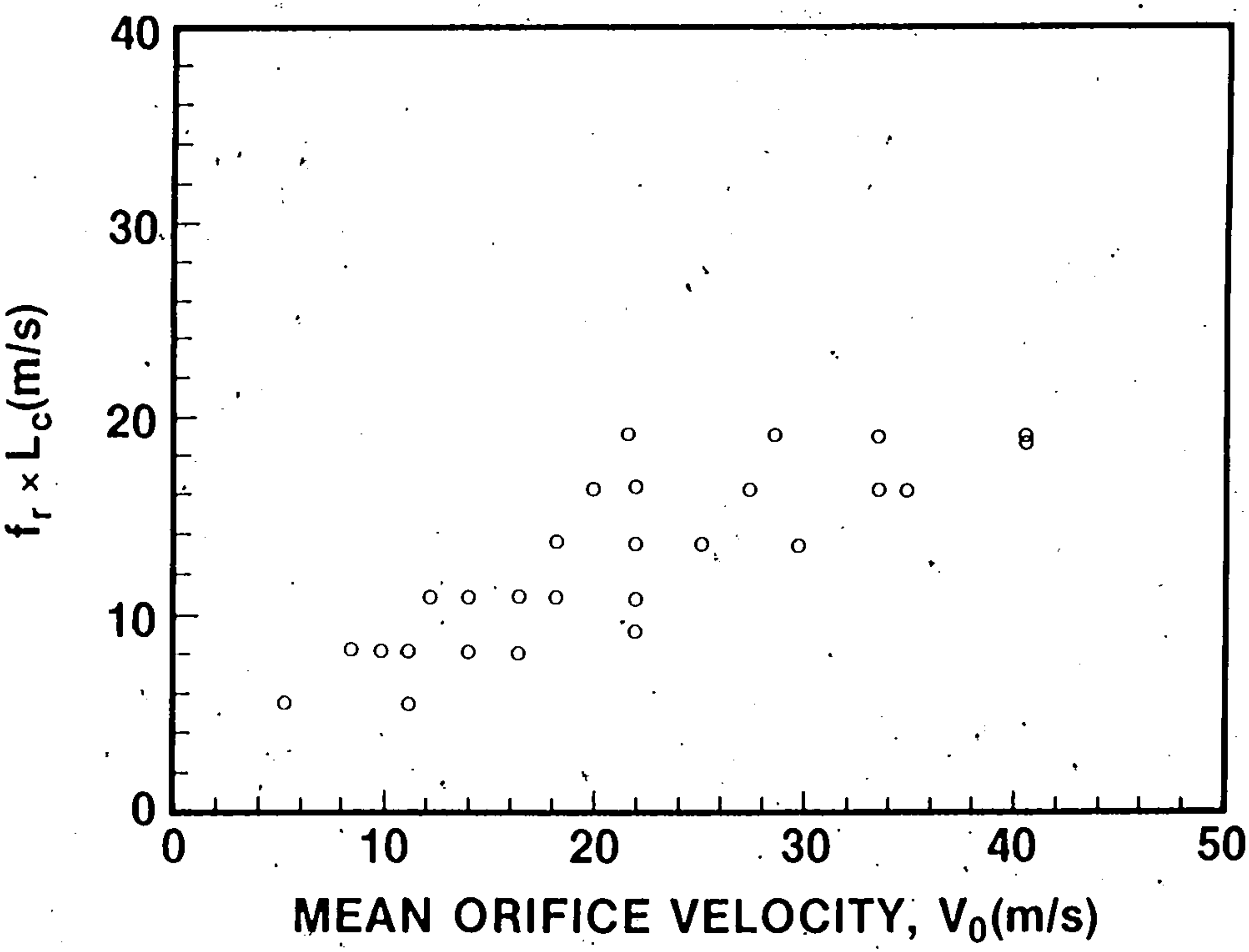

Figure 2.8 : Frequency at first occurance times cavity separation versus mean orifice velocity. (43mm <= Lc <= 87mm, Ls=5.3m, Lt=8.04m)

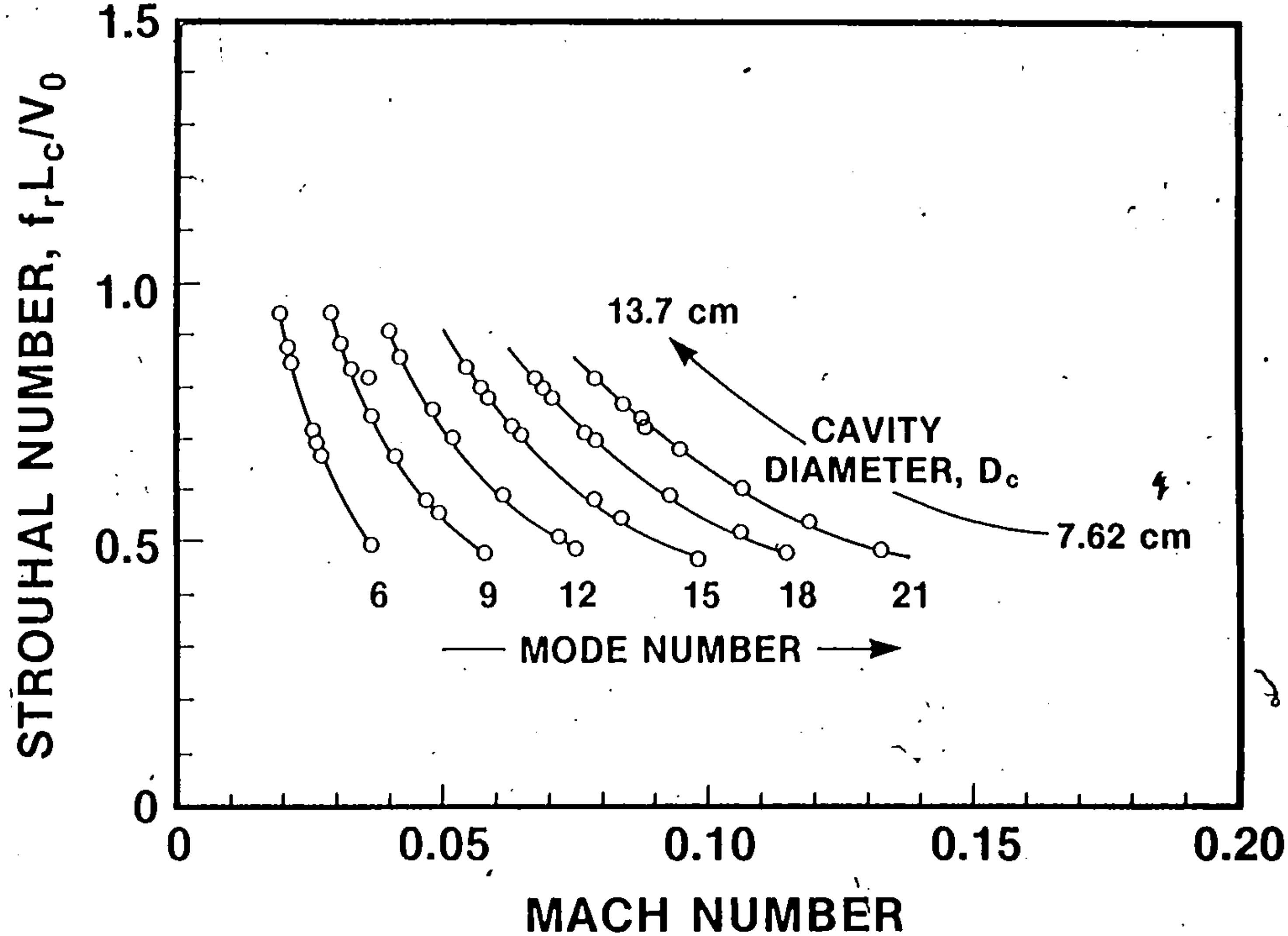

Figure 2.9 : Strouhal number versus Mach number. ($Lt=8.04m$, $Ls=5.33m$, $Lc=4.9m$)

was again determined by the apparent dipole nature of the source and the corresponding position of the resonator in the acoustic mode shape. If the frequency of maximum acoustic output times cavity separation is plotted against mean orifice velocity for any particular cavity diameter, the data lies on a straight line with virtually no scatter. For the largest diameter case (Dc = 13.72 cm) the data is described by the equation:

$$Fr^{*}Lc\,(m/s) = 0.75^{*}Vo + 1.66$$

$$R^2 = 0.998$$

For the smallest diameter tested (Dc = 7.62cm) the data is fit with:

$$Fr^{*}Lc\,(m/s) = 0.48^{*}Vo + 0.0758$$

$$R^2 = 0.999$$

Figure 2.10 summarizes the change in slope versus cavity diameter. Also included is a data point obtained from the series of experiments investigating the effect of cavity length. It is clear that there is a decrease in the sensitivity of the slope with increasing cavity diameter.

A transition from plane wave resonance to transverse, local cavity resonance will occur at higher flow velocities. The details of this transition have not been investigated. However, the theoretical linear decrease in cut-on frequency with increasing cavity diameter provides a mechanism in which the local acoustic environment of the cavity can influence the shear layer. To investigate this further, all of the Strouhal data (acquired by varying cavity separation or cavity diameter) were plotted against a non-dimensional cavity diameter. This is presented in figure 2.11. To reduce the number of points on this graph, only the maximum, minimum, and mean Strouhal values for a particular Dc/Do were plotted. Presented in this fashion, the dependency of number on cavity diameters clearly decreases with the increase in cavity diameter. At the lowest ratio tested there appears to be a unique Strouhal number, while at the larger cavity diameters the spread in the data indicates that a different

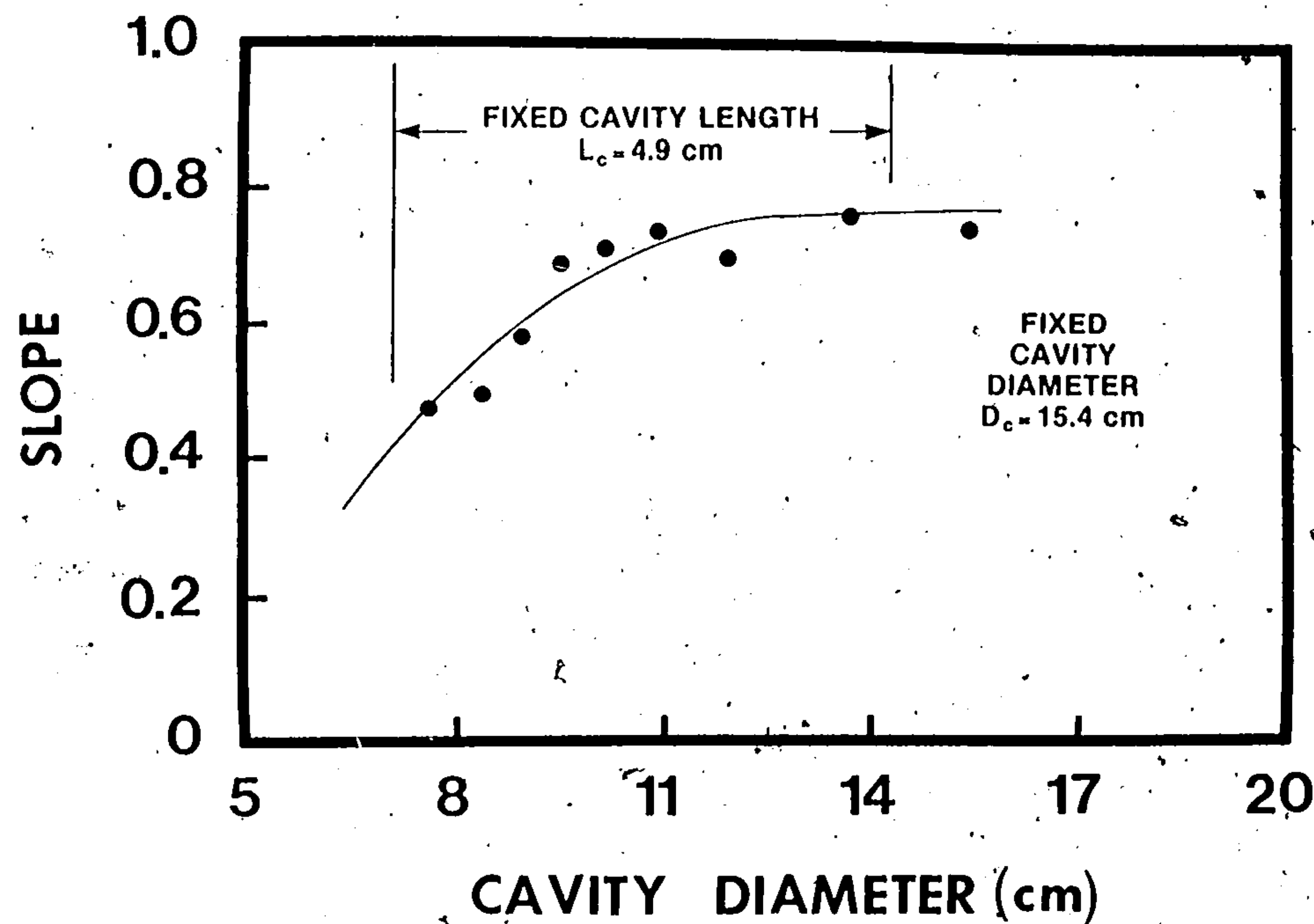

Figure 2.10 : Slope of (Fr*Lc versus Vo) versus cavity diameter. (Lt=8.04m)

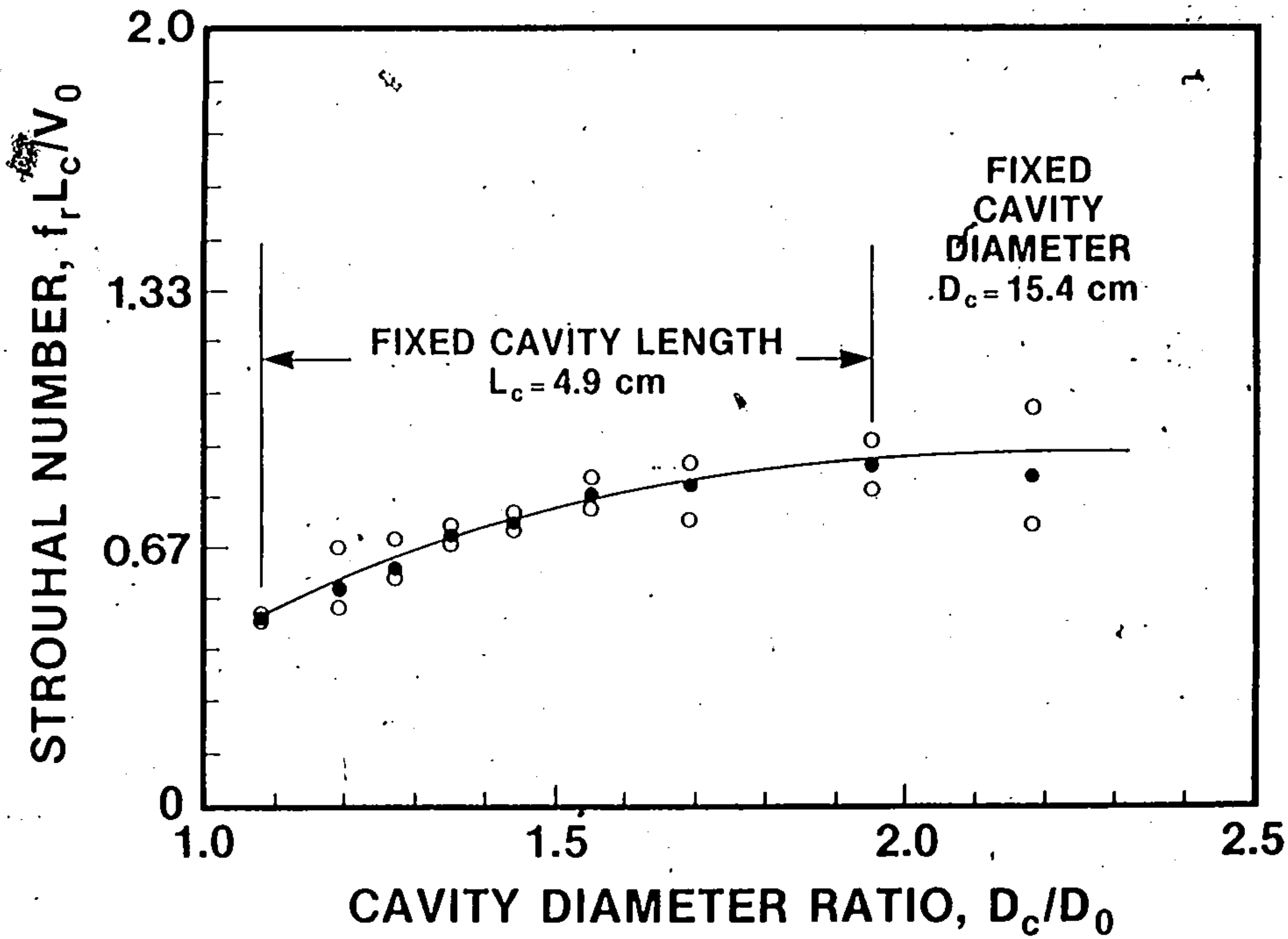

Figure 2.11 : Strouhal number versus non-dimensional cavity diameter (Lt=8.04m)

parameter is influencing the results. It is expected that the effect of cavity diameter on the acoustic plane wave resonance is primarily a fluid mechanic effect altering the growth and propagation of the shear layer. It is important to note that at the smallest value of Dc/Do tested (1.1) the resonator maintains a high acoustic output (>110 dBa) as measured just outside the bellmouth.

2.4 Flow Visualization Results

A flow visualization study was performed to examine in more detail the basic flow characteristics of the acoustic source. A square cavity was mounted between the two orifice plates to reduced the scattering of light at the plexiglass interface. This modified slightly the performance characteristics of the source, but did not alter the basic phenomenon. The "smoke" was generated by mixing Ammonia gas and Sulphur dioxide in an exothermic reaction to produce inert solid white Ammonium Sulphate particles [2.25]. The two gases must be introduced separately into the flow just upstream of the cavity. If the mixing is done externally and injected into the flow the solid particles will quickly block the injection probe. The correct proportions were best achieved by first introducing the Sulphur dioxide into the flow, and then adjusting the Ammonia gas until the smoke is a pure white (and a maximum of generation) or until the presence of each gas cannot be detected. Both gases are easily detected before the concentrations are sufficient to cause a problem. The Ammonia gas has a very strong and unique odour at 5 ppm. The Sulphur dioxide which is odourless is first detected as an irritation at the back of the throat resulting from the formation of Sulphuric acid (acid rain!). For long term storage and usage, the pressure regulators should be stainless steel since both gases are corrosive with brass.

A strobe technique similar to that used in [2.15] was developed. The strobe was triggered by the zero crossing of the acoustic pressure (from positive to negative) measured downstream of the cavity. It was not possible to trigger the circuit using the fluctuating pressure at the cavity location since the source is located in the vicinity of a plane wave pressure node. A phase delay circuit was developed and placed between the microphone output and the strobe trigger signal. This allowed control of the capture point in the acoustic cycle. The primary advantage of this flow visualization approach over high speed photography is the ability to freeze high frequency oscillations in a low light level environment. As well, the capture point in the acoustic cycle is known and maintained independent of any slight variation in the oscillation. From the experimentalist's perspective, any change in the fluid motion resulting from a change in the apparatus can be seen immediately, without the need for film development. Figure 2.12 illustrates the relationship between the locations of the microphone, cavity resonator and the acoustic pressure and particle velocity mode shapes. The acoustic mode shapes are estimated assuming open end boundary conditions for a pipe length Lt = 9.2 m. From examination of figure 2.12 the relationship between the phase angle of the trigger signal (with respect to the zero crossing) and the acoustic velocity at the cavity location can be determined. Table 2.1 summarizes the extreme values:

Time	P (mic)	Vel (cavity)
0	0	0
0 + .25t	-P max	+ V max
0 + 0.5t	0	0
0 + 0.75t	+ P max	- V max

t = 1/(181 Hz)

Table 2.1: Relationship between strobe trigger and acoustic velocity at cavity location

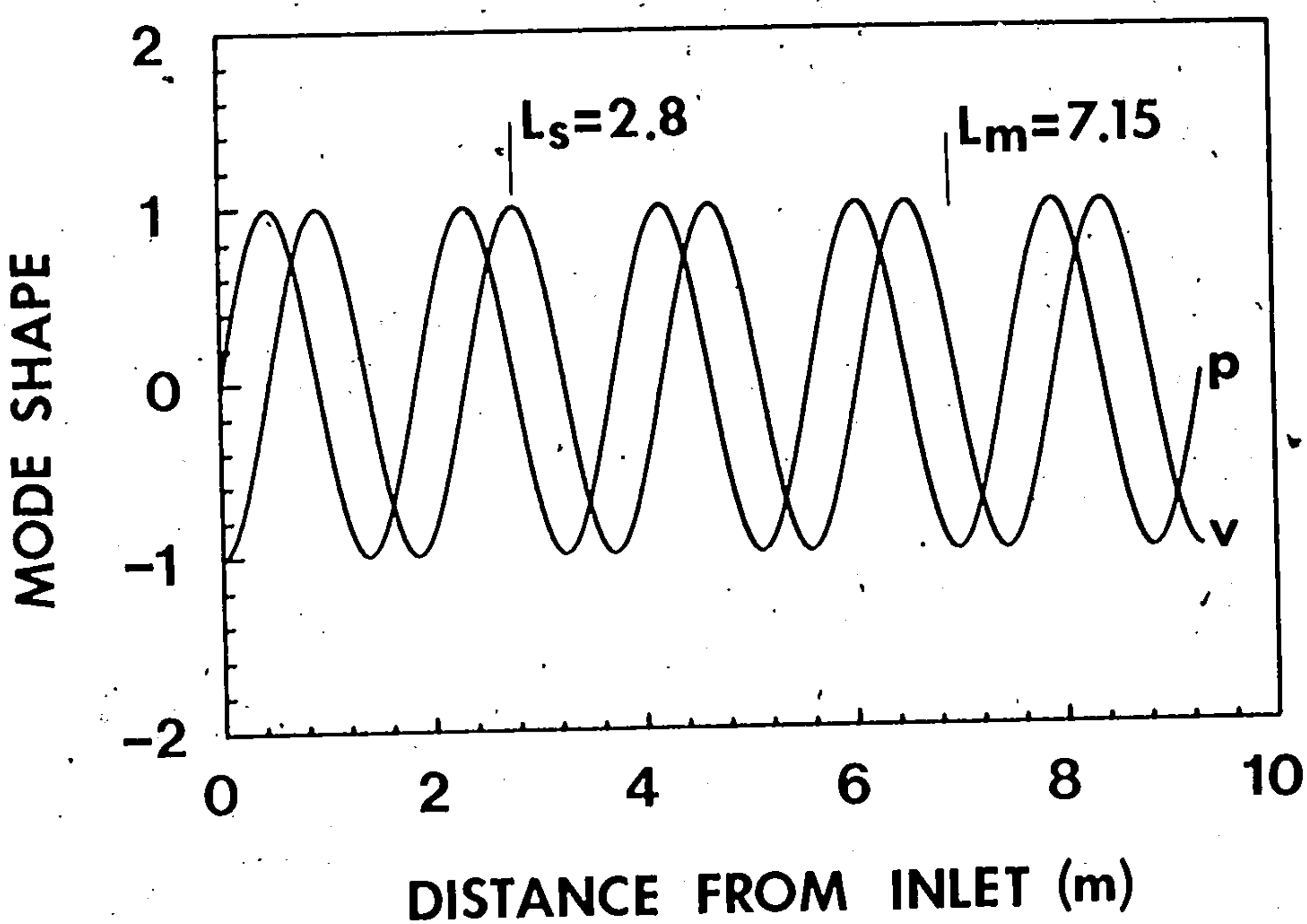

Figure 2.12 : Acoustic pressure and particle velocity mode shape. (Ls= location of cavity, Lm location of trigger microphone)

The "smoke" was illuminated using a sheet of light, essentially producing a 2 dimensional image of the torispherical shear layer. The photographs were taken using long exposures (0.5-2 sec) with ASA 400 speed film and a standard 35mm SLR camera. Figures 2.13 present a sequence of still pictures describing the fluid motions in the cavity. Figure 2.13b is taken within 0.06t of the point of maximum acoustic velocity in the cycle. This coincides with the minimum radial position of the fluid particle path at the downstream orifice plate. The roll up of the shear layer into an unseparated vortex is clear at a point about 1/2 the distance to the downstream orifice plate. The shear layer appears to be "cut" as the shear wave passes the lip of the downstream orifice plate. This generates initially an organized vortex within the volume bounded by the cavity and the shear layer. Although not evident in the still pictures but visible during the experimental study is the entrainment of fluid from the downstream pipe section up into the cavity, moving against the mean flow. This fluid passes very close (< 1 mm) to the lip of the downstream orifice plate. This reverse flow up into the cavity coincides with the separated vortex formation. The pressure gradient associated with the circular flow in the discrete vortex would be a possible driving force for this fluid. Examination of the cavity indicates significant Ammonium Sulphate deposits on the face of the downstream orifice plate as well as on the top surface of the test section, covering approximately 1/2 the distance to the upstream orifice plate. As the shear wave moves down towards the pipe centerline and reaches the minimum radial position, the flow visualization pictures indicate that the organized vortex has been destroyed and leaves the volume bounded by the cavity walls and the shear layer. The lower extension of the shear layer is seen to lie roughly half way between the pipe centerline and the downstream orifice lip.

Figure 2.14 presents the rms velocity fluctuation profiles across 3 locations in the cavity resonator. The first profile was measured 1 mm behind the downstream face of the

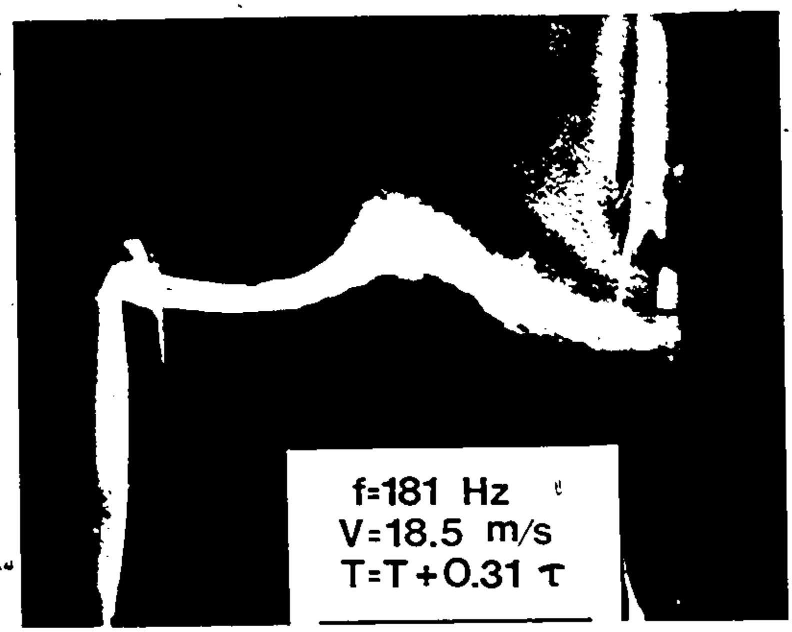

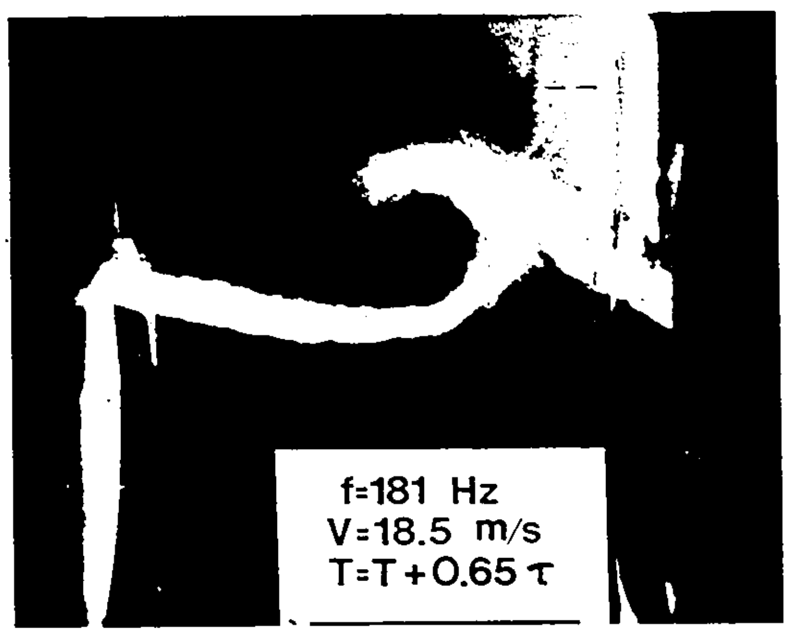

Figure 2.13 : Sequence of flow visualization photographs

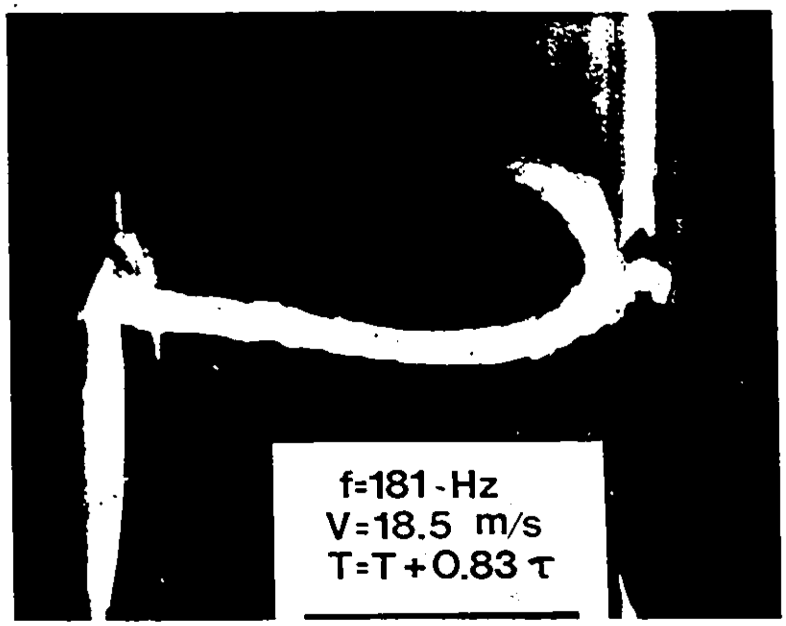

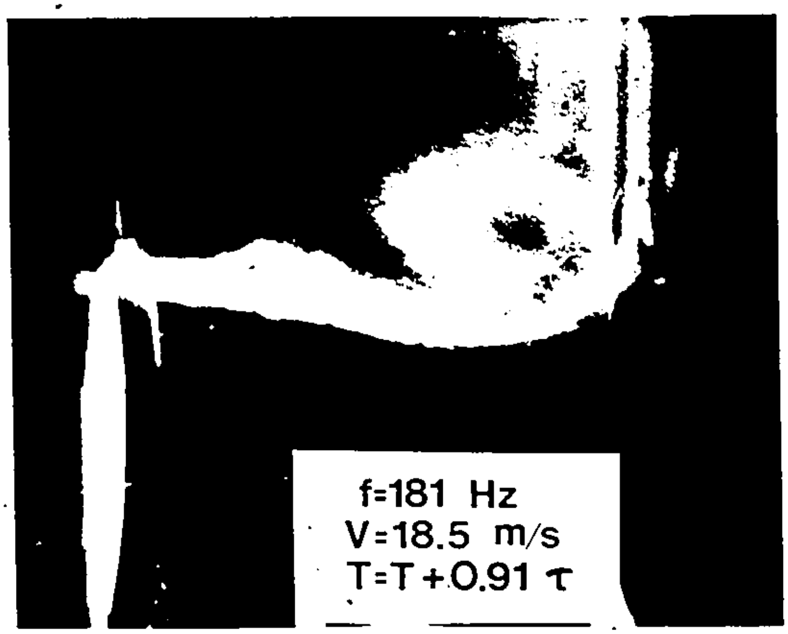

Figure 2.13 : Continued

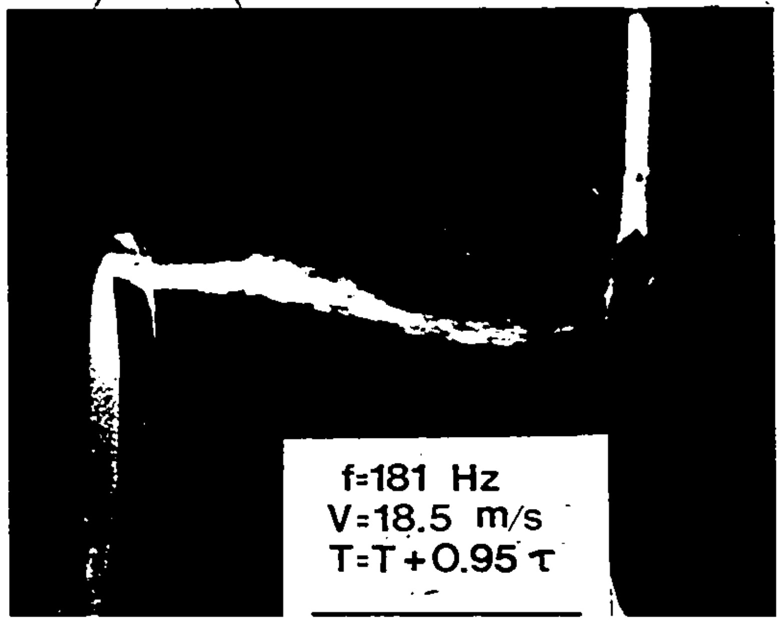

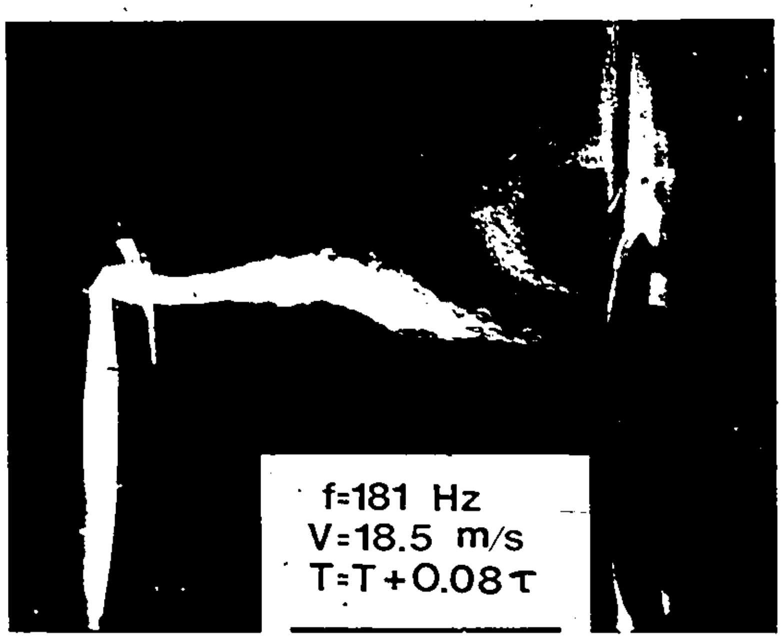

Figure 2.13 : Continued

upstream orifice plate. Velocity profiles were also measured across the plane of the upstream face of the downstream orifice plate, and 1 cm behind the downstream face of the downstream orifice plate. Utilizing hotwire anemometry, the rms velocity fluctuations are calculated using:

$$\text{Vel rms (m/s)} = 2^*\text{Vdc}^*\text{Vrms}^*\text{vel}/[\,n^*\text{Vdc}-A^2) \qquad [2.3]$$

where: Vdc = dc voltage on hotwire

Vrms = peak value in hotwire rms spectrum at 125 Hz.

vel = mean velocity (m/s)

(A) and (n) are constants in the hotwire calibration equation given by:

$$\text{Vdc}^2 = A + B * \text{vel}^n$$

A copy of the calibration data and least squares fit is provided in Appendix I.

The hotwire was orientated such that it measured the total velocity fluctuations (sum of axial and radial). However, it is clear from the flow visualization pictures that the velocity fluctuations measured near the centerline are axial.

The velocity profile measured across the upstream orifice plate indicates strong axial velocity fluctuations at the centerline of the pipe. The crossing of the radially oscillating shear layer is seen as the sharp increase in the rms fluctuations near the orifice lip. The location of this peak at a radius less than the orifice radius indicates the contracting nature of the flow, resulting from the absence of any flow conditioners immediately upstream of the upstream orifice plate. The velocity profile at the downstream orifice plate indicates a centerline velocity amplification of 2.1 through the cavity. This corresponds well to the values measured in [2.19-2.20]. The minimum total velocity fluctuations at the downstream orifice plane occur at d/Do of 0.96. There is a rapid increase in the rms velocity from this location to the measurement point closest to the lip of the downstream orifice plate. This apparent discontinuity may be associated with the flow reversal passing close the lip of the

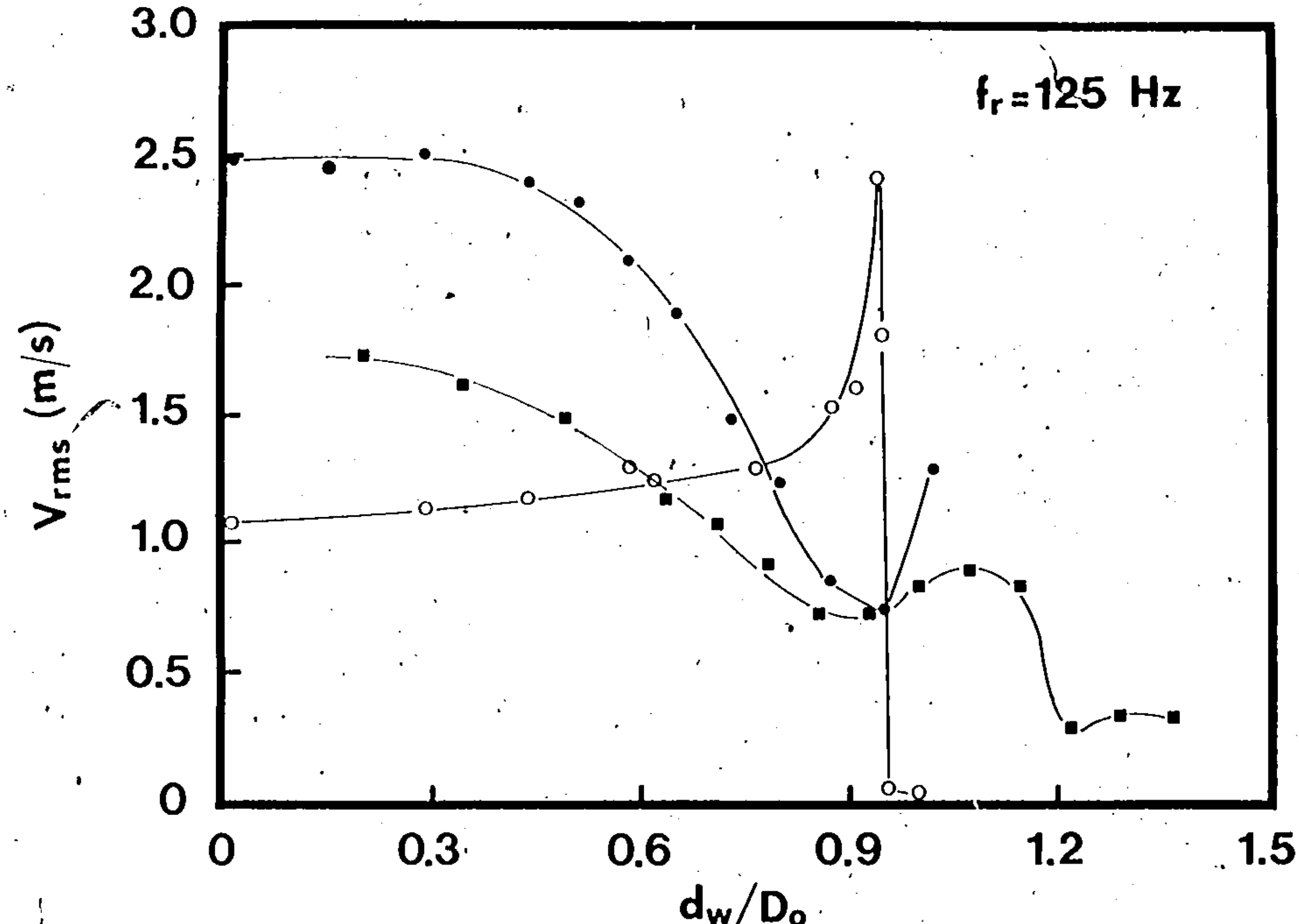

Figure 2.14 : RMS velocity versus non-dimensional hotwire location. (○ - 1mm behind downstream face of upstream orifice plate, ● - upstream face of downstream orifice plate, ■ - 1cm behind downstream face of downstream orifice plate)

downstream orifice plate seen during the flow visualization study. The use of hotwire anemometry for estimations of velocity fluctuations when the mean velocities are small, and the fluctuating components are large is not a reliable technique. Essentially this inherent weakness in the measurement approach arises from the rapid change in the slope of the calibration curve at lower flow velocities. A laser doppler anemometer would be ideal for obtaining detailed information of the mean and RMS velocity values near the lip of the orifice plate. This would require a modification to the test section allowing access to the orifice lip by the laser light. The final rms velocity profile examines the expansion of the flow jet into the downstream portion of the piping system. As seen in the figure, this expansion results in a general decrease in the measured rms velocity levels across the section. An important feature to note is the clear broadening of the peak associated with the previous discontinuity in the rms velocity profile. If the peak in the rms velocity profile at $d/Do = 1$ at the lip of the downstream orifice plate is associated with flow reversal, one would expect to see some measure of this downstream. As well, the presence of predominately stagnant flow conditions behind the downstream orifice plate would allow the higher velocity fluid moving upstream between the shear layer and the orifice plate to influence a greater volume of fluid. Thus, increasing the width of the peak in the RMS velocities for $d/Do > 1$.

2.5 Effect of Turbulence on Acoustic Source

Recently Blevins [2.26] has examined the effect of sound and turbulence on the organized vortex shedding behind a single cylinder under cross flow in a duct. Based on physical arguments and verified with limited experimental data, Blevins proposed that the organization of vortex shedding behind the cylinder by an externally applied (or self excited) sound field will be lost if the turbulence levels at the separation point exceed the acoustic particle velocities at the same location. The conceptual model for the self sustained shear layer oscillations using the acoustic feedback to excite and perturb the shear layer would also predict a strong sensitivity to the mean turbulence level at the shear point. Destruction of the correctly phased and coherent fluid disturbance at the shear layer by a random fluid disturbance arising from large mean turbulence levels should also "turn off" the shear layer oscillations.

A series of experiments were conducted to examine the effect of mean turbulence level on the acoustic source. Figure 2.15a presents the normalized RMS velocity spectrum (turbulence intensity) with a single turbulence screen made from 1.5 mm expanded aluminum (approx. 70% open area) mounted to the upstream face of the upstream orifice plate. The hotwire was located along the centerline of the pipe and positioned along the plane of the downstream face of the upstream orifice plate. The cavity geometry, location in the rig, and nominal resonating frequency are identical to those used in the velocity profile measurements. The mean velocity at the centerline was 20.9 m/s. Using the rms velocity fluctuations at the centerline from figure 2.14 results in a log of the turbulence intensity at the resonating frequency, without the turbulence grid of -1.3. This is virtually identical to the value at the resonating frequency (nominally 125 Hz) of figure 2.15a with a single grid. A second, identical screen was mounted over the first screen, such that the meshes of each screen were perpendicular to one another. Figure 2.15b presents the turbulence intensity measured at the same location for this experiment. The mean velocity was adjusted to within 2% of the previous case. The turbulence intensity spectrum is flat, and at a higher mean level than obtained using a single grid. The peak in the spectrum at 125 Hz has been reduced, however, there is still the presence of a strong periodic component (and fluctuating shear layer as seen utilizing the flow visualization apparatus).

The upstream orifice plate was turned on a lathe, removing material from the upstream face and reducing the thickness from 7.6mm to 3.8 mm. This allowed mounting of

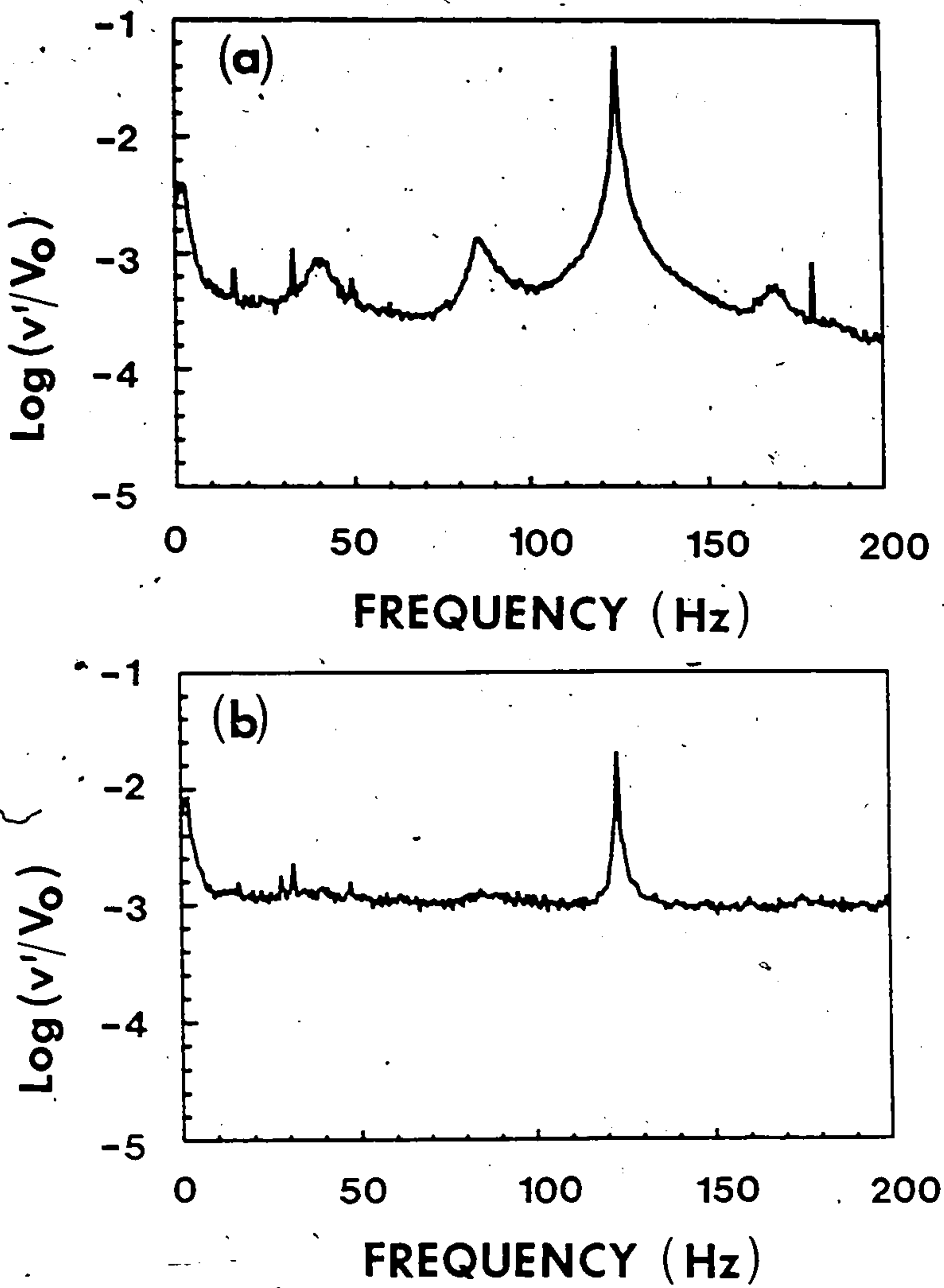

Figure 2.15 : Turbulence intensity measured at downstream face of upstream orifice plate. (a: Single turbulence grid, thickness=7.6mm, Vo=20.9 m/s), (b: Two turbulence grids, thickness=7.6mm, Vo=20.4 m/s)

the turbulence grids closer to the point of separation, without altering the geometry of the separation point. A significant change in the turbulence spectra as seen in figure 2.16a resulted from the mounting of the single turbulence grid. The resonating frequency of 125 Hz disappeared, however it was replaced by two peaks of reduced amplitude. These two frequencies which are seen as small peaks in the original spectra of figure 2.15a are resonant frequencies of the pipe, with pressure nodes at or very near the cavity location. The second grid was mounted again over the first grid, aligning the grid of the screens at 90 degrees. The flow velocity was adjusted within 0.4% of the previous experimental value. The turbulence intensity spectrum is presented in figure 2.16b. The spectrum is flat, and does not exhibit any periodic components at either the original resonating frequency of 125 Hz, or the side band frequencies seen in figure 2.13a. The low frequency peak near 30 Hz is not associated with sound production in the pipe. The mean turbulence intensity across the frequencies 120 Hz to 130 Hz is 1.6×10^{-3}. The resulting fluctuating velocity is 4.75×10^{-2} m/s. Assuming a simple acoustic plane wave mode, neglecting the end and flow impedances allows the estimate of peak acoustic pressures to be calculated as:

$$P_{-} = \rho c * u \qquad [2.4]$$

Assuming standard values for density and sound speed ($\rho = 1.2, c = 340$) results in peak acoustic pressures of 120 dB (re 20×10^{-6} Pa). This is in good agreement with the range of peak acoustic pressures measured for this cavity and flow velocity. It was possible to re-instate the fluid oscillations inside the cavity by driving the piping system with a speaker located just outside the bellmouth entrance. The oscillations were evident on the hotwire measurements as well as using the flow visualization equipment. The introduction of the "smoke" upstream of the turbulence grids removed the possibility of high contrast photographs. Although this aspect of the phenomenon was not investigated in detail, it was possible to force the fluid oscillation in the cavity to occur over wide frequency range ($\pm$ 5 Hz

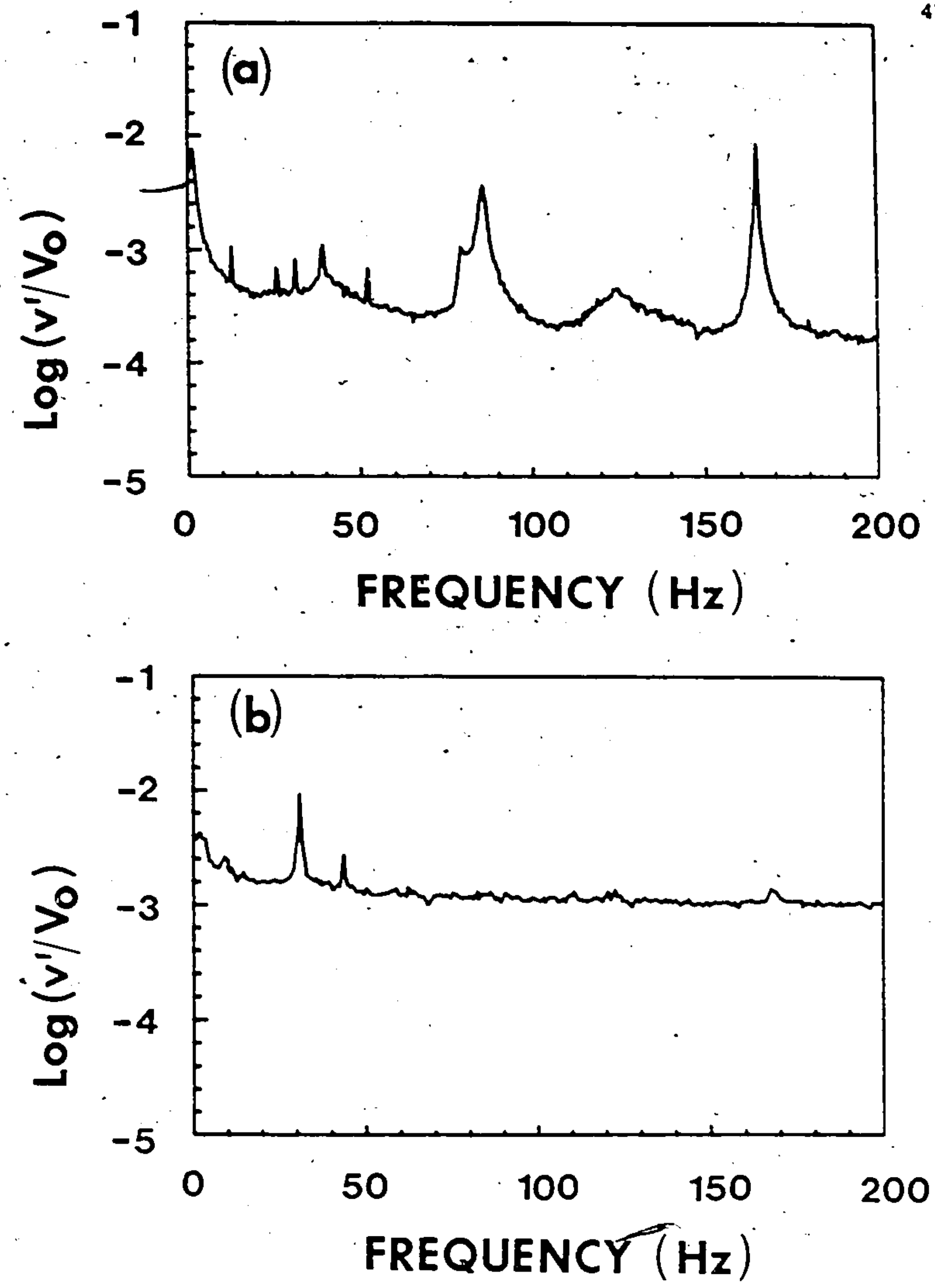

Figure 2.16 : Turbulence intensity measured at downstream face of upstream orifice plate. (a: Single turbulence grid, thickness=3.8mm, Vo=21.1 m/s), (b: Two turbulence grids, thickness=3.8mm, Vo=21.1 m/s)

centered about 125 Hz) with moderate levels of applied sound (approximately 90 dB maximum in the pipe). The generation of high turbulence levels at the separation point has not eliminated the flow separation. Thus it is not surprising that the shear layer will still amplify disturbances introduced at the shear point by the external speaker.

2.6 Summary

The main acoustic and fluid mechanical characteristics of the cavity source have been investigated. The source has been shown to interact primarily with those modes locating a pressure node (velocity antinode) at or near the double orifice cavity. The flow visualization photographs show a rolled up, but unseparated vortex between the two orifice plates. The acoustic particle velocity is a maximum at the cavity location when the shear layer at the downstream orifice location is at the minimum radial position. The hotwire anemometry measurements across the downstream orifice plate indicate a strong axial fluid oscillation at the centerline of pipe of roughly 10-15 percent of the mean centerline velocity. The axial amplification through the cavity is on the order of 2-3. It has been shown that significant turbulence levels at the upstream separation point can eliminate completely the fluid and resulting acoustic oscillations. Using a simplified acoustic model, it has been demonstrated that the random velocity fluctuations necessary to "turn off" the oscillations are of the same scale as the acoustic particle velocities before the introduction of the turbulence. It is important to note that the shear layer characteristics in higher shear layer modes (when more than 1 vortex exists between the orifice plates) have not been investigated.

CHAPTER 3

ACOUSTIC MEASUREMENT TECHNIQUES

3.0 Introduction

In the previous chapter, the main features of the cavity resonator were identified, including the strong interaction of the flow with particular acoustics modes of the piping system. Before this flow/acoustic interaction can be theoretically investigated, it is necessary to generate an accurate model of the piping acoustics. This criterion in turn leads to an experimental determination of the test piping system impedance values, ensuring accurate estimates of net system damping.

This chapter examines fundamental acoustic measurement techniques which can be used to accurately model the acoustic environment of the cavity resonator, as well as measure directly the acoustic power of the source. An impedance measurement method which is suitable for measuring the impedance of passive (non radiating) piping components is selected, implemented and tested. This basic approach is extended in this chapter to allow determination of the source impedance during sound production. The equations required for acoustic intensity calculations are developed which can be combined with measurements similar to those required for impedance measurements to allow the direct determination of acoustic power generation. Also, the applicability of using a two microphone technique incorporating a two channel FFT analyser for selective acoustic intensity and impedance identification is examined in detail.

3.1 Impedance measurement techniques

Several methods are available for determining the impedance characteristics of acoustic systems. Traditionally, the impedance tube approach has been used [3.1]. This method examines the ratio of successive maxima and minima of a standing acoustic wave in a tube terminated by an unknown end condition. From this information the reflection coefficient and subsequently the impedance values can be calculated. This technique can be tedious since discrete frequency excitation is combined with a microphone traverse along the length of the resonant tube. Errors in the estimation of the end impedance will occur with this basic approach if a correction for dissipation effects is not included, or if the location of the first pressure minima is not determined to a high degree of accuracy [3.2].

A tone bursting technique examined by Gately and Cohen [3.4] utilized an acoustic pulse generated at a discrete frequency which is measured (both incident and reflected) by a single wall mounted microphone. This approach requires a long resonant tube to clearly separate the incident and reflected waves which can introduce significant dissipation effects.

Kathuriya and Munjal [3.4] developed an impedance tube method which removed the need for a microphone traverse. This method eliminated the requirement for a lengthy resonant tube for low frequency measurements and the associated dissipation effects. The formulation which requires the measurement of the acoustic field at three (or more) fixed locations included the effect of mean flow in the parameter estimation. Improvements on this approach allowing independent determination of the phase angle and magnitude of the reflective coefficient were presented later by Panicker and Munjal [3.5]. This later modification to the original identification procedure requires the measurement of acoustic pressures at more than 3 locations in the resonant tube.

The removal of the microphone traverse for evaluation of system parameters is a significant improvement on the basic impedance tube approach. However, the discrete frequency excitation still involves a lengthy experimental procedure when impedance values over a wide range of frequencies are required. This limitation was removed by the method developed by Seybert and Ross [3.6]. Their solution was to excite the resonant tube with a broad band frequency source, and measure the auto and cross spectra of the acoustic pressure at two locations. The measured spectra were analytically developed in terms of the unknown frequency dependent incident and reflective waves in the tube. The solution for these wave components allowed determination of the complex valued reflective and impedance functions. This approach removes many of the problems associated with the traditional impedance tube method. However, it introduces constraints for microphone location and separation to limit errors in solution of the unknown system parameters. The effect of mean flow on the solution was also incorporated into the analysis. In chapter 4 of this thesis a technique which utilizes a transfer function approach to model the acoustic waves for determination of the impedance function is examined. It is however only a slight modification to the basic approach of Seybert and Ross.

An advanced spectral technique using a Ceptrum analysis has been used by Bolton and Gold [3.7] to determine impedance values. This method allows the use of a series of tone bursts containing a broad band of frequencies to be analysed as incident and reflected waves. This very interesting approach requires significant digital off line processing. The accuracy of this method when applied to lower frequency physical systems was not presented.

Selection of an impedance determination technique suitable for in situ determination of the system parameters eliminated the traditional impedance tube approach. The broad frequency range determination necessary in the system parameters encouraged the selection of the two microphone random excitation technique of reference [3.6]. The close relationship between the processing and information acquisition used in this method and that required for acoustic intensity measurements (to be discussed in section 3.3) also suited the particular application. The cepstrum analysis for impedance estimation required more data acquisition hardware than available with the present experimental apparatus.

3.2 Two microphone random excitation technique for impedance estimation

The basic approach of the two microphone random excitation method is to analytically develop the measured sound field in terms of incident (right running) and reflected (left running) acoustic waves. The total pressure at the measurement points is expressed in terms of the acoustic field generated by these two waves. The ratio and phase of the separated sound field at the measurement points are functions of the position of the two microphones within the impedance tube (which is known), and the reflective coefficient (both mag. and phase) of the unknown termination condition. The method of Seybert and Ross differs from that proposed in [3.4] in that the Fourier transform of the time delay components in the model and the unknown reflective coefficient are incorporated into the solution. The auto and cross spectra of the acoustic pressure at the measurement points are then the dependent variables in the system. This transformation to the frequency domain allows for the solution of the unknown system parameters over a wide frequency band if the system is excited by band limited white noise.

Incident or right running waves in the resonant tube are assumed harmonic and spatially dependent as:

$$P_i(x,t) = a(t) * e^{j(\omega t - K_i x)} \qquad [3.1]$$

where:

$K_i = k/(1+M)$

$k = \omega/c$ the wave number

M = Mach number

c = sound speed

x = distance from unknown termination condition

Reflected or left running waves are assumed harmonic and spatially dependent as:

$$P_r(x,t) = b(t) * e^{j(\omega t - K_r x)} \tag{3.2}$$

where:

$K_r = k / (1 - M)$

Equations 3.1 and 3.2 imply that points to the right, lag points to the left by $e^{K_i x}$ for right running (incident) waves. For left running (reflected) waves, points to the right, lead points to the left, by $e^{K_r x}$. Using this notation, the time domain block diagram producing the incident, reflected and total acoustic field in the resonant tube is presented in figure 3.1. The measured quantities in the system are the total acoustic pressure at the measurement points x1,x2. The required unknown quantities using the formulation presented by Seybert and Ross are the total pressure and particle velocity at X = 0 (the termination point).

Figure 3.2 presents the block diagram suitable for determination of the total pressure at the measurement points, given the incident and reflected waves at x = 0.

Using the notation of Bendat and Piersol [3.8] the measured pressures at x1,x2 can be computed as:

$$P1 = h2 * Pb + h3 * Pa \tag{3.4}$$

$$P2 = h1 * Pb + h4 * Pa \tag{3.5}$$

where:

$h1 = e^{-j(K_r x2)}$

$h2 = e^{-j(K_r x1)}$

$h3 = e^{j(K_i x1)}$

$h4 = e^{j(K_r x2)}$

and:

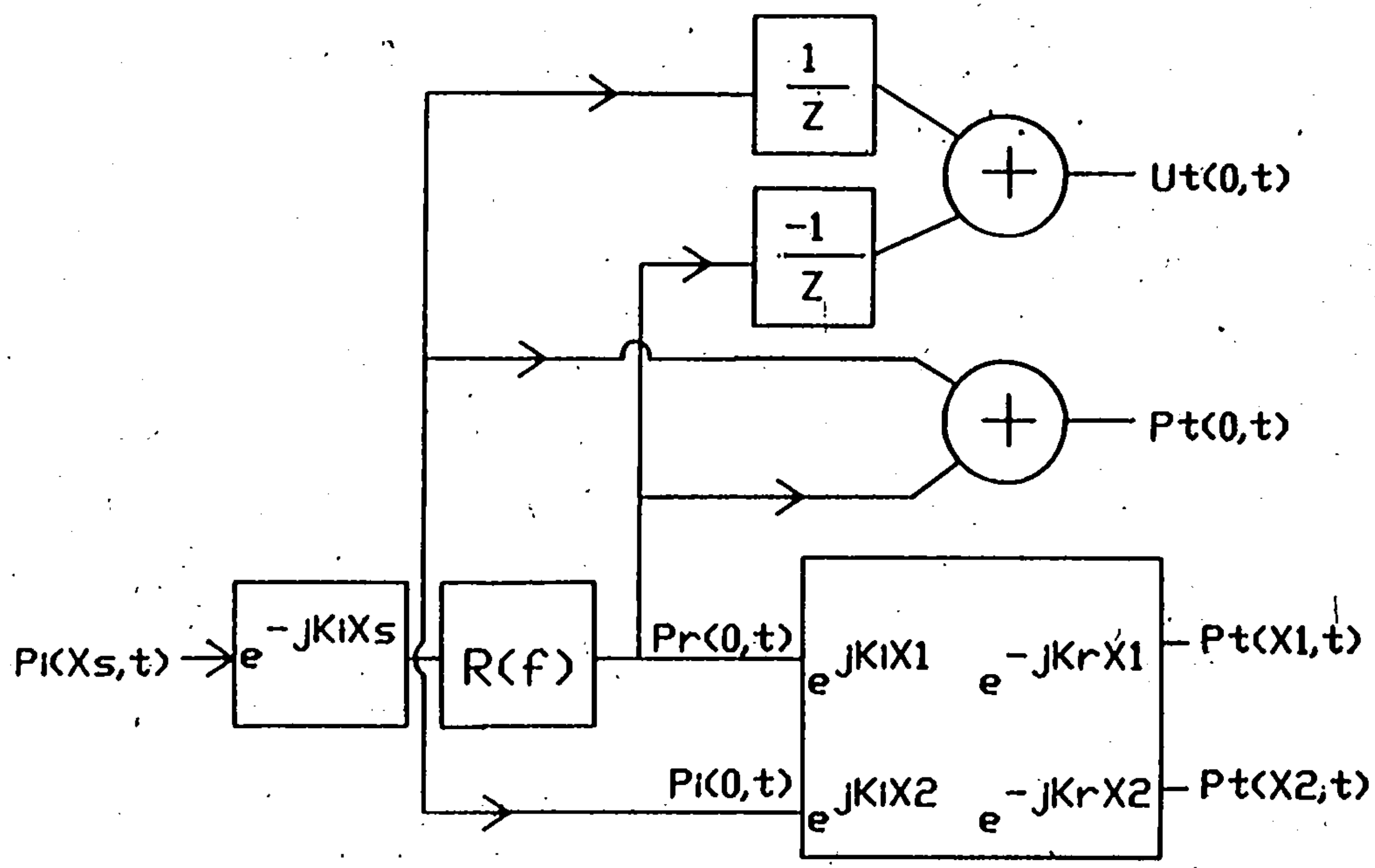

Figure 3.1 : Time domain block diagram describing wave system in impedance tube.

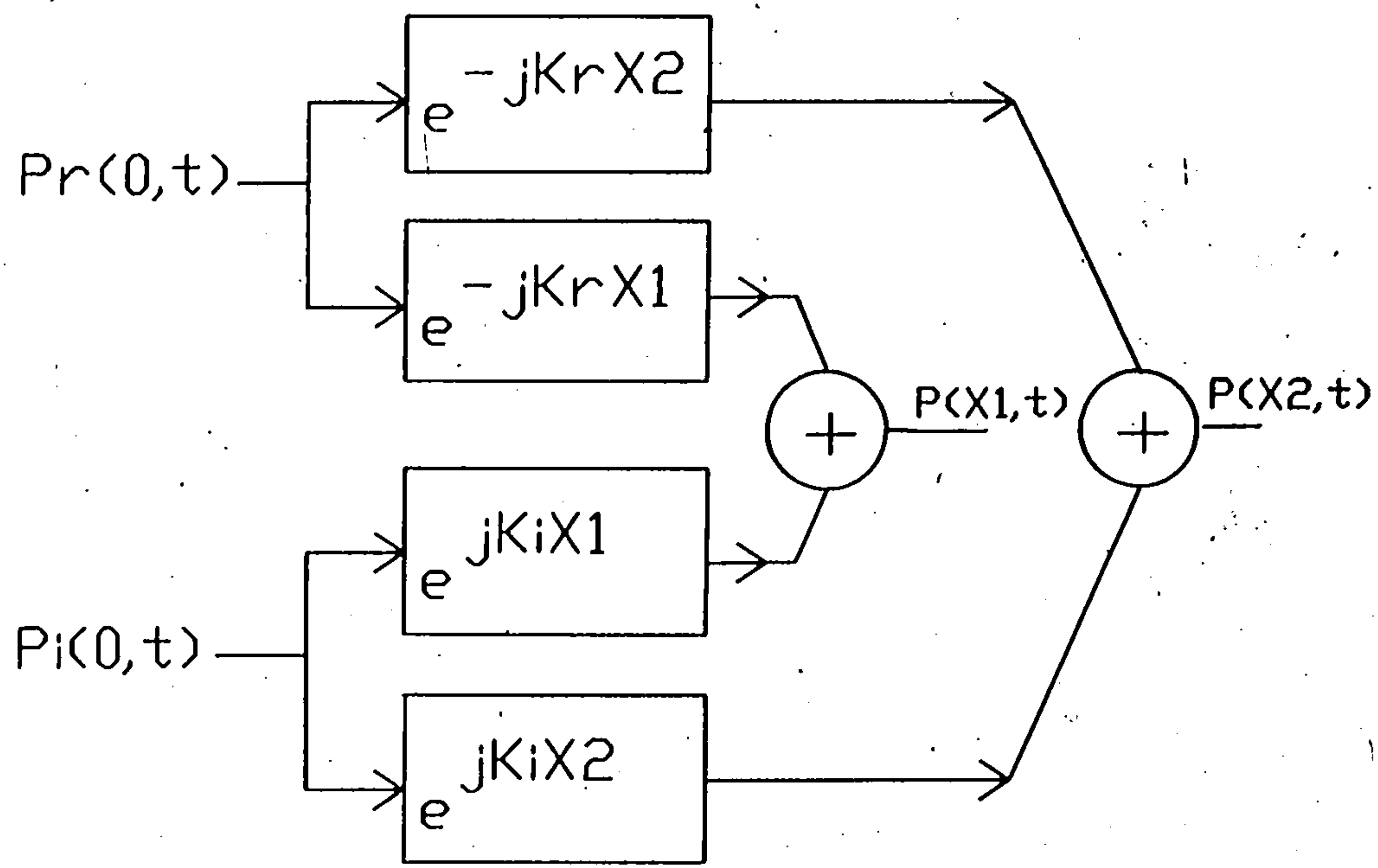

Figure 3.2 : Frequency domain block diagram relating incident and reflected pressure components at impedance location to total pressure at microphone location.

$P1$ = Fourier transform of $Pt(x1,t)$

$P2$ = " " $Pt(x2,t)$

Pa = " " $Pi(0,t)$

Pb = " " $Pr(0,t)$

The auto spectrum of the total acoustic pressure at x1 is given by:

$$G11 = 1/T \ E[\, c(P1) * P1 \,] \qquad [3.6]$$

where:

c(P1) represent the complex conjugate of P1

Substituting 3.4 into 3.6 results in:

$$G11 = /h2/^2 * Gbb + /h3/^2 * Gaa + c(h2)h3 * Gba + c(h3)h2 * Gab \qquad [3.7a]$$

Similarly, the auto spectrum of the total acoustic pressure measured at x2 is given by:

$$G22 = /h1/^2 * Gbb + /h4/^2 * Gaa + c(h1)h4 * Gba + c(h4)h1 * Gab \qquad [3.7b]$$

The cross spectrum of the measured microphone signals at x1 and x2 is given by:

$$G12 = 1/T \ E[\, c(P1) * P2 \,] \qquad [3.8]$$

Substitution of equations 3.4 and 3.5 into 3.8 results in:

$$G12 = c(h2)h1 * Gbb + c(h3)h4 * Gaa + c(h2)h4 * Gba + c(h3)h1 * Gab \qquad [3.9]$$

Equations 3.7 and 3.9 can be simplified as:

$$G11 = Gaa + Gbb + 2 * \cos(a) * Re(Gab) + 2\sin(a) * Im(Gab)$$

$$G22 = Gaa + Gbb + 2 * \cos(b) * Re(Gab) + 2\sin(b) * Im(Gab) \qquad [3.10]$$

$$Re(G12) = \cos(c) * Gaa + \cos(d) * Gbb + (\cos(f) + \cos(g)) * Re(Gab) + (\sin(f) + \sin(g)) * Im(Gab)$$

$$Im(G12) = -\sin(c) * Gaa - \sin(d) * (Gbb) + (\sin(g) - \sin(f)) * Re(Gab + (\cos(f) - \cos(g)) Im(Gab)$$

where:

$$a = (K_i + K_r)^* x1$$

$$b = (K_i + K_r)^* x2$$

$$c = (x1 - x2)^* K_i$$

$$d = (x2 - x1)^* K_r$$

$$f = (K_i x1 + K_r x2)$$

$$g = (K_i x2 + K_r x1)$$

Equations 3.10 are a 4x4 system of linear equations which are mathematically identical to equations 13 of reference [3.6]. The complex reflective coefficient can be calculated directly from the solution of the incident and reflected waves. That is:

$$R(f) = Gab / Gaa \qquad [3.11]$$

The desired non dimensional impedance function can be calculated directly from equation 3.11 as:

$$Z(f) = (1 + R(f)) / (1 - R(f)) \qquad [3.12]$$

Practical use of equations 3.10 are restricted to frequencies whose half wave length are greater than the microphone separation. Frequencies whose half wave length equal to the microphone separation result in a singular solution matrix.

3.3 Acoustic Intensity measurements

The two microphone technique for acoustic intensity measurements has received considerable attention in recent years. This is in part due to the direct extension to the calculation of acoustic power radiation, as well as the proliferation of two channel on line FFT analysers. The formulation for acoustic intensity calculation presented here follows closely that of reference [3.9].

The acoustic intensity for a stationary signal is given by:

$$I(r) = \overline{[p(r,t) * u(r,t)]} \qquad [3.13]$$

where:

$p(r,t)$ = acoustic pressure

and:

$u(r,t)$ = acoustic particle velocity

The two microphone method for intensity analysis uses a finite difference approximation for estimation of the acoustic pressure at a point midway between the two microphones. That is:

$$p(r,t) = 1/2\,[\,p(r+s/2) + p(r\text{-}s/2)\,] \qquad [3.14]$$

where:

s = microphone separation.

The Euler equation is used to estimate the particle velocity as:

$$u(r,t) = -\,1/\rho \int [\partial/\partial r\,\{p(r,t)\}]\,dt \qquad [3.15a]$$

where:

ρ = air density

Using equations 3.14 and 3.15a, the particle velocity can be estimated using:

$$u(r;t) = \text{-}1/(\rho s) \int [p(r+s/2) - p(r-s/2)]\,dt \qquad [3.15b]$$

Equations 3.14 and 3.15b can be substituted into 3.13 to generate an approximation to the intensity vector:

$$I(r) = -\,1/(2\rho s)\,\overline{[(p(r+s/2) + p(r-s/2)) \int (p(r+s/2) - p(r-s/2))\,dt]} \qquad [3.16]$$

A more useable form for the intensity vector can be generated using the cross-correlation function between $p(r,t)$ and $u(r,t)$.

$$Rpu(\tau) = \overline{[p(r,t) * u(r,t+\tau)]} \qquad [3.17]$$

where Rpu(r,0) is identical to the intensity vector of equations 3.13. The cross-correlation function can be generated from the inverse Fourier transform of the cross spectrum Gpu. Using this approach the intensity vector (both real and imaginary) can be generated from spectral estimates of the microphone signals.

Defining:

$P(f)$ = Fourier transform of $p(r,t)$

and:

$U(f)$ = " " $u(r,t)$

The cross spectrum is generated as:

$$G_{pu} = 1/T \; E\,[c(P(f)^{*}\, U(f)\,] \qquad [3.18]$$

where:

$$P(f) = [(Pa(f) + Pb(f)]\,/\,2$$

$$U(f) = -\,[Pb(f) - Pa(f)]\,/\,(j\,\omega\rho s) \qquad [3.19]$$

and:

$Pb(f)$ = Fourier transform of $p(r+s/2,t)$

$Pa(f)$ = " " $p(r-s/2,t)$

Substitution of 3.19 into 3.18 results in:

$$G_{pu} = -\,1/(2\rho\omega s)\,[2\,\mathrm{im}(G_{ab}) + j(G_{bb} - G_{aa})] \qquad [3.20]$$

where:

G_{bb} = auto spectrum of mic. at $(r+s/2)$

G_{aa} = auto spectrum of mic. at $(r-s/2)$

G_{ab} = cross spectrum of two mic. signals.

The frequency dependent intensity vector is given by the real part of equation 3.20.

$$I(f) = -\,\mathrm{im}(G_{ab})/(\omega\rho s) \qquad [3.21]$$

The intensity vector is given by the integral over the frequency domain of 3.21

$$I = -\int im(Gab)\,/\,(\omega ps)\,df \qquad [3.22]$$

Fahy [3.10] is credited with the first presentation of equation 3.22 for calculation of the acoustic intensity vector. The units of acoustic intensity are watts/meter squared. Thus, the acoustic power radiated by a source can easily be estimated by area integration.

It is important to recognize the separation of reactive and active acoustic fields implicit in the acoustic intensity calculation. In reactive fields (typical of pure standing waves),the particle velocity is 90 degrees out of phase with the acoustic pressure, resulting in no net flow of acoustic energy. This distinction is not made with simple acoustic pressure measurements. It is interesting to note [3.11] that the forward and backward components of the radiating intensity vector can be calculated from the spectra of the incident and reflected wave components (equation 3.10). This ties together more closely the intensity analysis, with the impedance formulation presented in section 3.2.

The errors and appropriate microphone orientation effects have been investigated by several authors [3.12,3.13,3.14,3.15]. The effect of finite difference errors and the proximity to the source were investigated by Thompson and Tree [3.12]. They proposed that:

$$0.1 \le K^{*}s \le 1.3$$

and: [3.23]

$$0.0 \le s/Xs \le 0.5$$

for a maximum inaccuracy of 1.5 dB in the acoustic intensity estimate. For a fixed microphone separation this constrains the frequency range which can be effectively investigated. Elliot [3.13] has questioned the lower limiting proximity guidelines of equations 3.23. He has suggested that Thompson and Tree's estimates are overly conservative. However, the basic guidelines are adequate for most applications.

3.4 Source impedance estimation

The two microphone technique described in section 3.2 is applicable for estimation of the impedance characteristics of passive (non-radiating) acoustic systems. Using standard spectral analysis techniques, a method is developed to measure the impedance of a radiating source. The approach utilizes equations 3.10, where the known spectra (G11,G22,G12) contain only information coherent with the external source.

Figure 3.3 presents a block diagram suitable for determination of the conditioned spectra. The total pressure at the measurement points is given by:

$$P1(f) = (H11 * S1) + (H21 * S2)$$

$$P2(f) = (H12 * S1) + (H22 * S2)$$

The 2 auto spectra and cross spectrum of the acoustic pressure are given by:

$$\begin{aligned} G11 &= c(P1(f)) * P1(f) \\ G22 &= c(P2(f)) * P2(f) \\ G12 &= c(P1(f)) * P2(f) \end{aligned} \qquad [3.24]$$

The acoustic inputs in the analysis representing the externally generated (s1) and flow generated (s2) noise sources can be assumed incoherent with each other (Gs1s2 = 0.). With this assumption, equations 3.24 can be calculated using:

$$\begin{aligned} G11 &= /H11/^2 * Gs1s1 + /H21/^2 * Gs2s2 \\ G22 &= /H12/^2 * Gs1s1 + /H22/^2 * Gs2s2 \\ G12 &= H11*H12 * Gs1s1 + H21*H22 * Gs2s2 \end{aligned} \qquad [3.25]$$

The portions of the two auto spectra coherent with the externally generated sound field (and fully incoherent with the flow generated noise) are given by:

$$G11.s2 = \gamma^2_{s11} * G11 \qquad [3.26]$$

$$G22.s2 = \gamma^2_{s12} * G22$$

where:

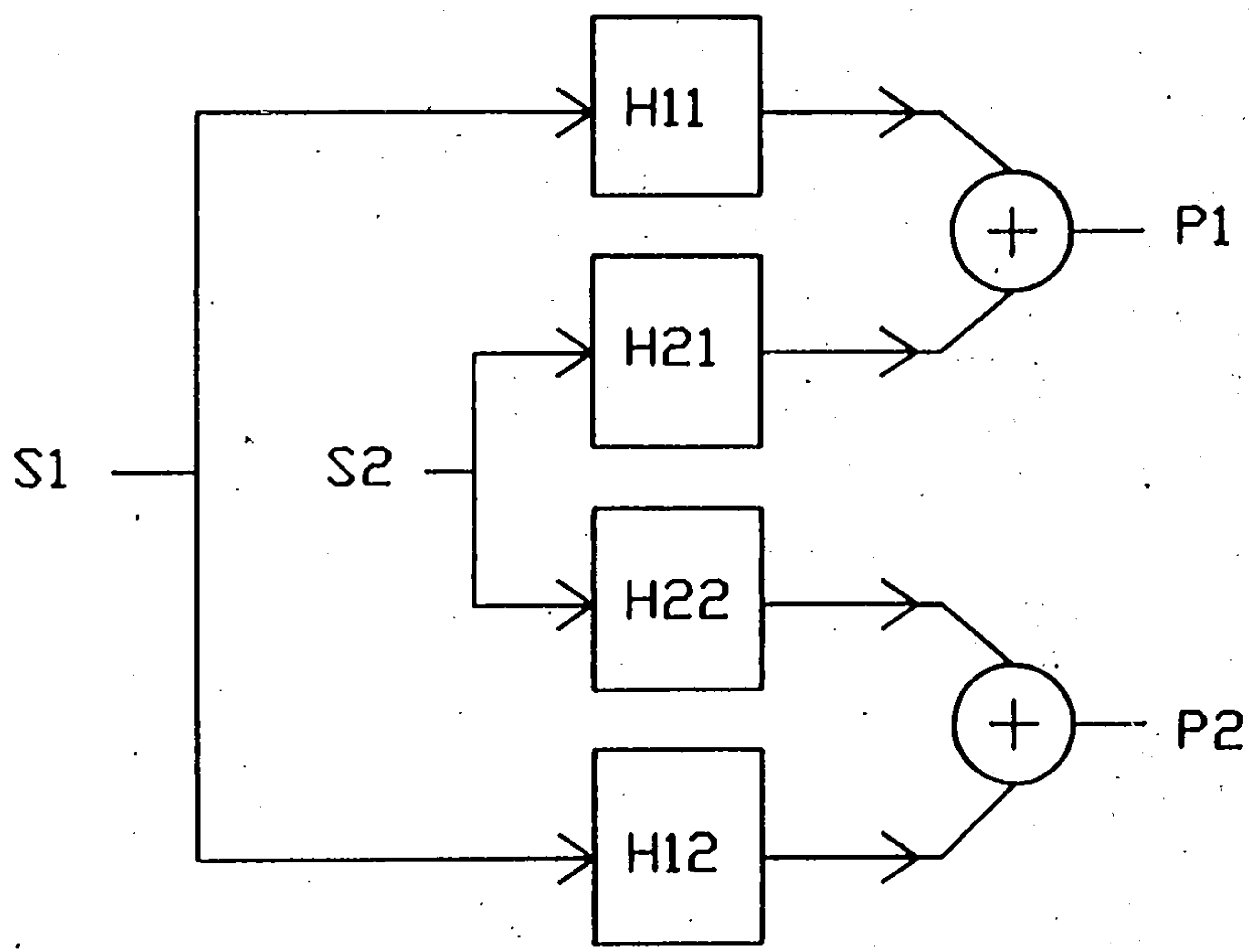

Figure 3.3 : Two input two output block diagram suitable for coherent power analysis.

γ^2_{s11} = ordinary coherence function between s1 and P1

γ^2_{s12} = ordinary coherence function between s1 and P2

The coherent cross spectrum is generated using the transfer function between the externally driven source and P1(f). That is:

$$G12.s2 = c(H11) * Gs12 \qquad [3.27]$$

where:

H11 = Gs11 / Gs1s1

and:

Gs12 = ordinary cross spectrum between external source and mic. 2

Gs11 = ordinary cross spectrum between external source and mic. 1

3.5 Multipass approach for source impedance estimation.

Implementation of the method outlined in section 3.4 is straight forward, requiring the measurement of 6 spectra (Gs1s1,G11,G22,G12, Gs12,Gs11) with the ordinary coherence functions as derived quantities. However, this is more information that can be acquired with a standard 2 channel on line FFT analyser. Bucheger et al. [3.16] have applied a similar approach to measure selectively the acoustic intensity output in an environment of multiple radiating sources. Moreover, it was suggested that a two channel FFT analyser could be used with multipasses of data acquisition if the coherence between sources was less than 0.1. Subsequently Wagstaff and Henrio [3.17] demonstrated the selective acoustic intensity measurement approach with 2 passes of data acquisition in a two source environment. The speed, availability and convenience of 2 channel FFT analysers encourage their use as applied to the source impedance determination. For this reason a series of experiments were conducted to examine the feasibility of a two pass approach.

Figure 3.4 presents a schematic diagram of the experimental apparatus used to implement the two pass impedance identification. In this experiment S(t) represents the externally applied sound, while n(t) represents the undesired background (or flow) noise. The coherence between the two independent noise sources was measured and found to be less than 0.01 over the entire frequency range. The resonance tube is made of 6 mm thick plexiglass tubing. The unknown end impedance consists of a 2.5 cm thick plexiglass sheet rigidly mounted to the resonance tube. This configuration generates a highly resonant (reactive) sound field in the impedance tube, with a known reflective coefficient of magnitude 1, and provides a "worst case" environment for intensity and impedance estimations. In all experiments a two channel Nicolet 660b FFT analyser was used with 150 ensemble averages performed to reduce the random error. With a display window of 1000 Hz, the Nicolet analyser has a frequency resolution of 2.5 Hz.

Initially, a separate experiment was performed to account for any relative gain or phase mismatch between the two microphones and data processing hardware [3.18]. The two microphones were flush mounted with the rigid termination and the impedance tube excited with band limited white noise. The transfer function between the two microphones, relating the relative gain and phase was measured and transferred to the VAX 730 for off line calibration. The calibration transfer function is defined as:

$$Hc12 = G12 / G11$$

The relative calibration is performed using:

$$\begin{aligned}(G11)c &= G11 \\ (G22)c &= G22 / |Hc12|^2 \\ (G12)c &= G12 / Hc12\end{aligned} \qquad [3.28]$$

where the uncalibrated spectra of equations 3.28 represent either the directly measured (single pass) auto and cross spectra, or the coherent spectra of equations 3.26 and 3.27.

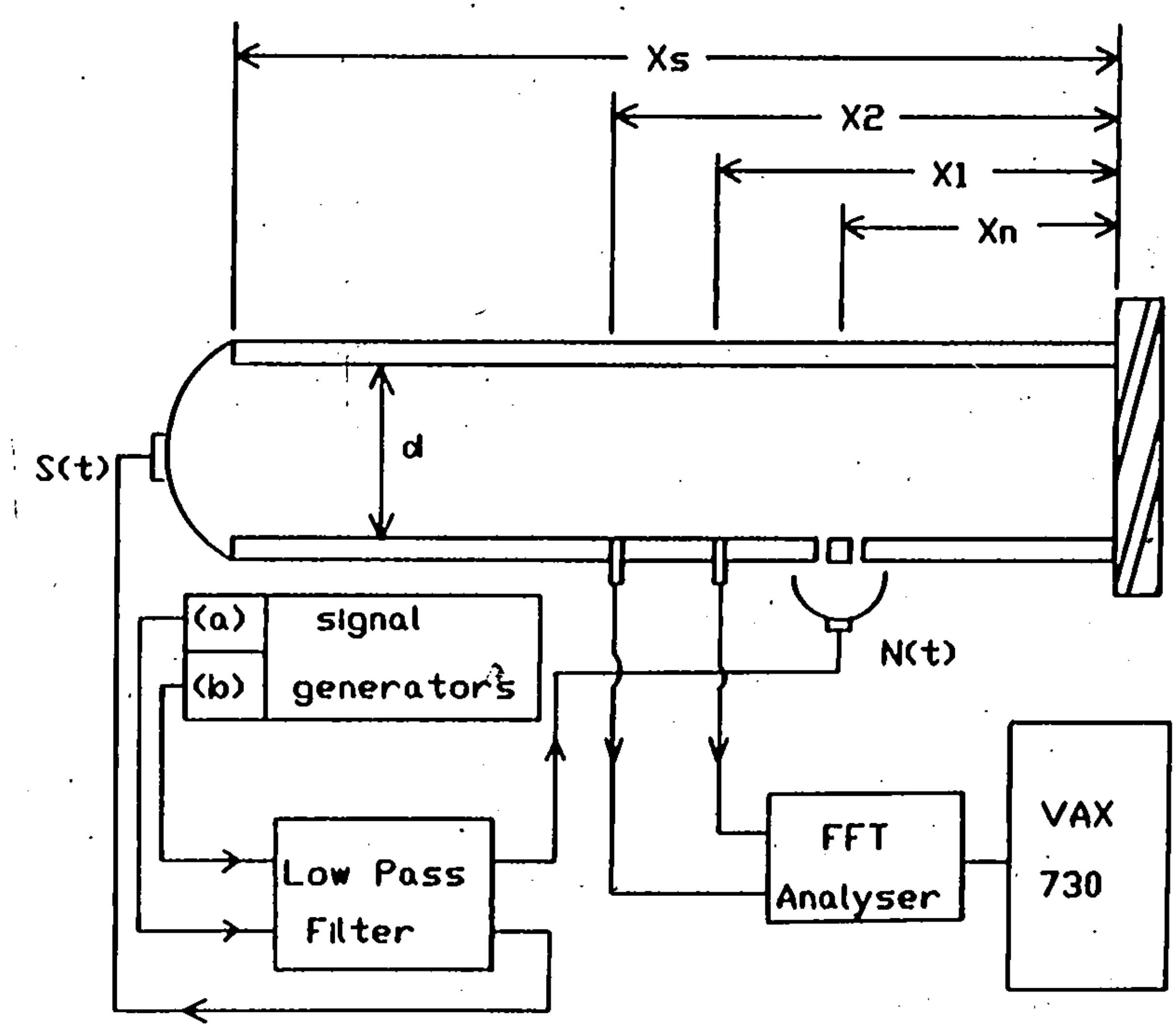

Figure 3.4 : Schematic diagram of experimental apparatus utilized in testing feasibility of two pass data acquisition.

Verification of the developed software package,and implementation of the two microphone technique was conducted with the parasitic source (n(t)) off and the reflective coefficient computed directly. This negates the need for the two pass acquisition and allows an assessment of the basic approach. The results, presented in figure 3.5, indicate a slight dip in the computed reflection coefficient below 200 Hz and a "smooth" evaluation over the frequency range. The obvious errors below 50 hz are associated with the lack of available speaker input at these frequencies. The dip below 200 Hz and the overall evaluation just below the expected value of 1 is attributed to the frequency dependent acoustic losses through the perforations in the resonant tube at the location of the second source. In general the results are very good over the entire frequency range.

The second experiment was conducted with the parasitic source on. However, no attempt was made to account for its presence. The reflective coefficient was calculated using a single pass data acquisition and illustrates the possible errors involved when the effect of the second source is ignored. As seen in figure 3.6 the calculated reflective coefficient is a poor estimate of the expected value.

The third experiment was conducted with the parasitic noise source on and utilized the full conditioned spectra approach of section 3.4. The output level of n(t) was the same as the previous experiment. The ordinary coherence functions between the primary noise source (s1) and one of the microphone signals are presented in figure 3.7. The very low coherence values seen just over 200 Hz, and again at 600-700 Hz are due to the destructive interference patterns in the resonant tube and the resulting poor signal to noise ratio at these frequencies. This loss of coherence is typical of the bias error problems associated with measurements in highly resonant environments [3.8]. The peak coherence values at the resonance frequencies indicate that the parasitic source contributed to roughly 10 percent of the measured acoustic pressures. The computed reflective coefficient is presented in figure 3.8, and is seen to be a

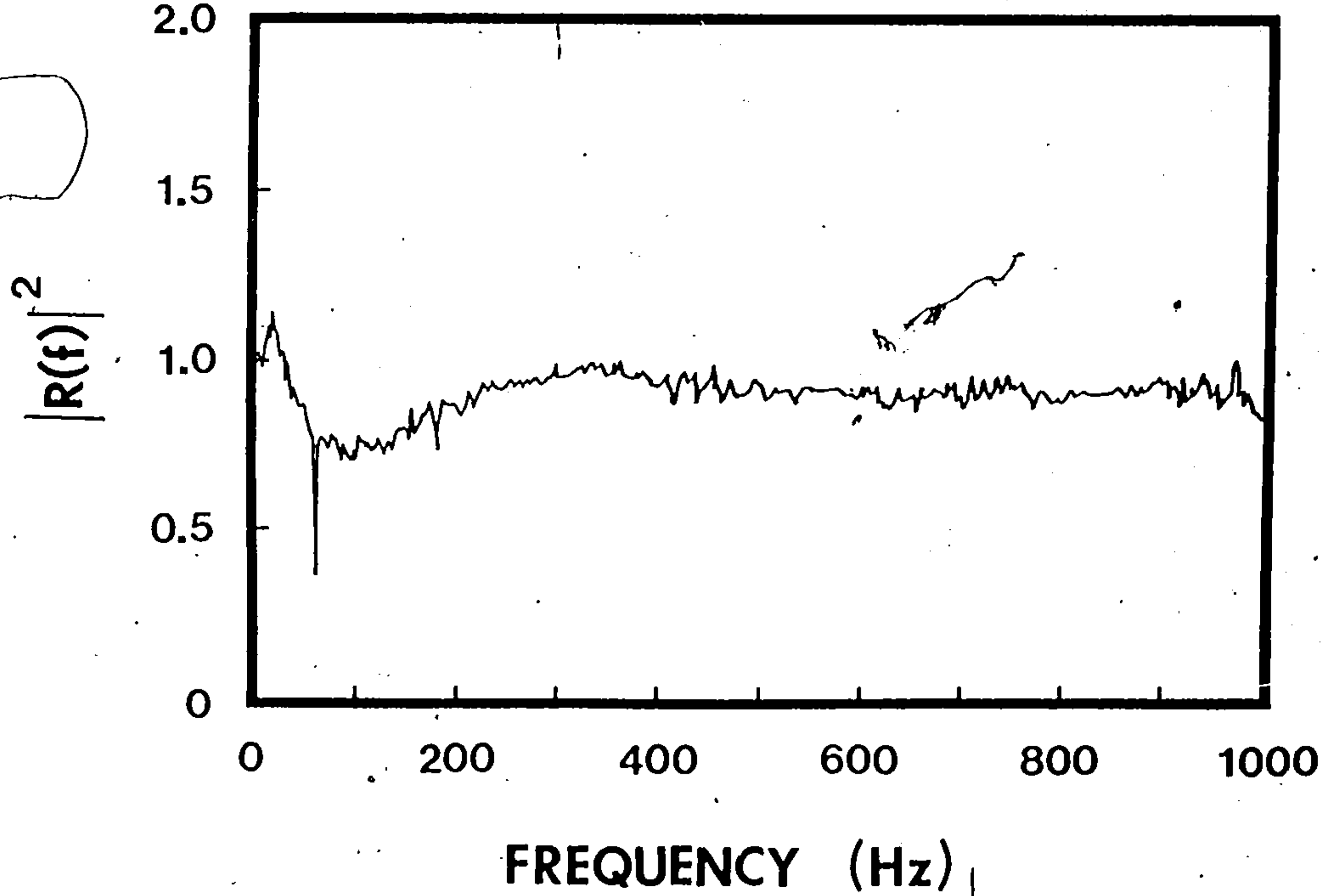

Figure 3.5 : Reflective coefficient computed using single pass data acquisition.

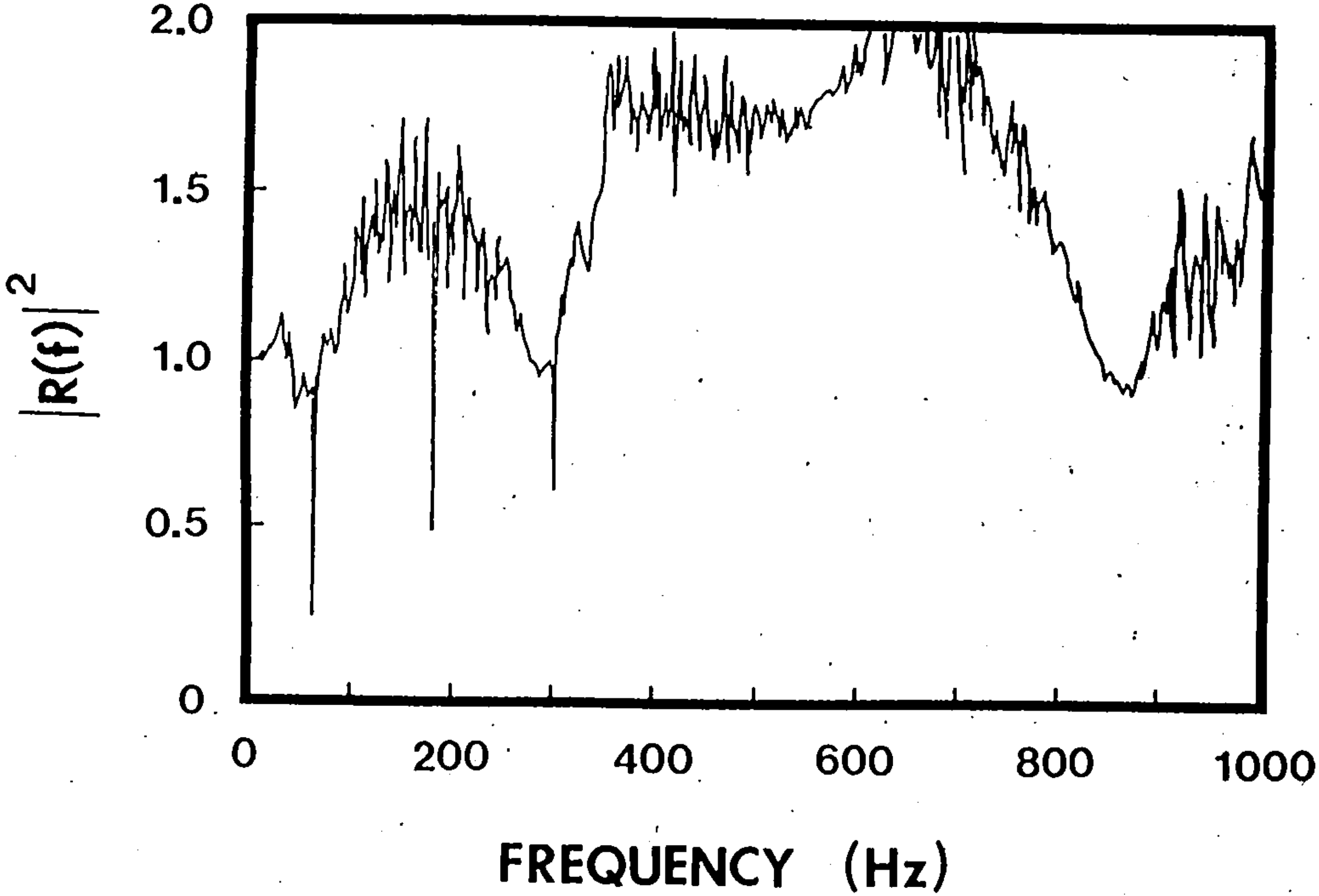

Figure 3.6 : Reflective coefficient computed using single pass data acquisition with n(t) on.

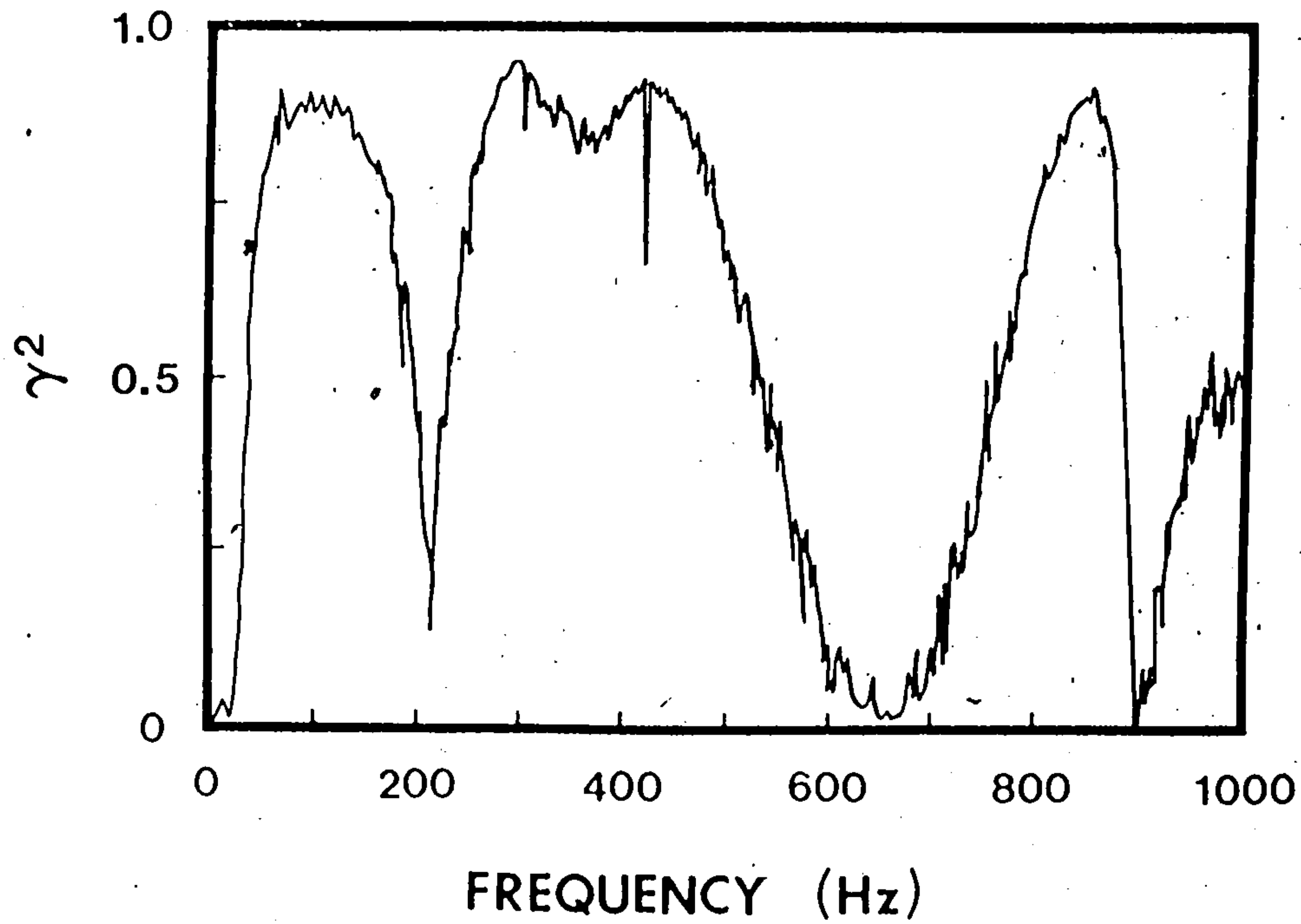

Figure 3.7 : Ordinary coherence function between microphone and primary source.

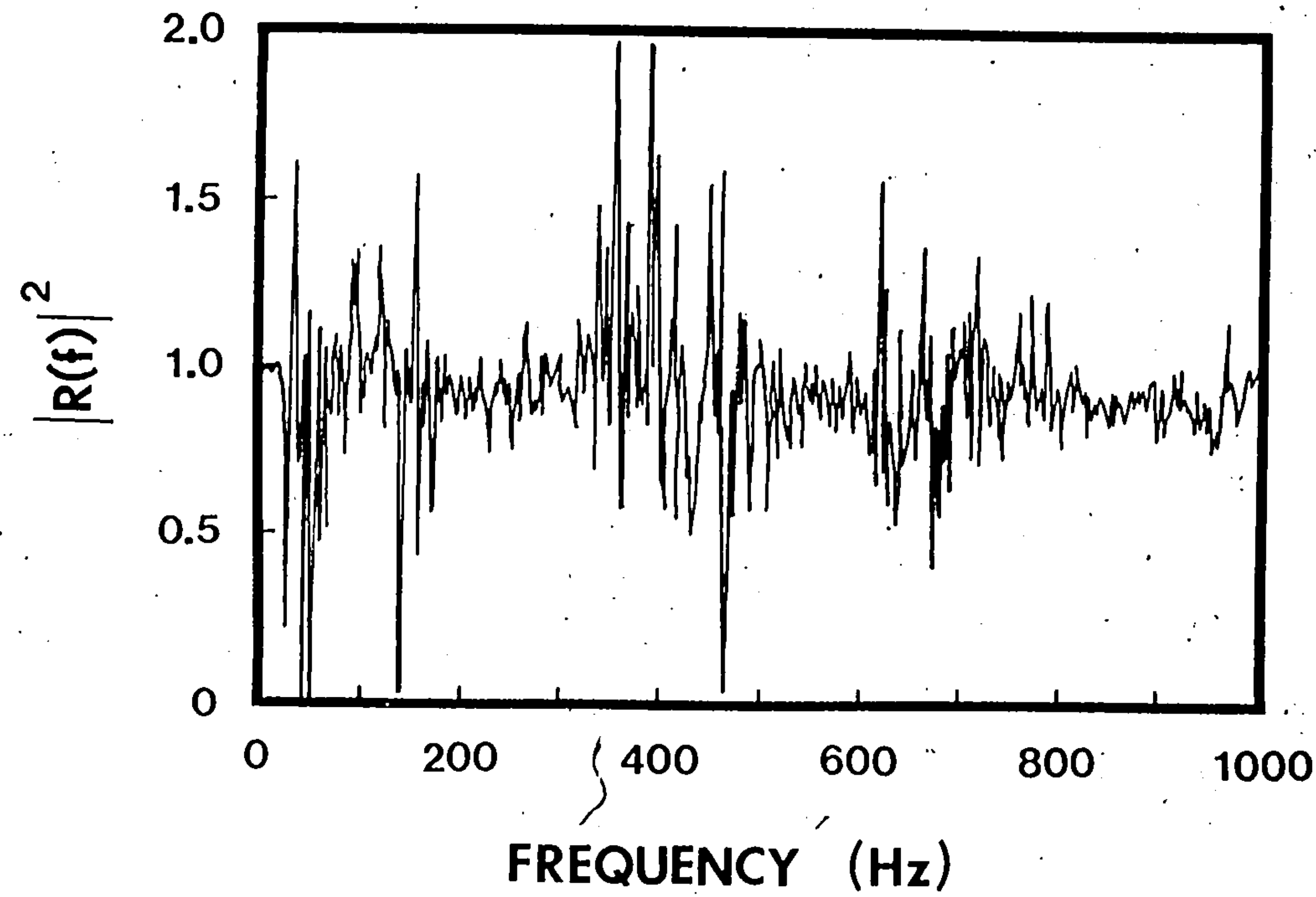

Figure 3.8 : Reflective coefficients computed using conditioned spectra approach with multipass data acquisition

"noisy" estimate, with the mean value (frequency smoothed) close to the results of the first experiment.

In the presence of stationary uncorrelated contamination noise, an alternative approach to using the coherence functions in the analysis is to measure and store the two auto and cross spectra with the primary source off, and subtract these from the corresponding spectra with the primary source on. This is again a two pass experiment and assumes that there are no transfer function modifications when both sources are operating. The resulting reflective coefficient computed using this approach is presented in figure 3.9. There is an improvement in the estimate below 200 Hz from that seen in figure 3.8. However, there still exists significant "noise" superimposed on the expected value in the regions of 350-800 Hz, and again at 900-1000 Hz. Again the frequency smoothed value is a good estimate of the original value presented in figure 3.5.

The absence of a smooth estimate in figures 3.9 and 3.8 indicate that the "noise" introduced into the computation is not associated with the use of the coherent power analysis but is related to the two pass data acquisition. An experiment was conducted to investigate the effect of decreasing the frequency resolution (and changing the associated bias error) when using the two pass approach. An upper frequency limit of 5000 Hz with a corresponding frequency resolution of 12.5 Hz on the Nicolet analyser was used in the experiment. This is the same frequency resolution of reference [3.16] when the two pass approach was used for a selective acoustic intensity analysis. The results of this experiment are presented in figure 3.10. Below 1000 Hz the reflective coefficient is a reasonably smooth estimate of the expected value. The results above 1000 Hz should be ignored as both low pass filters were removing any acoustic input to the system. The "apparent" improvement in coefficient estimation in this case over the more frequency detailed example illustrates the smoothing effect of a reduced frequency resolution in the analysis.

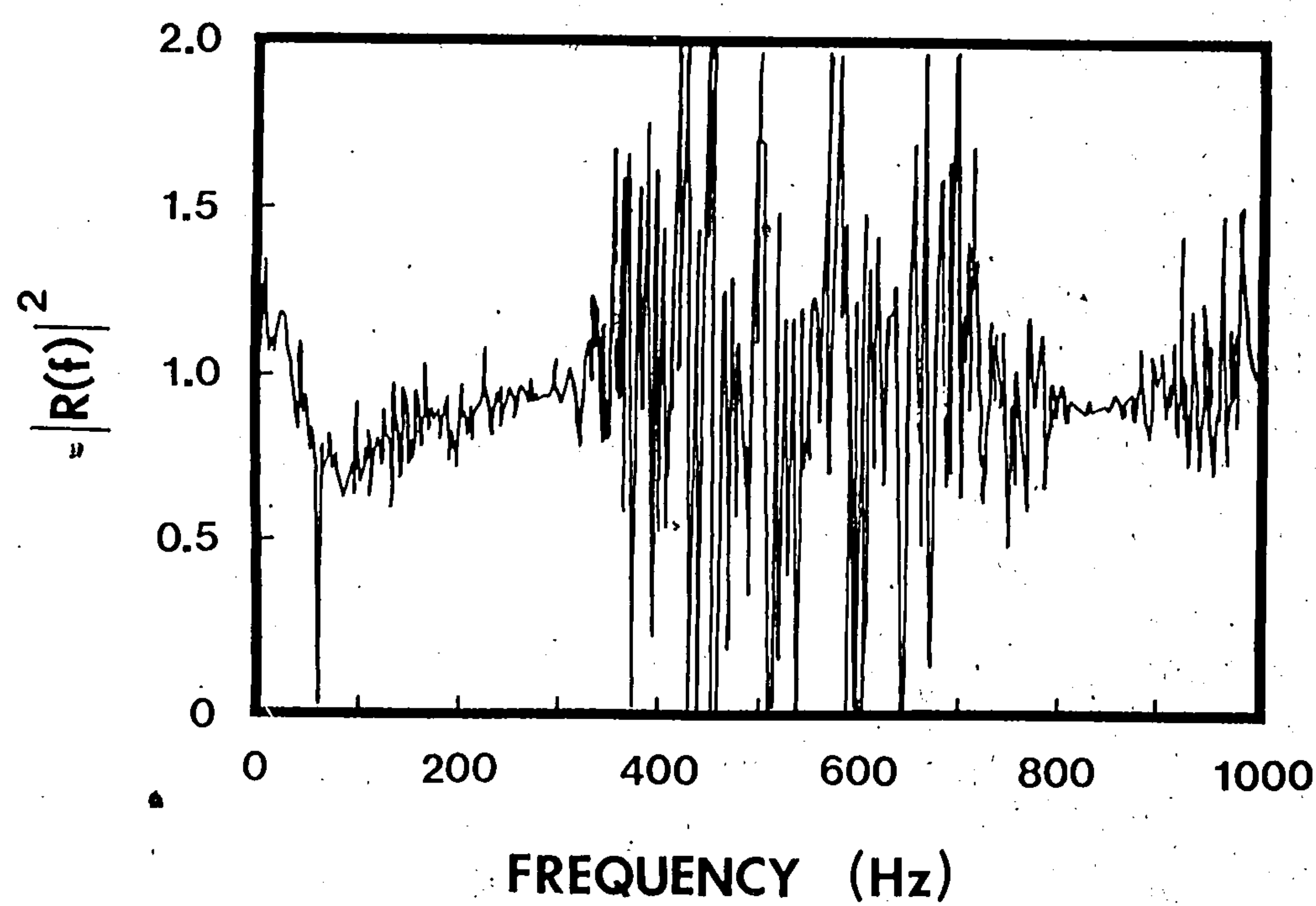

Figure 3.9 : Reflective coefficient computed using two pass data acquisition, using subtraction technique.

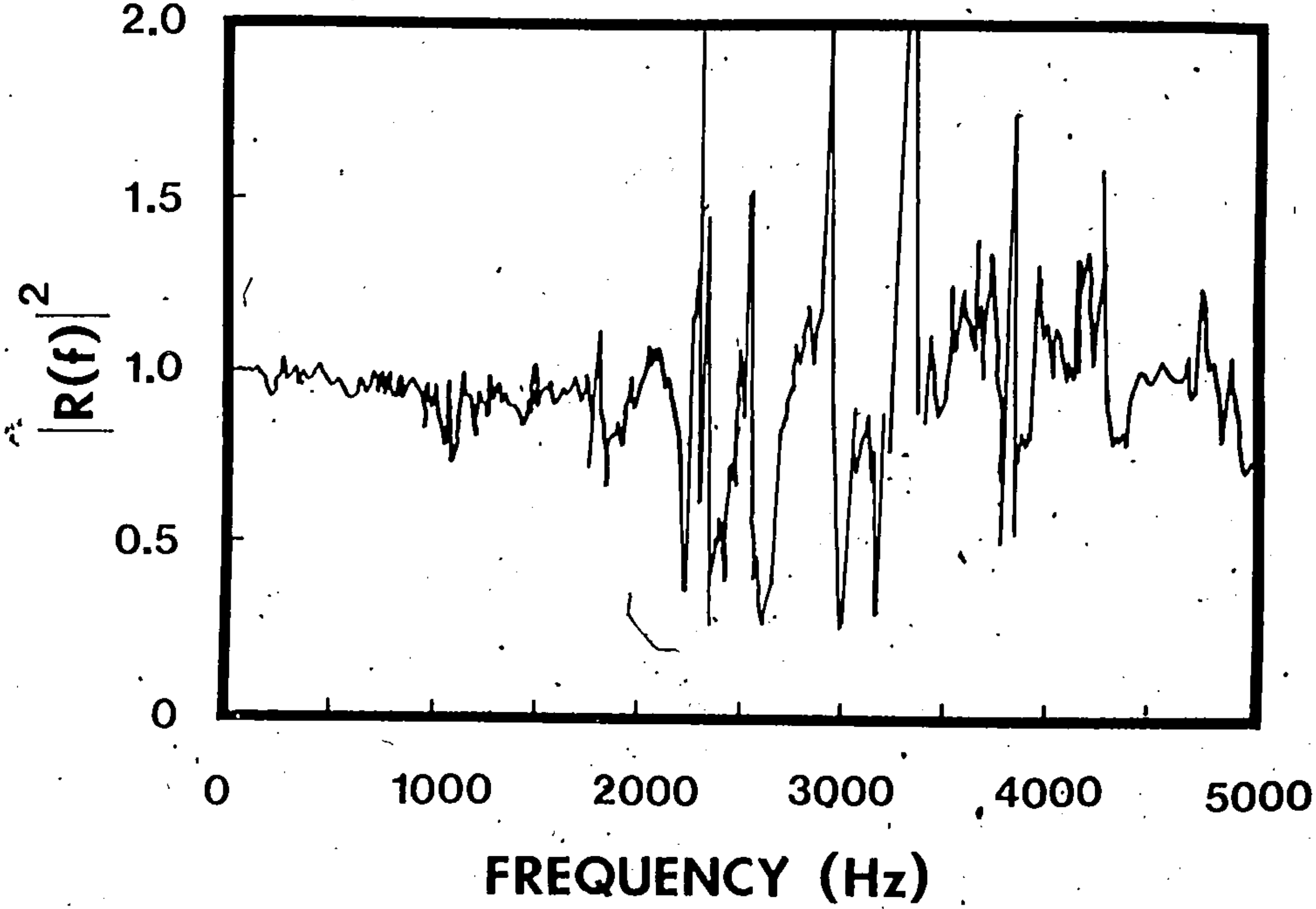

Figure 3.10: Reflective coefficient computed using conditioned spectra approach with reduced frequency resolution.

In highly resonant environments an increase in frequency resolution will improve the measured estimates of the modal peaks, improving the ability to separate the differences in pressure over the frequency range at the two measurement points. This should in turn improve the quality of the final parameter estimations. Two final experiments were conducted to further examine the effects of frequency resolution (and corresponding bias error) on the two pass measurement approach. Figure 3.11a presents the estimation of the reflective coefficient using a frequency resolution of 1.25 Hz. The parasitic noise source was off and the perforations in the tube plugged. A single pass data acquisition was used, measuring G11,G22,G12 directly. Again the poor estimation below 150 Hz is a result of the lack of significant source input at these frequencies. Figure 3.11b presents the results using the coherent power analysis and two passes of data acquisition for the same conditions. In the absence of the secondary noise source the ordinary coherence function at the resonance peaks exceeded 0.98. Comparison of these two figures indicate clearly the introduction of "noise" into the solution when a two pass approach is used without altering the frequency resolution and number of ensemble averages.

The presence of "noise" in a spectrum is usually attributed to random error resulting from insufficient ensemble averaging. In the two pass approach, the increase in arithmetic operations increase error propagation to the final solution. However, the two pass approach can also introduce time delay bias errors in the spectral estimates resulting in poor phase estimation in the transfer functions. The final two experiments were examined in more detail to locate the introduction of noise into the solution. Figure 3.12a presents the calibrated auto spectra (G11,G22) of the two microphone signals from the direct (single pass) experiment. Figure 3.12b contains the conditioned spectra ((G11)c,(G22)c) from the two pass experiment. Except for the very low (<20 Hz) region the corresponding spectra are virtually identical and noise free. Figure 3.13a presents the calibrated cross spectra of the single pass

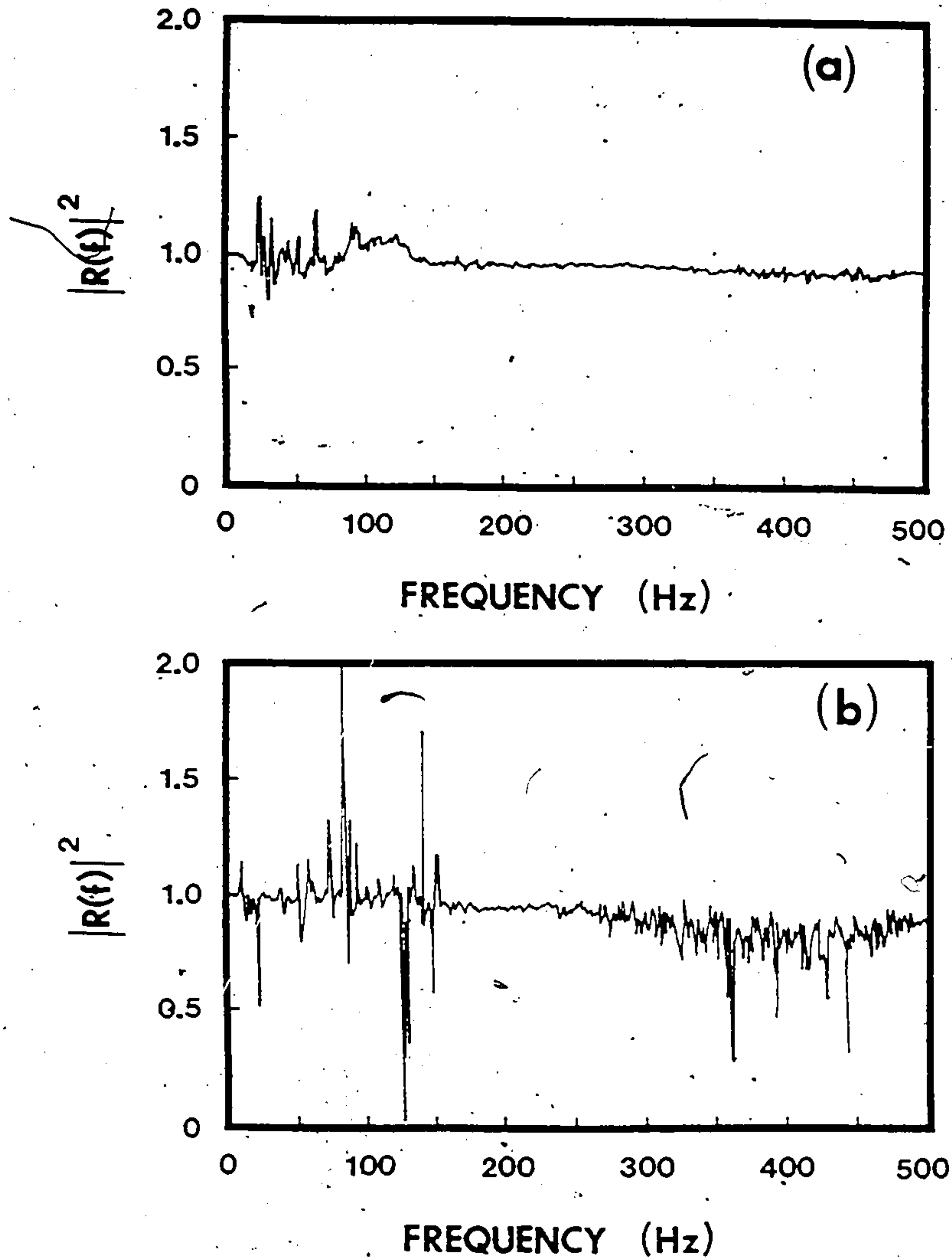

Figure 3.11 : Reflective coefficient compute using increased frequency resolution [a: single pass, n(t) off, b: two pass, n(t) on]

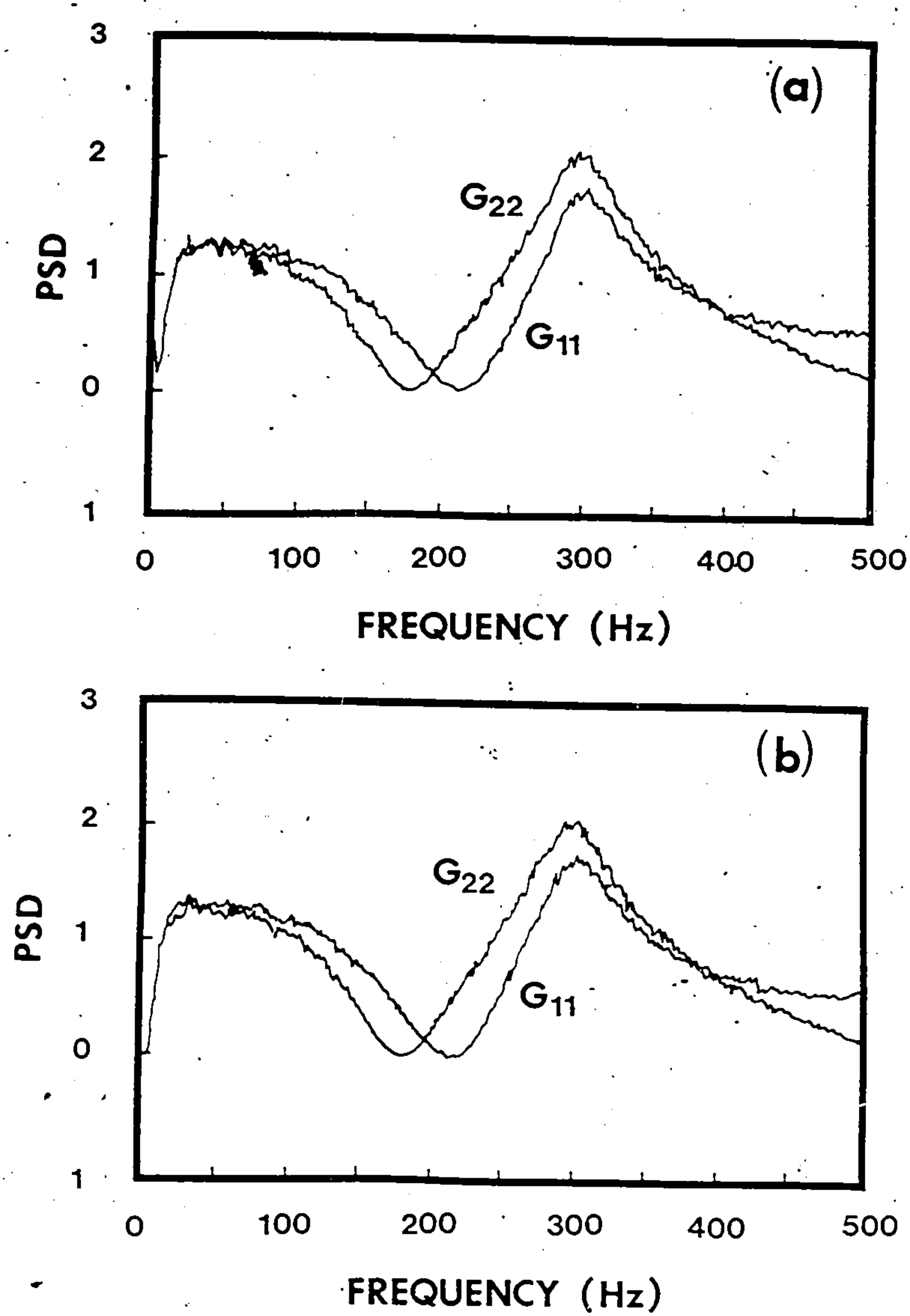

Figure 3.12 : a: Calibrated auto spectra from single pass experiment.
b: Calibrated coherent auto spectrum from two pass experiment.

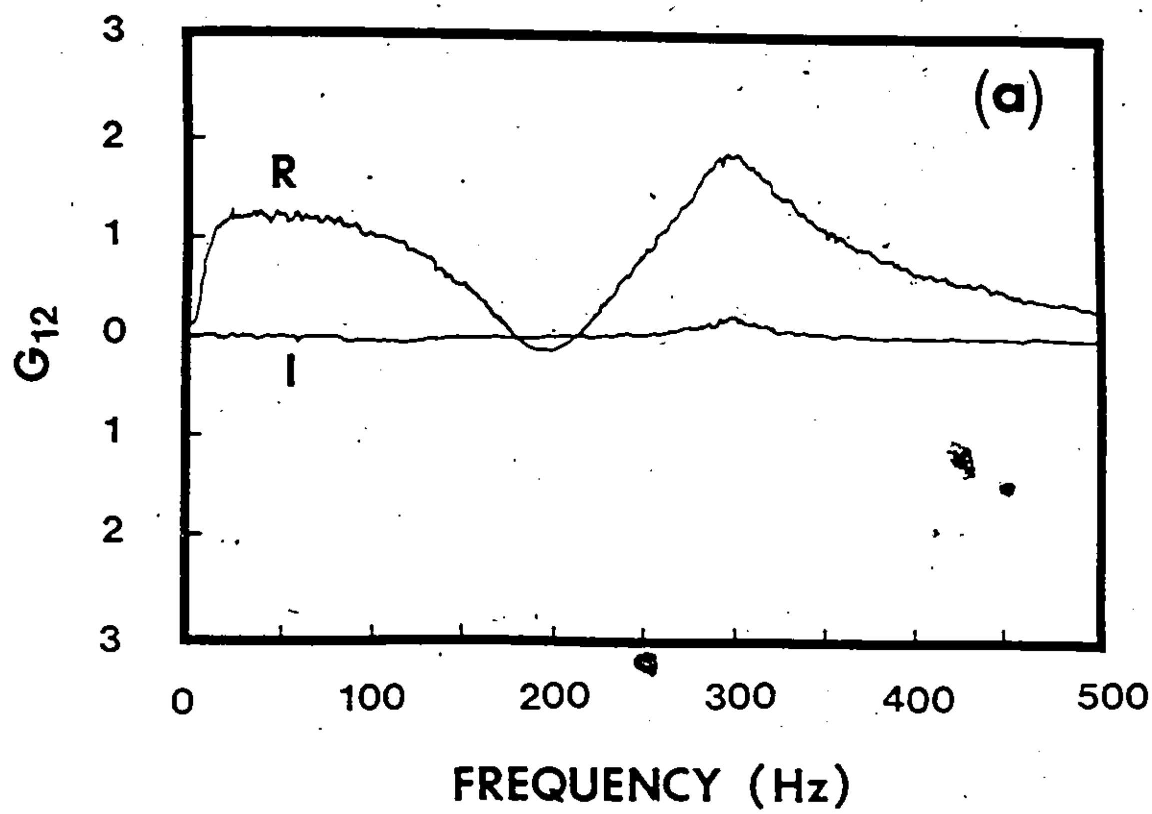

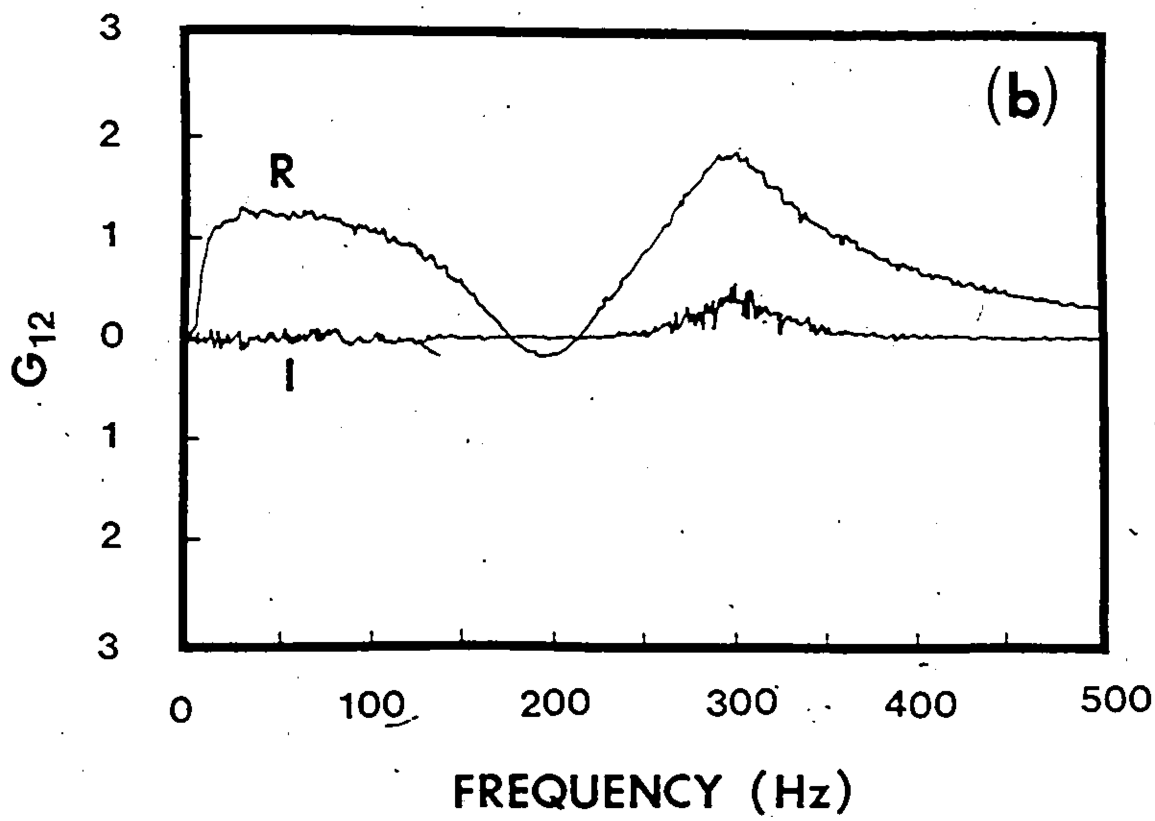

Figure 3.13 : a: Calibrated cross spectrum from single pass experiment.
b: Calibrated, coherent cross spectrum from two pass experiment.

(directly measured) experiment. Note that figures 3.12 through 3.13 have been scaled and plotted such that logarithmic units can be used in both positive and negative directions about zero. The imaginary part of the spectrum is linearly related to the intensity vector at the microphone location (section 3.3). For highly resonant (reactive) fields, this should be zero as measured in this spectra. There is, however, a very slight "bump" in the imaginary component of the cross spectrum near 300 Hz. Figure {3.13b} presents the coherent cross spectrum calculated from the two pass data. The spectrum is significantly noisier, and the hump near 300 Hz larger. Thus the frequency dependent intensity vector calculated from these results would be noisier, and obviously incorrect in this region. This noise is amplified through the solution by the matrix inversion necessary to generate the reflective coefficient. Note that the noise in the computed reflective coefficient of figure 3.11b is located in the frequency regions of the noise in the cross spectrum.

3.6 Summary

A review of existing impedance identification methods resulted in the selection of a two microphone, broad band excitation approach. This method is suitable for in situ determination of the entrance and exit impedance values of the piping system used in the experiments described in chapter 2 of this thesis. The impedance identification equations were modified in this chapter using a conditioned spectra analysis to allow determination of the source impedance during sound production.

It was proposed in the open literature that a multipass data acquisition could be used in conjunction with a conditioned spectra analysis to determine selectively the power production of multiple radiating sources. The feasibility of applying a multipass data acquisition to measure the impedance of non passive (radiating) components was investigated in detail in this chapter. It was demonstrated that the use of a two channel FFT analyser and correspondingly two passes of data acquisition can introduce significant errors and noise into the calculation of both the reflective coefficient and implicitly the acoustic intensity vector. The errors and noise seen in the reflective coefficient are significantly greater that those produced in the intensity vector. This is a result of the matrix inversion required in the solution (equations 3.10). It appears that bias errors are the root cause of the problem. However, a significant decrease in frequency resolution can smooth the computed functions and perhaps give unwarranted confidence in the results. With the increase in arithmetic operations required in the coherent power analysis, significant attention to detail (3.19, authors reply), in particular relative phase calibration and an increase in ensemble averaging may also reduce the noise to an acceptable level. The calculation of the source impedance is an important aspect in modelling the acoustic characteristics and output of radiating sources. The use of the coherent, conditioned spectra approach can be easily combined with alternative impedance estimation methods (to be discussed in chapter 4) to estimate the required system parameter.

CHAPTER 4

SOURCE SIGNATURE ANALYSIS

4.0 Introduction

An accurate plane wave acoustic model of the piping system is necessary before the interaction between the fluid mechanics of the cavity resonator (experimentally examined in chapter 2) and the acoustic environment can be investigated. The resonant frequencies and basic mode shapes for such a simple system can be easily and accurately calculated without developing a detailed model. However, the accurate prediction of acoustic particle velocities along the pipe given the acoustic pressures requires a detailed study of the acoustic system.

In this chapter, the 4 pole method is used to generate an acoustic model of the experimental rig. System impedance functions necessary for accurate acoustic modelling are obtained using the techniques described in chapter 3, and are incorporated into the 4 pole model.

A general source characterization technique utilizing the developed model is presented and applied to the cavity resonator. This approach has been used previously to characterize a variety of flow control devices, all of which can be classified as "broad band" noise sources. This method has not been applied previously to acoustic sources exhibiting lock in, a characteristic typical of highly resonant pure tone sources.

4.1 Four Pole Modelling

The 4 pole method is an efficient technique for modelling the plane wave acoustics in piping systems. Essentially it involves the generation of a 2x2 matrix (4 terms) relating the acoustic pressure and particle velocity between 2 locations in the duct. One of the inherent strengths of the method is that for many situations the terms of the 4 pole matrices can be derived explicitly. Using this approach a continuous model is developed (as opposed to a discrete model generated using the finite element method) ~~which~~ incorporates a reduced set of variables allowing determination of both the acoustic pressure (P) and particle velocity (v) at any point in the model. As well, experimentally measured impedance values, crucial to accurate modelling can be easily incorporated into the model.

Munjal (4.1) presented the 4 pole approach as applied to muffler design where the effect of flow on the state variables (P,V) was included. Recently, there has been considerable discussion regarding the validity of Munjal's solution and the correct formulation for the 4 pole parameters for a straight pipe section in the presence of mean flow (4.2,4.3,4.4). Observers of these discussions are led to believe that the original formulation presented by Munjal is correct, and that the confusion generated by To (4.2) was unnecessary. The development of the 4 pole parameters for a straight pipe section will be presented here to illustrate the basic equations of motion and assumptions used in the modelling approach.

The 1 dimensional momentum equation in the absence of body forces, and assuming potential flow (viscosity = 0) is given by:

$$\bar{\rho}\,[\partial V/\partial t + V \cdot \nabla V] = -\nabla P \tag{4.1}$$

The instantaneous variables(velocity,pressure,density) are expressed in terms of their time averaged mean values and a small perturbation. That is:

$$P = P_o + p$$
$$V = V_o + v \tag{4.2}$$
$$\bar{\rho}_{t} = \rho + \rho'$$

A potential (ϕ) is chosen such that:

$$\nabla \phi = v \tag{4.3}$$

Equation 4.3, and equations 4.2 can be combined to produce a 1 dimensional momentum equation given by:

$$(\rho+\rho')[\partial V_0/\partial t+\nabla(\partial\phi/\partial t)+(V_0+\nabla\phi)\cdot\nabla(V_0+\nabla\phi)] = -\nabla P_0 - \nabla p \quad [4.4]$$

Equation 4.4 can be simplified assuming an homogeneous fluid (resulting in the gradient of mean values to be zero) and neglecting products of first order terms. That is:

$$\rho\,[\partial(\nabla\phi)/\partial t + (V_0\cdot\nabla)\nabla\phi] = -\nabla p \quad [4.5]$$

or:

$$\nabla\,[\rho\,(\partial\phi/\partial t + V_0\cdot\nabla\phi) + p] = 0 \quad [4.6]$$

Equation 4.6 can be integrated with respect to x to give:

$$p = -\,\rho\,(D\phi/Dt) \quad [4.7]$$

where the substantive derivative is given by:

$$D(\,)/Dt = \partial(\,)/\partial t + V_0\cdot\nabla(\,)$$

The continuity equation for 1 dimensional flow is given by:

$$\partial(\bar{\rho})/\partial t + \nabla\cdot(\bar{\rho}\,V) = 0 \quad [4.8]$$

Equations 4.3,4.2 can be used with equation 4.8 to generate:

$$\partial\rho'/\partial t + \nabla\cdot(\rho+\rho')(V_0+\nabla\phi) = 0 \quad [4.9a]$$

The dot product can be expanded to produce:

$$\partial\rho'/\partial t + (\rho+\rho')\,\nabla\cdot(V_0+\nabla\phi) + (V_0+\nabla\phi)\cdot\nabla(\rho+\rho') = 0 \quad [4.9b]$$

Neglecting products of first order terms results in:

$$\rho\nabla\cdot\nabla\phi + \partial\rho'/\partial t + V_0\cdot\nabla\rho' = 0 \quad [4.10a]$$

This can be further simplified as:

$$\rho\nabla\cdot\nabla\phi + D\rho'/Dt = 0 \quad [4.10b]$$

Equations 4.10b and 4.6 represent two equations with 3 unknowns. A form of the state equation which assumes the wave propagation to be reversible and adiabatic is used to eliminate (ρ') from 4.10b. That is:

$$dp/d\rho' = c^2 \quad [4.11a]$$

Thus:

$$\rho' = p/c^2 \quad [4.11b]$$

The continuity equation becomes:

$$\rho \nabla \cdot \nabla \phi + 1/c^2 D(p)/Dt = 0 \qquad [4.12]$$

Taking the gradient of 4.12, and the total derivative of 4.5, and eliminating $D(\nabla p)/Dt$ results in the classical wave equation which includes the effects of flow. That is:

$$D^2(\phi) / Dt^2 = c^2 \nabla^2(\phi) \qquad [4.13]$$

The solution of equation 4.13 for harmonic waves is given by:

$$\phi = [A\, e^{(-Kix)} + B\, e^{(Krx)}]\, e^{j\omega t} \qquad [4.14]$$

where:

$$Ki = k/(1+M)$$

$$Kr = k/(1\text{-}M)$$

Equation 4.7 can be combined with 4.14 to generate the acoustic pressure in terms of the unknown coefficients (A,B) at x equal to 0 and x equal to L. Similarly,equation 4.4 can be combined with the solution of the wave equation (4.14) to generate the acoustic particle velocity in terms of the unknown coefficients (A,B) at x=0 and x=L. Elimination of the coefficients generate the 4 pole solution as [4.3]:

$$\begin{Bmatrix} p \\ Sv \end{Bmatrix}_1 = \begin{Bmatrix} a11 & a12 \\ a21 & a22 \end{Bmatrix} \begin{Bmatrix} p \\ Sv \end{Bmatrix}_2 \qquad [4.15]$$

where:

$$a11 = e^{(-jMkL/(1-M^2)}\cos(kL/(1-M^2)$$

$$a22 = a11$$

$$a12 = j\,\rho c/S\, e^{(-jMkL/(1-M^2)}\sin(kL/(1-M^2))$$

$$a21 = a12 * (S/\rho c)^2$$

Explicit formulations for a variety of sections or acoustic conditions are available, including anechoic terminations, horns [4.5,4.6] and variable duct or nozzle sections [4.7].

Acoustic models of complicated systems can be generated using the four pole method. Series connections are modelled by multiplication of the matrices to generate a final matrix relating the state variable at the two locations. Parallel components are modelled assuming uniform acoustic pressure at the junction, and addition of acoustic particle velocity. A more detailed description of the modelling process for complicated systems has been presented by To [4.8]. The method is easily programmed (see for example the software package discussed in 4.9) allowing a "finite element" type description of the acoustic system in terms of elements (piping sections) and nodes (acoustic junctions).

Across sections of complicated geometry, or unknown geometric detail (ie mufflers),the elements of the 4 pole matrices are not easily predicted. In general the 4 pole matrix relating the state variables at two locations is given by:

$$\begin{Bmatrix} p \\ u \end{Bmatrix}_1 = \begin{Bmatrix} a & b \\ c & d \end{Bmatrix} \begin{Bmatrix} p \\ u \end{Bmatrix}_2 \qquad [4.16a]$$

where the u1,u2 represent the volume velocity, obtained by multiplying the acoustic particle velocities (v1,v2) by the duct area S. When a,b,c,d are not known, they can be determined using techniques presented by To and Doige [4.10,4.11]. In the most basic case, this involves the blockage at various locations in the piping loop, imposing that the volume velocity is zero at that point. When the system under analysis cannot be blocked, the 4 equations are generated by pressure measurements at locations other than at the two stations of interest. The solution procedure for more complicated situations results in the generation of products of known and unknown 4 pole parameters requiring a lengthy solution procedure for the unknown system parameters.

Alternatively, a much more concise method utilizing a two load approach has been used by Lung and Doige [4.12]. Equations 4.16 can be rewritten as:

$$p1/p2 = a + b/z2$$

$$z1 = (az2+b)/(cz2+d)$$

where:

$$z1 = p1/u1 \qquad [4.16b]$$

and: $z2 = p2/u2$

The impedance values at the stations 1,2 (z1,z2) are generated using a transfer function measurement between two microphones on each side of the unknown element, combined with known 4 pole elements. If p1/p2,z1,z2 are measured versus frequency for 2 separate boundary conditions, then a system of 4 linear equations in the 4 unknowns is generated.

4.2 Equivalent source characterization methods

A characterization of the acoustic pressure generated by flow control devices (valves, bends, sudden expansions) is necessary before the structural response of pipelines resulting from these flow dependent pressure oscillations can be predicted. Implicit in the identification of equivalent acoustic source parameters is the uniqueness of the characterization, and selection of the appropriate scaling parameters used to reduce the acoustic data. Satisfaction of the uniqueness of the solutions allows information obtained in a test rig to be applied in plant environments. Selection of the appropriate scaling parameters ensures that the correct level of sound production is calculated, provided the basic flow environment and geometric detail (scaling parameters) are known and that a unique solution is known to exist. In general the details of the flow field through the flow control device (piping singularity) are not known. This forces a characterization to be made from far field measurements combined with an acoustic model of the source environment. Considerable work has been devoted to the development of measurement techniques and modelling procedures suitable for the identification and characterization of an equivalent acoustic source. Most of this work which has been applied to the problem of silencing engine noise has used an electrical analogy in describing the duct acoustics [4.13,4.14,4.15]. A Thevenin equivalent circuit for the acoustic system is generated, where voltage and current are replaced in the analogy with pressure and volume velocity. Using this modelling approach, pressure sources drive series connections of the load and source impedance, and volume velocity sources drive a circuit containing the load and source impedance in parallel. The two models are equivalent as measured in the far field if the pressure and velocity at the source are related through the source impedance Zs. The parameters to be determined in the identification procedure are then the source strength (either P(f) or U(f)) and the source impedance (Zs) which can be used to calculate insertion loss. Several approaches have been used to identify these parameters, two of which have been applied to a variety of sources by Doige and Alves [4.16,4.17]. The "direct" approach described in [4.16] involves the measurement of the load and source impedance (with the source off in the case of the above reference) in separate experiments from that used to measure the source strength. The "two load" method determines the source strength and impedance under operating conditions by measuring acoustic pressures for two separate source loads. Doige and Alves have indicated that the "two load" method is more suitable for strongly periodic signals since both unknown quantities are determined during source sound production. Clearly when the source impedance and the source strength are related (as in the case of the cavity resonator under study via the flow velocity) determination of the particular source impedance for a given operation point is necessary. Under these conditions the "direct" approach is still possible if the source impedance is measured using the conditioned spectra approach described in chapter 2. For broadband sources, the two load method is not applicable since the phase information is lost. This is not true of the "direct" approach. The ability to predict the peak acoustic output ~~level~~ using either of these two methods for strongly periodic outputs with varying acoustic load is quite remarkable (fig 4,reference 4.16). This is especially true of the high frequency results where a loss of frequency resolution in the measurements must occur. For a given source load, the approach used in [4.16] to measure the source and load impedance using the same microphone location as those used to measure the equivalent source will guarantee the accurate prediction of the measured acoustic pressures, independent of the accuracy of the 4 pole model. Thus careful attention to detail must be made to ensure that the load and source impedance values are correct.

A four load method [4.18,4.19] for identifying source parameters utilizes 4 different lengths of ducting to vary the load impedance. Perhaps the most significant advantage of this approach is that both of the unknown quantities can be estimated using simple pressure level measurements outside of the ducting facility without the need for independent excitation of the ducting system.

An alternative source identification procedure utilizes the 4 pole model of the ducting in a more direct fashion. In this model an unknown step change in the state variable across the piping singularity (or source) is assumed to occur. This approach (which has not received the same attention in the open literature) is presented below in conjunction with the development of the 4 pole model for the piping system.

The inlet conditions at the bellmouth entrance are related to those at the source impedance location by:

$$\{p,U\}_{zi} = [A] * \{p,U\}_i \qquad [4.17]$$

Note that the formulation of the model (for example the matrix [A] in the above equation) utilizes the inverse of the four pole matrix of equation 4.15. The state variables across the singularity are related using:

$$\{p,U\}_{ze} = [B] * \{p,U\}_{zi} \qquad [4.18]$$

where:

B(1,1) = 1

B(2,2) = B(1,1)

B(1,2) = −Zv (real and imaginary)

$B(2,1) = 0$

In the absence of flow, the parameters of matrix [B] can be evaluated using the methods discussed in the previous section. In the presence of flow the singularity impedance (Zv) can be measured using the source impedance technique presented in chapter 2. Under no flow conditions, the impedance (Zv) for rigid singularities is primarily determined by the local geometry, whereas in the presence of flow, the acoustic characteristics are dominated by the pressure (and density) changes across the singularity. In the absence of flow, the acoustic production of the singularity is zero. Thus, it is only under flow conditions that the singularity impedance is required. A significant simplification is achieved using the quasi static estimate of the Zv. That is:

$$Zv = (K \bullet Vp)/S \qquad [4.19a]$$

where the static pressure drop across the singularity is given by:

$$P_{zi} - P_{ze} = 0.5 \bullet K \bullet (Vp)^2 \qquad [4.19b]$$

For low Mach number flows the change in the impedance estimates using equation 4.1 is small (for a detailed examination of the effects of flow on the acoustic parameters see reference 4.20). With this assumption the impedance across the singularity can be approximated as the summation of the no flow estimate (Zvo) and the quasi static value. That is:

$$(Zv)c = B(1,2) = (Zvo) + (K \bullet Vp)/S \qquad [4.20]$$

The state variables at the impedance location are related to the acoustic pressure and volume velocity at the source location using:

$$\{p,U\}_{si} = [C] \bullet \{p,U\}_{ze} \qquad [4.21a]$$

Across the source there is an unknown increase in the acoustic pressure and volume velocity: That is:

$$\{p,U\}_{se} = \{p,U\}_{si} + \{dP,dU\} \qquad [4.21b]$$

The acoustic pressure and volume velocity at the exit are related to the state variables at the source using:

$$\{p,U\}_e = [D] * \{p,U\}_{se} \qquad [4.21c]$$

Equations 4.18,4.19,and 4.21 can be combined to generate an overall transfer function matrix between the inlet and exit conditions. That is:

$$\{p,U\}_e = [D][C][B][A]*\{p,U\}_i + [D]*\{dP,dU\} \qquad [4.22]$$

The boundary conditions of the acoustic system are imposed using the end impedance functions:

$$\{p\}_i = [Z]_i * \{U\}_i \qquad [4.23]$$

$$\{p\}_e = [Z]_e * \{U\}_e$$

Equations 4.23 can be combined with 4.22 to generate a 2x2 system of equations relating the volume velocities at the ends of the acoustic system {Ui,Ue}, to the unknown source parameters {dp,dU}. The acoustic pressure at the upstream microphone location is calculated using:

$$Pa = E(1,1)*\{p\}_i + E(1,2)*\{U\}_i \qquad [4.24a]$$

where [E] is the 4 pole matrix relating the state variables at the inlet and the upstream microphone location. The acoustic pressure at the downstream microphone location is calculated using:

$$Pc = F(1,1)*\{p\}_e - F(1,2)*\{U\}_e \qquad [4.24b]$$

where [F] is the 4 pole matrix relating the state variables at the downstream microphone location and the exit.

The solution for the unknown change in state variables across the singularity is found solving:

$$\{Y\} = [H] * \{V\} \qquad [4.25]$$

where:

$\{Y\} = (Gaa, Gcc, real(Gab), aimag(Gab)$

$\{V\} = (Gdp, Gdu, real(Gdpdu), aimag(Gdpdu))$

and:

$H(1,1) = |Hpa|^2$ $\qquad$ $H(1,2) = |Hua|^2$

$H(1,3) = real[c(Hpa)^{*}Hua + c(Hua)^{*}Hpa]$

$H(1,4) = -imag[c(Hpa)^{*}Hua - c(Hua)^{*}Hpa]$

$H(2,1) = |Hpc|^2$ $\qquad$ $H(2,2) = |Huc|^2$

$H(2,3) = real[c(Hpc)^{*}Huc + c(Hua)^{*}Hpa]$

$H(2,4) = -imag[c(Hpc)^{*}Huc - c(Huc)^{*}Hpc]$

$H(3,1) = real[c(Hpa)^{*}Hpc]$

$H(3,2) = real[c(Hua)^{*}Huc]$

$H(3,3) = real[c(Hpa)^{*}Huc + c(Hua)^{*}Hpc]$

$H(3,4) = real[c(Hpa)^{*}Huc - c(Hua)^{*}Hpc]$

$H(4,1) = imag[c(Hpa)^{*}Hpc]$

$H(4,2) = imag[c(Hua)^{*}Huc]$

$H(4,3) = imag[c(Hpa)^{*}Huc - c(Hua)^{*}Hpc]$

$H(4,4) = real[c(Hpa)^{*}Huc - c(Hua)^{*}Hpc]$

The complex valued impulse response functions Hpa,Hpc are obtained by solution of equations 4.24 assuming a unit step in {dP}. The complex valued impulse response functions Hua,Huc are obtained by solution of equations 4.24 assuming a unit step in {dU}. Full solution of equations 4.25 produce the auto spectrum (Gdp,Gdu) and cross spectrum (Gdpdu) of the unknown source.

Considerable effort has been devoted by Gibert [4.21,4.22] in developing the theoretical basis, and testing of this source identification technique. From examination of the theoretical characteristics of Gdp and Gdu, Gibert has concluded that the spectra occupy different regions of the frequency domain (Gdp lower and Gdu higher). With this assumption the two components of the source vector are fully uncorrelated, (Gdpdu = 0) and equations 4.25 are reduced to a 2x2 set of equations containing only auto spectra as both inputs and outputs. A sudden expansion and 7 degree diffuser were used by Gibert [4.21] to experimentally investigate this identification procedure. Assuming the source spectra to be uncorrelated apriori produced Gdp and Gdu displaying different characteristics. Both source autospectrum were non-dimensionalized using the square of the mean pressure drop across the singularity. As predicted by Gibert, the spectrum Gdp did not exhibit a dependency on Mach number, and decreased in amplitude with frequency. A cut off Strouhal number of 0.2 based on upstream velocity and (D-d) was determined. The auto spectrum of the step change in volume flow (Gdu) was flat, with the plateau level scaling with M^2. The results of a full analysis (with-out assuming Gdpdu = 0)were not presented.

Chadha [4.23], using a separate experimental facility, utilized the same identification procedure for the noise characterization of a standard geometry governor valve. Again the source spectra (assumed uncorrelated in the analysis) were non-dimensionalized with the square of the mean pressure drop across the valve. It is interesting to note that good agreement between measured and predicted pressure ratios across the valve was obtained using the quasi-static model for the valve impedance (equation 4.19a). The basic shapes of both source spectra determined for the governor valve were the same as those determined for singularities identified by Gibert. This is, of course, due in part by the assumption that the source spectra are uncorrelated.

Using a separate characterization procedure, Botros et al. [4.24] analysed the acoustic noise generated by a standard geometry orifice plate. Here the source was modelled as a branch piston (volume velocity) source. Although frequency dependent information was not presented, the r.m.s fluctuations for a variety of orifice area ratios were fit with an equation of the form:

$$Vrms = K * M * (delta\ P)^{1.0765} \tag{4.26}$$

where:

M = upstream Mach number

delta P = mean pressure drop across orifice plate

and:

K = constant dependent in part on sound speed and pipe area.

The rms volume velocity fluctuations using the approach of Gibert can be obtained by calculating the square root of the integral over the frequency range of Gdu. This results in the rms volume velocity to scale with Mach number and (delta P) $\sqrt{2}$.

Although the source identification procedures discussed here appear significantly different, the basic modelling procedures and parameters necessary for accurate identification and predictions remain the same. The electrical analogy approach appears more suitable for insertion loss calculations (muffler design) as the source is analysed looking at it from either an upstream or downstream direction.

4.3 Development and testing of 4 pole model

A software package was developed to implement the 4 pole modelling technique and source identification procedure outlined in the previous section. The program incorporates many user selected options allowing intermediate testing of the acoustic model. The state variables were chosen as acoustic pressure (P) and ρc*volume velocity, thus impedance has the units $(1/m)^2$. In this section further details of the model construction are presented and combined with experimental testing to illustrate the sensitive aspects of the model development.

The downstream reflective coefficient (presented in fig. 4.1) and impedance function were calculated using the two microphone random excitation technique described in chapter 3. The calculated impedance function was sensitive to both the separation distance and the distance to the plenum entrance. The best estimate was measured using a separation distance of 25.4 cm with the first microphone positioned 13 cm from the piping exit. Four hundred ensemble averages were used to minimize the random error in the spectral estimates.

The transfer function between two microphones on any side of the singularity is a function of the acoustic characteristics of the piping, and the termination condition on that side of the singularity. Figure 4.2a presents the measured transfer function (both real and imaginary) between microphone A, positioned 2.16 m from the plenum, and microphone B, positioned 0.9 m from the plenum. The complex valued transfer function was calculated as Gab/Gaa. The magnitude of the transfer function represents the acoustic pressure ratio (sqrt(Gbb/Gaa). A speaker was flush mounted to a piping flange upstream of the microphones and excited using a sine swept signal from 1 to 525 Hz. Figure 4.2b presents the predicted transfer function computed using the developed software package. The acoustic pressures were calculated using equation 4.24b at the two microphone locations assuming a source vector of (1,1). The transfer function is then computed using:

$$Hab = [c(Pa(f)) * Pb(f)]/[c(Pb(f) * Pb(f)] \qquad [4.27]$$

Several important observations can be made regarding the two sets of results. First, the amplitude of the peaks in the predicted transfer function are larger than those measured. There is, however, significant improvement in the estimation for the 3 highest modes. The phase angle is incorrect in the lowest mode (f = 80 Hz) for the predicted transfer function. Note that the width of the modal peaks in the higher modes (a measure of damping) is close to the measured values. It was felt that the gain over estimation was in part due to

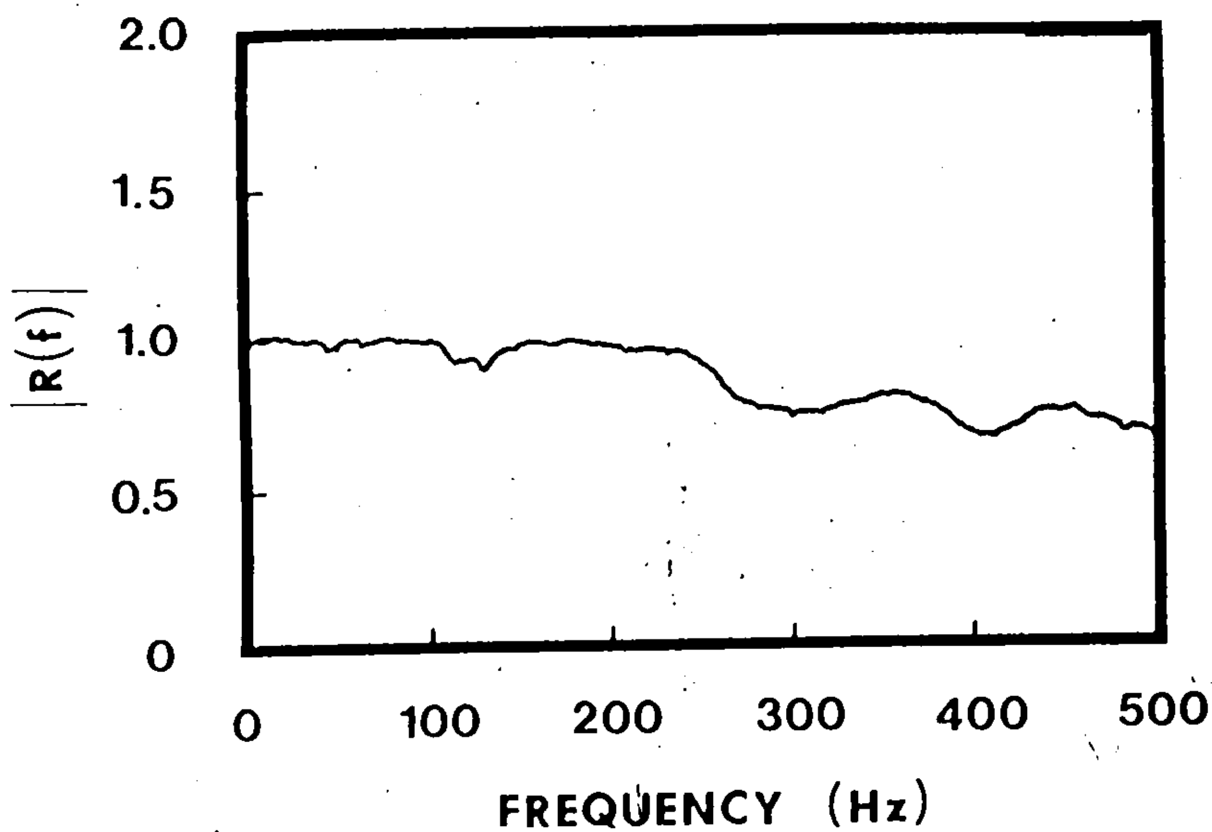

Figure 4.1 : Exit reflective coefficient ($x1=13$ cm, $x2=38.4$ cm, $Na=400$).

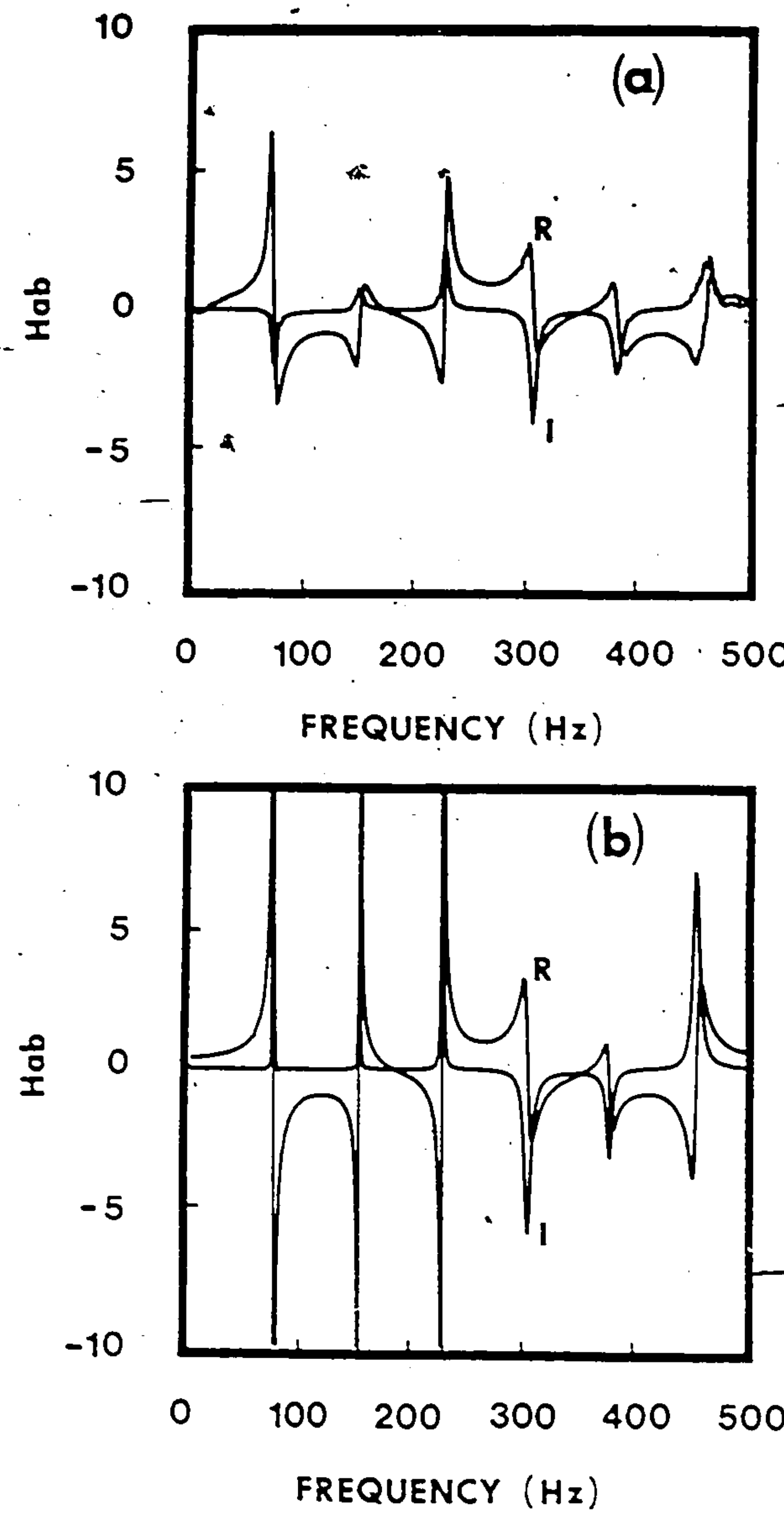

Figure 4.2 : Downstream acoustic pressure ratio (La=2.16m , Lb=0.9m). [a: Measured, b: Predicted]

the calculation of the pressures at a point, where the measurements are averages over the area of the microphone. This hypothesis was investigated by re-evaluating the predicted transfer function, where Pa(f) and Pb(f) of equation 4.27 were replaced with the average of 10 pressure functions evaluated at 10 equally spaced locations centered at the experimental microphone locations. The spacing between the computations was equal to the microphone diameter (6 mm) divided by 9. Although there was a slight modification in the peak values of the estimated transfer function at the higher frequencies, the reduction was not sufficient to warrant inclusion into the model.

A series of experiments were conducted to measure the attenuation coefficient of the piping section. With the singularity removed from the pipe, a wave train of 2-3 cycles at a given frequency was generated at the upstream bellmouth. The number of cycles was chosen to eliminate any interference at the downstream micophone by the reflected signal generated at the plenum entrance. The pressure amplitudes at two locations in the rig, separated by 7.3 m were recorded using a digital scope. The attenuation coefficient is calculated as:

$$\alpha = 1/7.3 \ \ln(P2/P1) \qquad [4.28a]$$

The two microphones used in the experiment had a relative calibration of magnitude 1.($\pm$0.02) over the entire frequency range of interest. Figure 4.3 presents a summary of the results, where each point is the mean of 10 separate experiments. Two straight lines were fit through the data as indicated in the figure, with the separation frequency chosen to be 250 Hz. The attenuation coefficient was used to calculate the complex sound speed as [4.25]:

$$c' = \omega / [\omega/c - j\alpha] \qquad [4.28b]$$

Figure 4.4 presents the predicted amplitude ratio utilizing the complex sound speed. There is significant improvement over the entire frequency range in the peak estimates. In addition, the sign of the phase in the lowest mode is now correct.

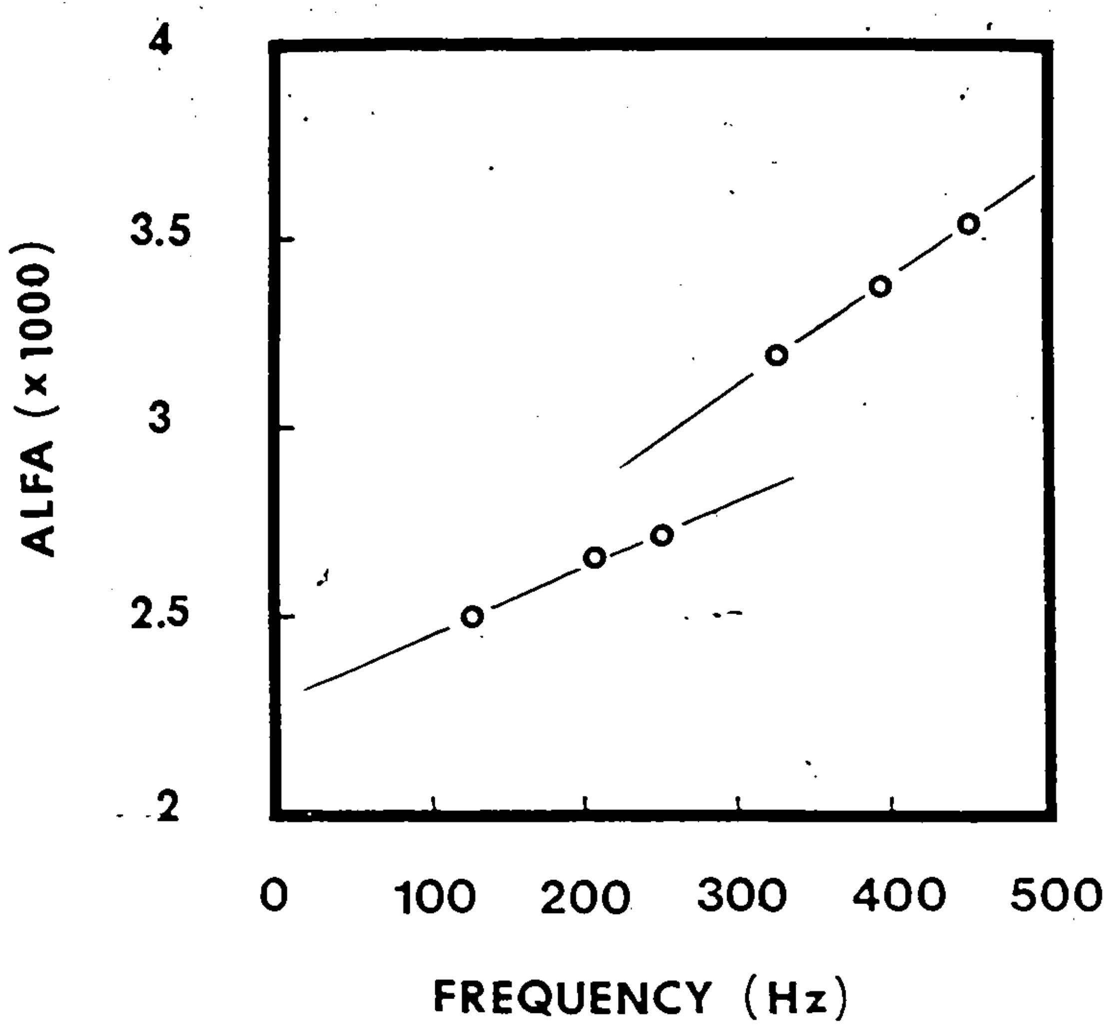

Figure 4.3 : Measured attenuation coefficient for acrylic pipe sections.

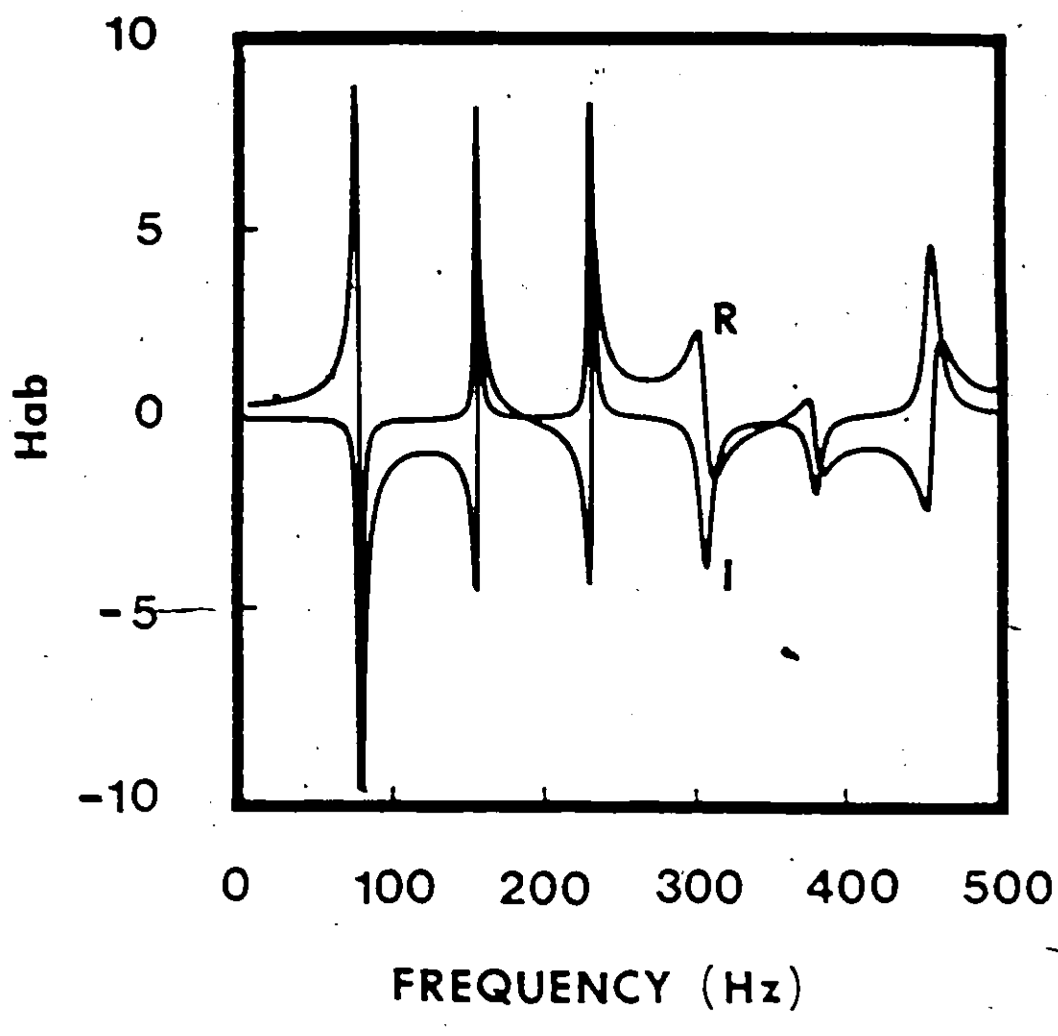

Figure 4.4 : Predicted downstream acoustic pressure ratio incorporating complex sound speed. [La=2.16, Lb=0.9]

The use of a discrete Fourier transform to measure the modal peaks introduces bias errors dependent primarily on the ratio of the minimum frequency resolution in the analysis to the actual width of the modal peaks in the data [2.10]. Thus, in highly resonant conditions,(typical of most acoustic environments) the peak of the estimated transfer function will be strongly sensitive to the frequency resolution used in the analysis. A series of experiments were conducted to determine if the over estimation of the peaks in the predicted transfer function could be attributed to the frequency resolution used in the analysis. The transfer function was measured between two microphones mounted upstream of the singularity, with the piping system excited by a speaker downstream of the microphones driven by a band limited white noise. Using the Nicolet FFT analyser, the frequency resolution in the measurements was varied from 0.08 Hz to 5.0 Hz. The maximum resolution was obtained using the zoom option. Two modal peaks in the transfer function were analysed in detail with modal damping values (measured using the maximum frequency resolution) of 0.69% and 0.54%. Figure 4.5 summarizes the results where the amplitudes of the transfer functions at the two frequencies were normalized with respect to the values measured with the frequency resolution of 0.08 Hz. As expected, the peak values in such a lightly damped system are very sensitive to small changes in the frequency resolution, particularly in the region less than 1.25 Hz (that used for upper frequency of 500 Hz).

The inlet impedance (as seen from inside the pipe) was measured using the random excitation method of chapter 3. The microphone separation distance was 0.284 m, with a distance from the bellmouth entrance to the closest microphone of 0.184 m. Figure 4.6 presents the measured reflective coefficient. The transfer function between two microphones located at positions other than those used for the impedance estimations was measured. A comparison of the transfer function calculated using the software package with the measured quantity revealed a quality of the prediction comparable to the downstream case. In

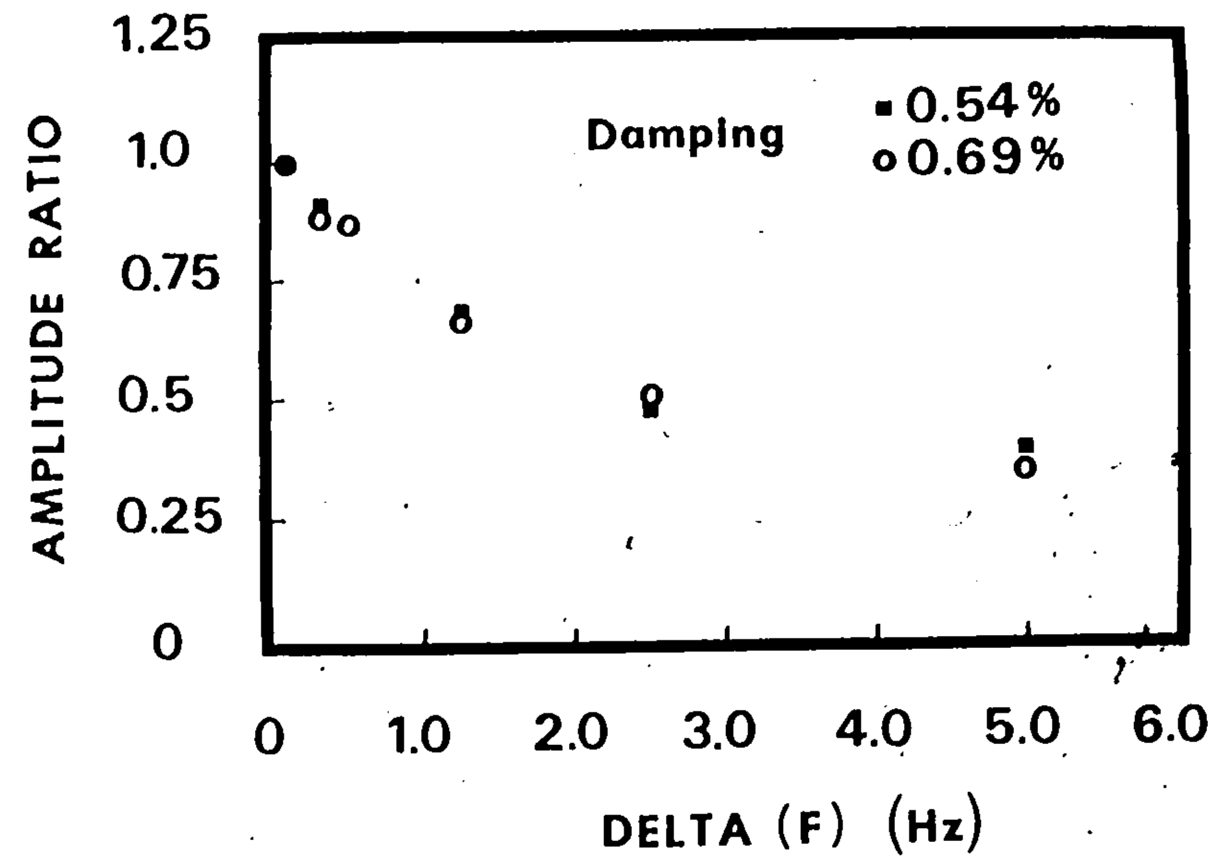

Figure 4.5 : Normalized gain in measured transfer function versus frequency resolution.

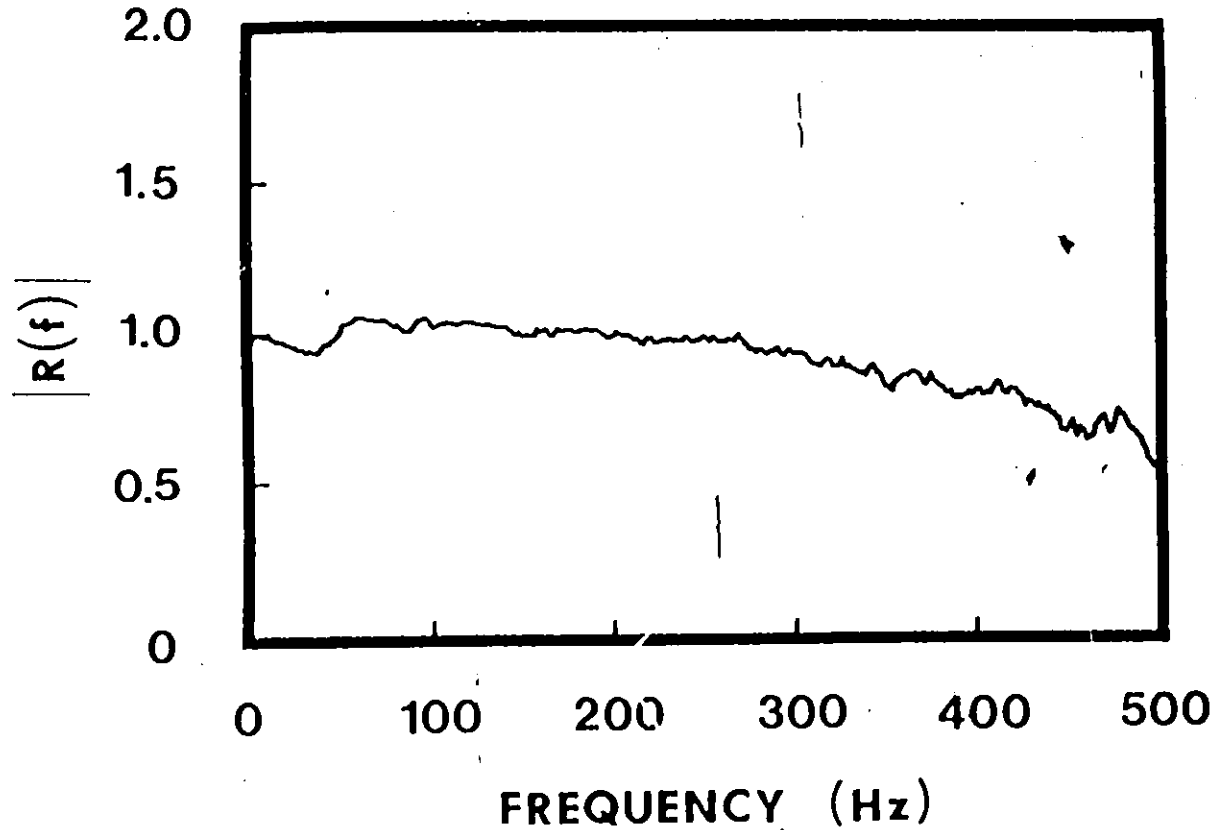

Figure 4.6 : Inlet reflective coefficient (x1=18.4cm, delta x = 28.4cm).

particular the magnitudes of the modal peaks were over predicted, more so at the lower frequencies than the higher. The widths of the peaks near the base were very close in comparison.

The use of the quasi static model of the singularity impedance [equation 4.19a] is a significant simplification in the acoustic modelling. This assumption was tested by measuring the amplitude ratio between two microphones located upstream of the singularity location with the pipe excited by a speaker just outside the bellmouth location. The change in the amplitude ratio was monitored as the flow velocity (and subsequent pressure drop across the singularity) was increased. A standard orifice plate was used as the singularity, as this was found to produce sound levels in the pipe significantly lower (20 dB) than that could be produced by the speaker over the frequency range and velocities tested . The microphones were situated 0.86 m and 1.01 m from the bellmouth entrance. Two hundred averages were used in the transfer function estimate as no significant change in the measured transfer function occurred beyond this number of averages. Figure 4.7 summarizes the mean pressure drop versus the square of the upstream velocity for this orifice. The quasi steady impedance estimate based on the slope of the line is calculated as:

$$Zs = 134 / (\rho cS) = 45 \, (1/m)^2$$

Figure 4.8 presents the sequence of the measured transfer functions for increasing flow velocity. The orifice plate significantly alters the acoustics of the upstream portion of the duct under flow conditions. In particular, under high flow velocity conditions, resulting in a large mean pressure drop, the orifice plate separates the upstream and downstream portions of the duct by approximating a rigid termination at the singularity location. Figure 4.9 presents the measured transfer function for a flow velocity of 4.92 m/s and that predicted by the software. The acoustic model used in the prediction utilized the exit impedance value previously measured and the quasi static estimates of the singularity impedance. The

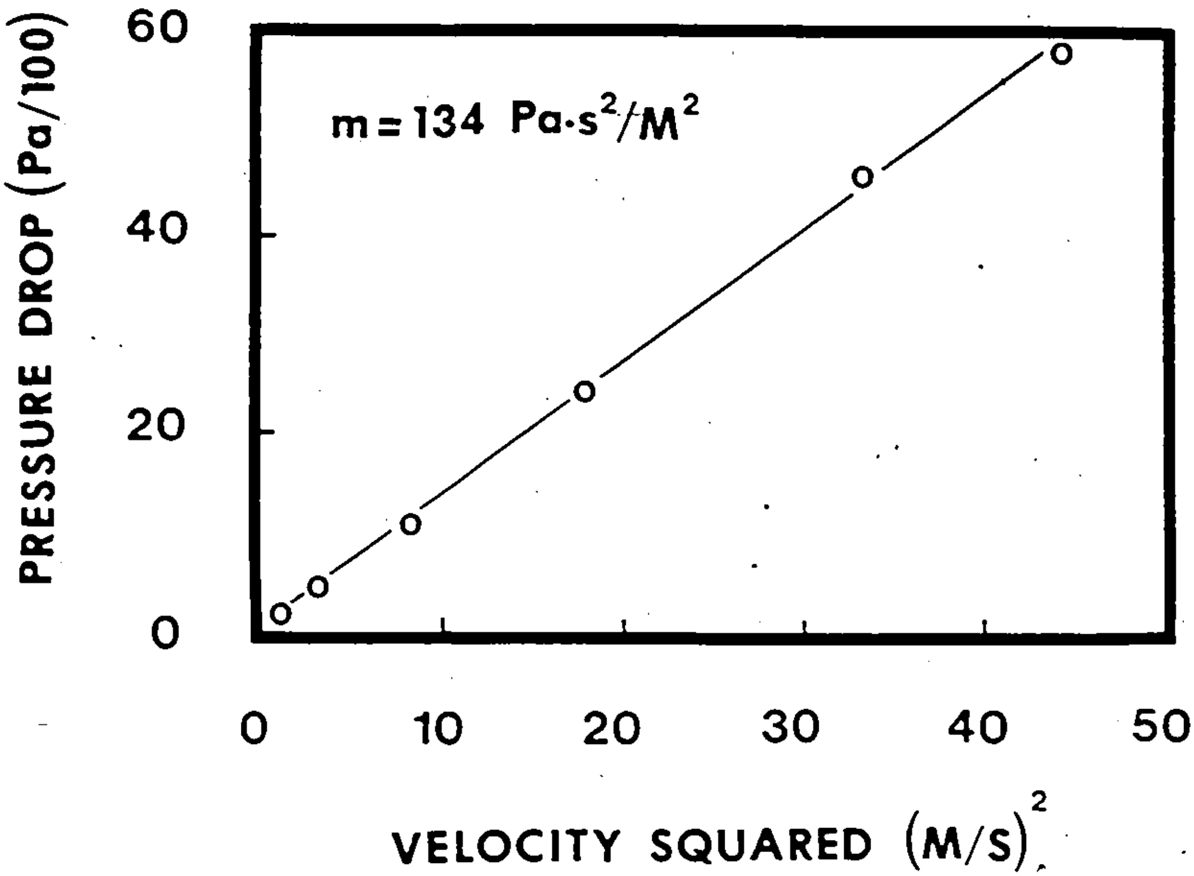

Figure 4.7 : Mean pressure drop across orifice singularity versus square of upstream velocity.

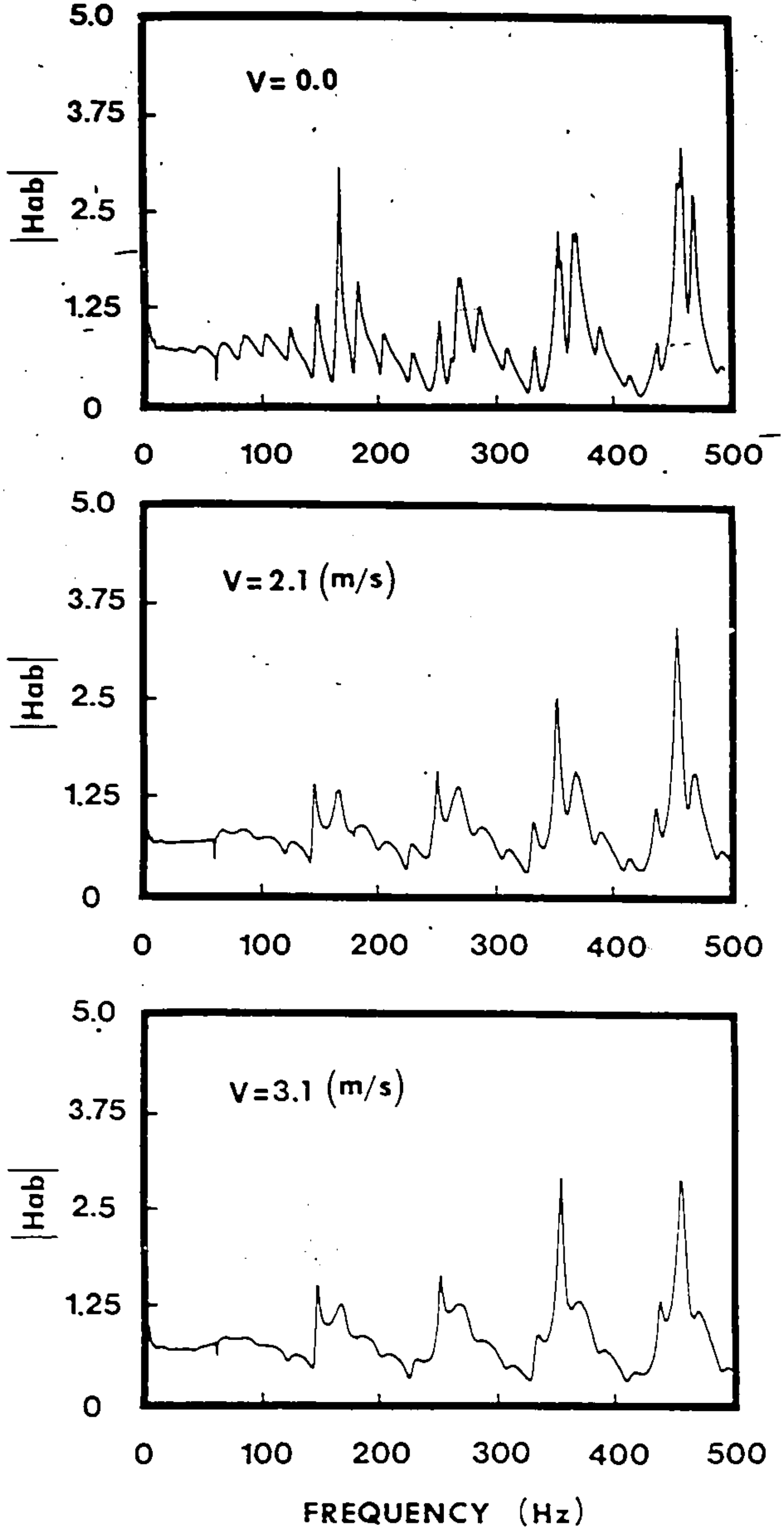

Figure 4.8 : Sequence of measured acoustic pressure ratios, microphones located upstream of orifice plate, system excited at bellmouth.

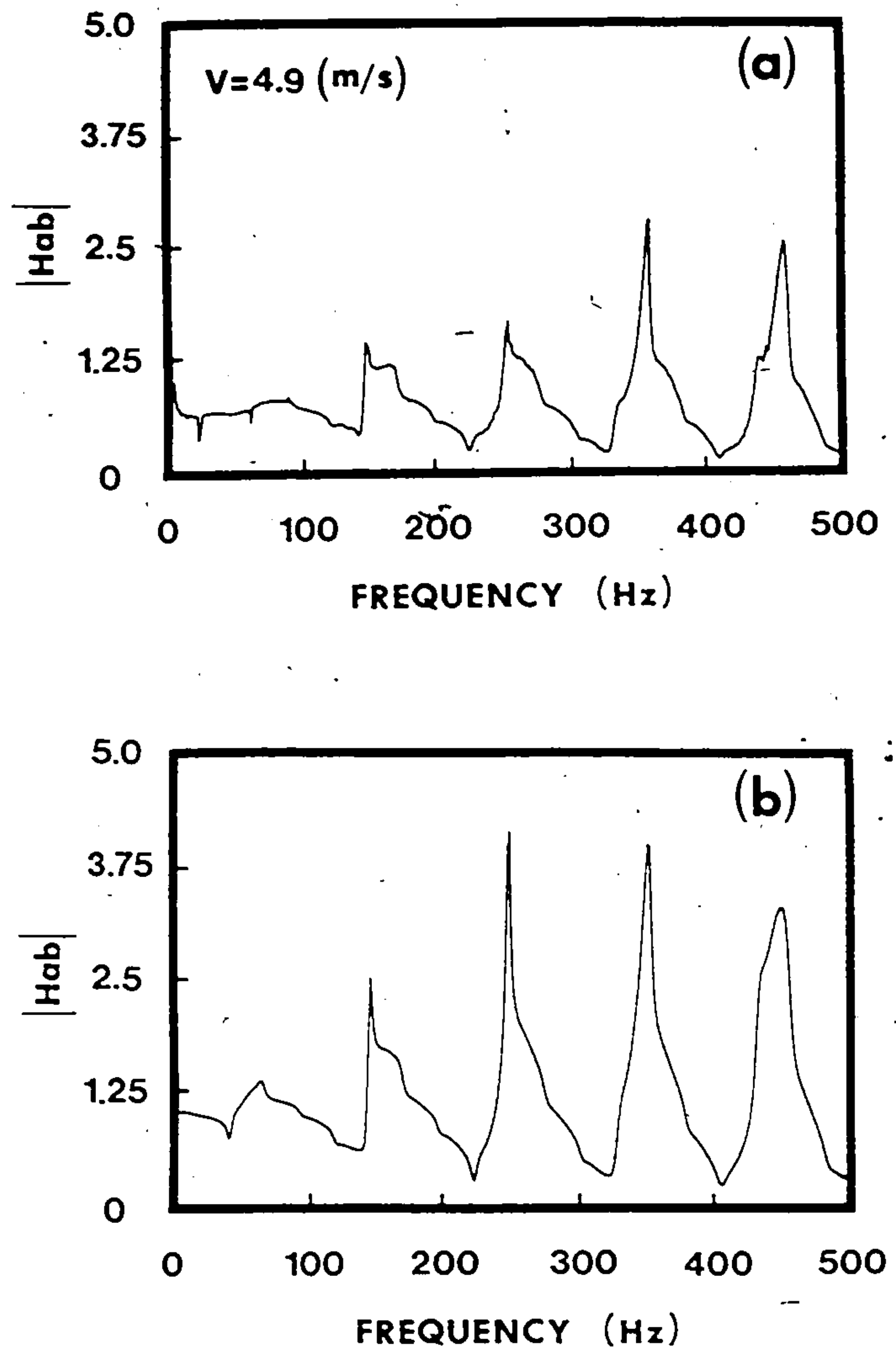

Figure 4.9 : Upstream acoustic pressure ratio, microphones located upstream of orifice plate. [a: Measured, b: Predicted]

inclusion of the no flow estimate of the orifice impedance (measured using the two microphone technique and a semi-anechoic termination downstream) did not significantly alter the predicted transfer function except for the no flow case. The amplitude ratio measurements were repeated for a variety of obstructions used as the singularity. The quasi static estimate for the singularity impedance was calculated and used to predict the amplitude ratio at the two microphone locations. Based on examination of the results it was felt that the modelling approach utilizing the quasi static estimate for the singularity impedance was reliable.

It is possible to use the measured amplitude ratios used to assess the quality of the end impedance estimates in conjunction with the 4 pole model to determine directly the desired impedance quantities [4.16,4.17]. This approach must be used carefully since the amplitude ratios predicted by the the 4 pole model will equal the measured values, independent of the quality and accuracy of both the impedance estimate and the 4 pole model. The downstream impedance can be found using:

$$Ze = [AM(1,2)-h21*BM(1,2)]/[h21*BM(1,1)-AM(1,1)] \quad [4.29a]$$

where:

$\{P,U\}_1 = [AM]*\{P,U\}_e$

$\{P,U\}_2 = [BM]*\{P,U\}_e$

and:

h21 = measured transfer function (P1/P2)

The upstream entrance impedance is found using:

$$Zi = [CM(1,2)-h21*DM(1,2)]/[h21*DM(1,1)-CM(1,1)] \quad [4.29b]$$

where:

$\{P,U\}_1 = [CM]*\{P,U\}_i$

$\{P,U\}_2 = [DM]*\{P,U\}_i$

and:

h21 = measured transfer function (P1/P2)

This approach can also be used to measured the source impedance during sound production. However, the transfer function used in the analysis must be conditioned with respect to the externally applied sound field. This can be achieved in the same manner as described for the source impedance measurement approach presented in chapter 2. Figure 4.10 presents the calculated exit impedance function evaluated using equation 4.29a. The corresponding exit reflective coefficient is also provided. Using this impedance estimate it was confirmed that the predicted amplitude ratio at measurement points equaled the measured quantity (presented in figure 4.2a). There are obvious errors in both the reflective coefficient and the impedance function despite the ability to predict the exact amplitude ratio at the measurement points using this impedance function. These errors occur primarily at frequencies corresponding to the peaks in the measured transfer function. This is consistent with the preceding discussion regarding the frequency resolution error and the corresponding bias error. Presentation of the calculated impedance function at locations other that the exit planes can mask these errors.

4.4 Pure tone source characterization

The acoustic power production for a source using the formulation of section 4.3 is given by:

$$Pw = U^* dP + P^* dU \qquad [4.30]$$

where P and U represent the acoustic pressure and volume velocity, respectively. From analysis of the results presented in chapter 3, it is clear that the cavity resonator interacts primarily with the acoustic modes which locate a pressure node (P = 0) at the source

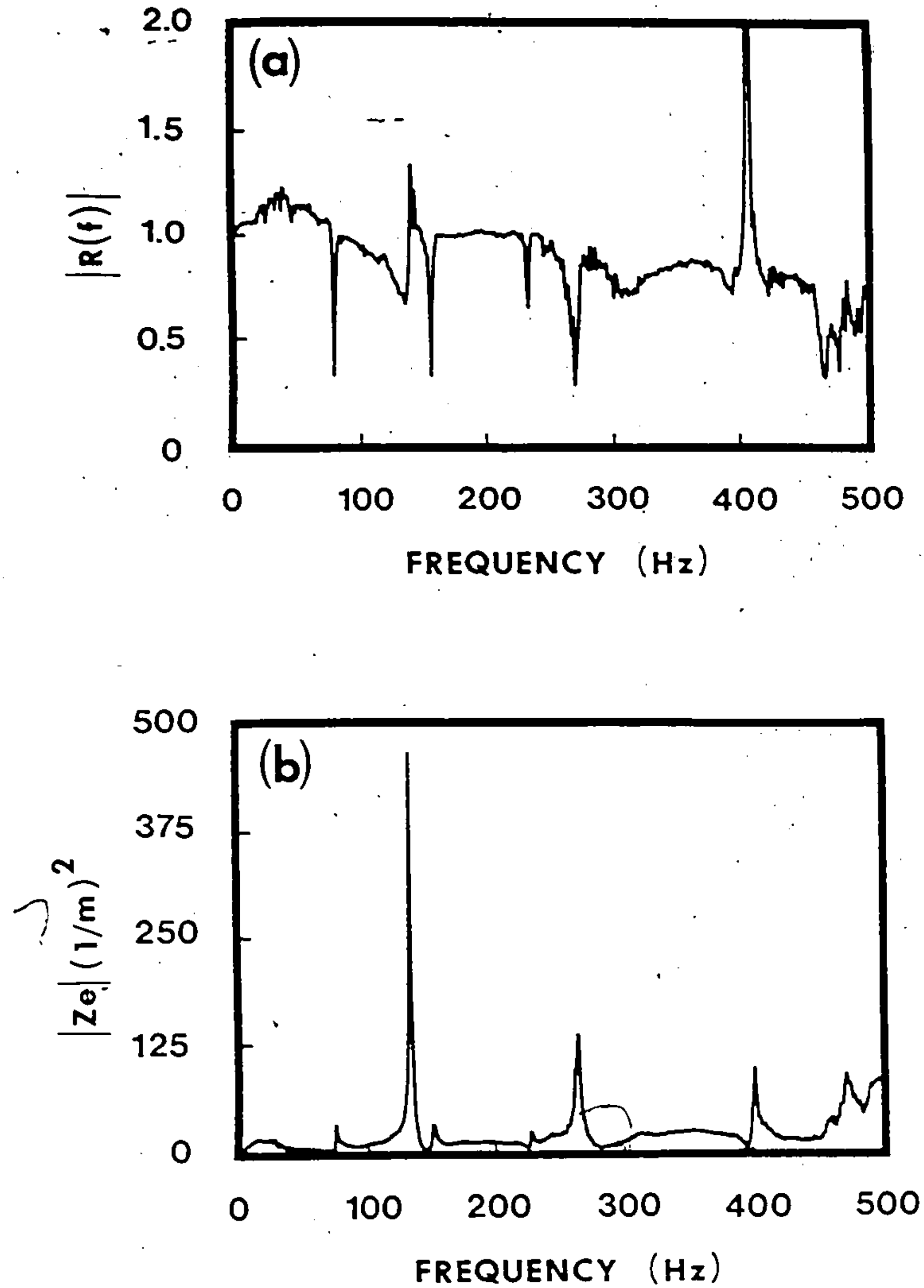

Figure 4.10 : Exit functions obtained using measured transfer function and 4 pole model directly. [a: reflective coefficient b: impedance function]

location. Thus the source characterization equations 4.25 are greatly simplified by solving only for the dp component as:

$$Gdp = 1/2\,[Gaa\,/\,/Hpa/^2 + Gcc/\,/Hpc/^2] \qquad [4.31]$$

The rig length used in the first source characterization experiment was 8.03 m, the upstream orifice was located 4.13 from the bellmouth entrance. The orifice diameter was 6.5 cm, giving an area ratio of 0.17. The cavity length was fixed at 9.5 cm. The upstream microphone was located 1.015 m from the bellmouth entrance, the downstream microphone was located 0.895 m from the plenum entrance. At the completion of an experiment (corresponding to one particular flow velocity) the data was transferred to the Vax 730 for the equivalent source evaluation. The flow velocity was adjusted such that the peak acoustic output was obtained for each particular resonating mode. A few spectra pairs at off peak resonance were also obtained. The quasi static impedance was obtained from the pressure drop versus velocity squared curve whose slope was equal to 14.04 Pa-sec^2/m^2. The resulting PSD of the dP type source (obtained from the solution of equation 4.31) was non-dimensionalized as:

$$Gdp(St) = [Gdp(f) * Vp/lc\,]/(\text{delta } P)^2 \qquad [4.32]$$

where:

St = reduced frequency (f*lc/Vp)

Vp = mean upstream pipe velocity

lc = cavity length

delta P = mean pressure drop across cavity.

The acoustic production is predominantly at one frequency for a given cavity separation and flow velocity. Thus from a design perspective it is only the conditions of peak production which requires characterization. Table 4.1 summarizes the results of the source identification where only the information at the peak sounding conditions are presented.

frequency Hz	Up (m/s)	St	Gdp(St)
125.0	1.52	6.2	0.077
168.75	2.31	5.48	0.017
208.75	3.34	4.69	0.024
250.0	4.38	4.28	0.013
333.75	5.96	4.20	0.029

Table 4.1 : Peak sounding data.

Uniqueness of the source characterization can be determined by varying the acoustic environment of the source, and re-evaluating the non-dimensional source spectrum utilizing the identical cavity resonator. The acoustic change necessary in the experimental rig was obtained in part by lengthening the piping to 9.29 m and positioning the upstream orifice plate of the cavity resonator 5.4 m from the bellmouth entrance. The downstream exit impedance was significantly altered by placing a sharp edged orifice (area ratio 0.1) at the exit plane between the piping and the plenum.

The effect of the downstream orifice plate was determined by measuring the transfer function between two microphones upstream of the pipe exit plane. The piping system was excited with band limited white noise at the bellmouth entrance with the singularity removed. Figure 4.11 presents the sequence of measured transfer functions for an upstream flow velocity ranging from no flow to 5 m/s. Comparison of figure 4.11a and 4.3a illustrates the effect of the orifice plate in the absence of flow. More importantly, however, is the significant change in the downstream impedance under flow conditions. The sequence of measured transfer functions provided in figure 4.11 indicates clearly an increase in damping in the measured modes of the transfer function. The reduction in amplitude of the modal

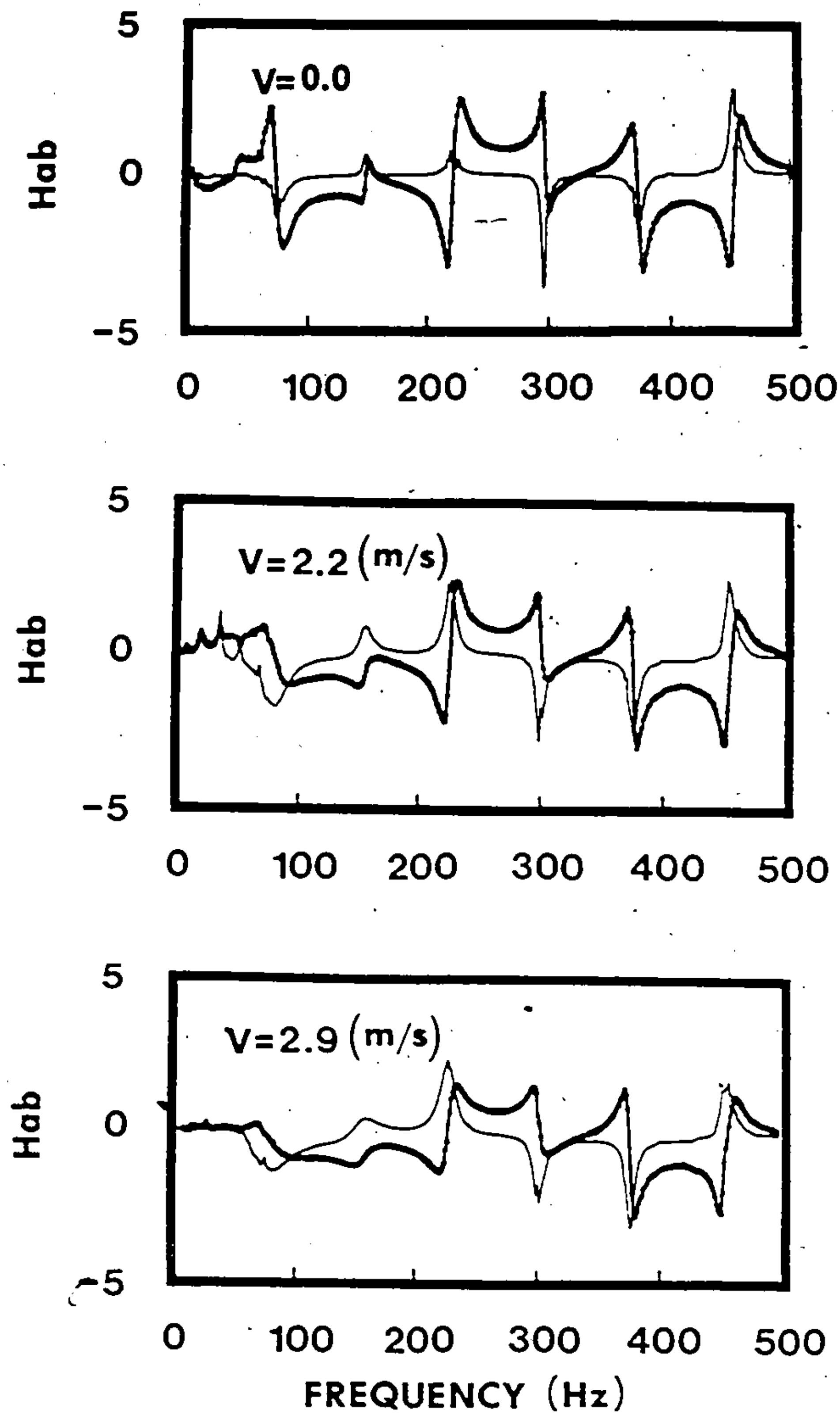

Figure 4.11 : Sequence of measured acoustic pressure ratios with orifice plate at exit plane (la= 2.16m, Lb=0.9m)

peaks starts at the lower frequencies and affects the higher frequencies as the flow velocity is increased.

The downstream end orifice for the no flow condition was modelled using the equivalent length data provided in [4.24]. The effect of flow was incorporated using the quasi static model. The slope of the line between the mean-pressure drop across the orifice plate versus the upstream velocity squared was found to be 73.8 Pa-sec^2/m^2. The pressure drop across the orifice plate was measured using pressure taps located 1 diameter upstream of the orifice plate, and 30 cm off the pipe centerline into the plenum wall. Figure 4.12a presents the predicted transfer function at the measurement points for a flow velocity of 5.0 m/s. The agreement between this figure and the measured quantity (figure 4.12b) is good. Examination of intermediate measurements indicated that the quasi-static approach over estimated the actual impedance. A reduction in the downstream impedance of 20% reproduced the measured transfer function more closely over the entire velocity range. It is interesting to note that at higher flow velocities the effect of the downstream orifice plate is to produce transfer functions (both measured and predicted) which approach those produced by a rigid termination at the exit plane.

The measured transfer functions under flow conditions can be used via equation 4.29a to determine directly the equivalent exit plane impedance. Figure 4.13 presents a sequence of 3 impedance estimates evaluated using this approach. Again it was confirmed that the amplitude ratios were predicted exactly at the measurement points using these impedance functions. There are obvious errors in the impedance estimate similar to those found for the no flow case using the same approach. The effect of flow on the exit boundary conditions is seen as an increase in the magnitude of the impedance function, starting at the lower frequency range and increasing in frequency with velocity. There is virtually no alteration in the exit impedance above 250 Hz with flow velocity.

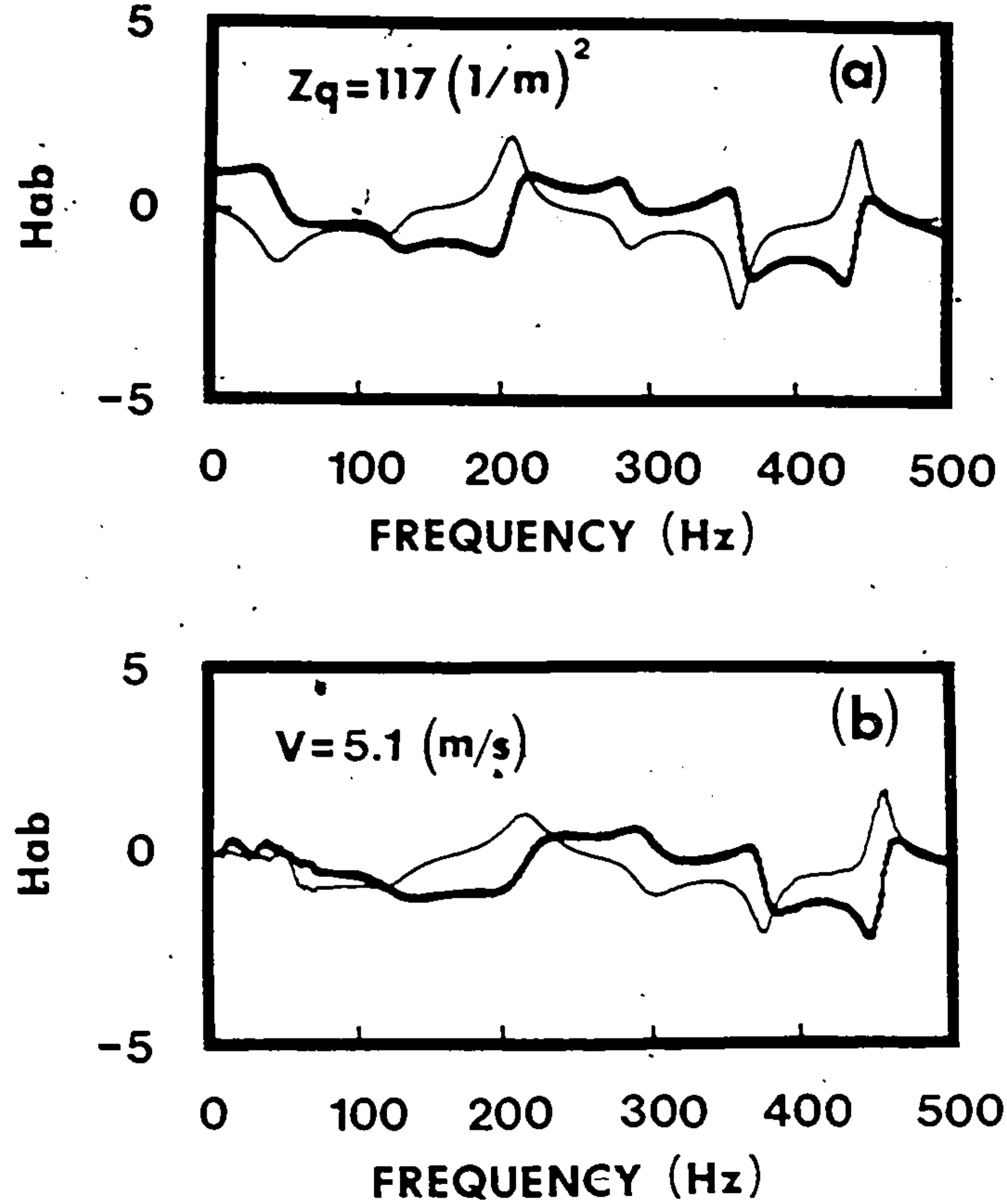

Figure 4.12 : Acoustic pressure ratio with orifice plate at exit plane. (a: predicted using quasi-static model, b: measured)

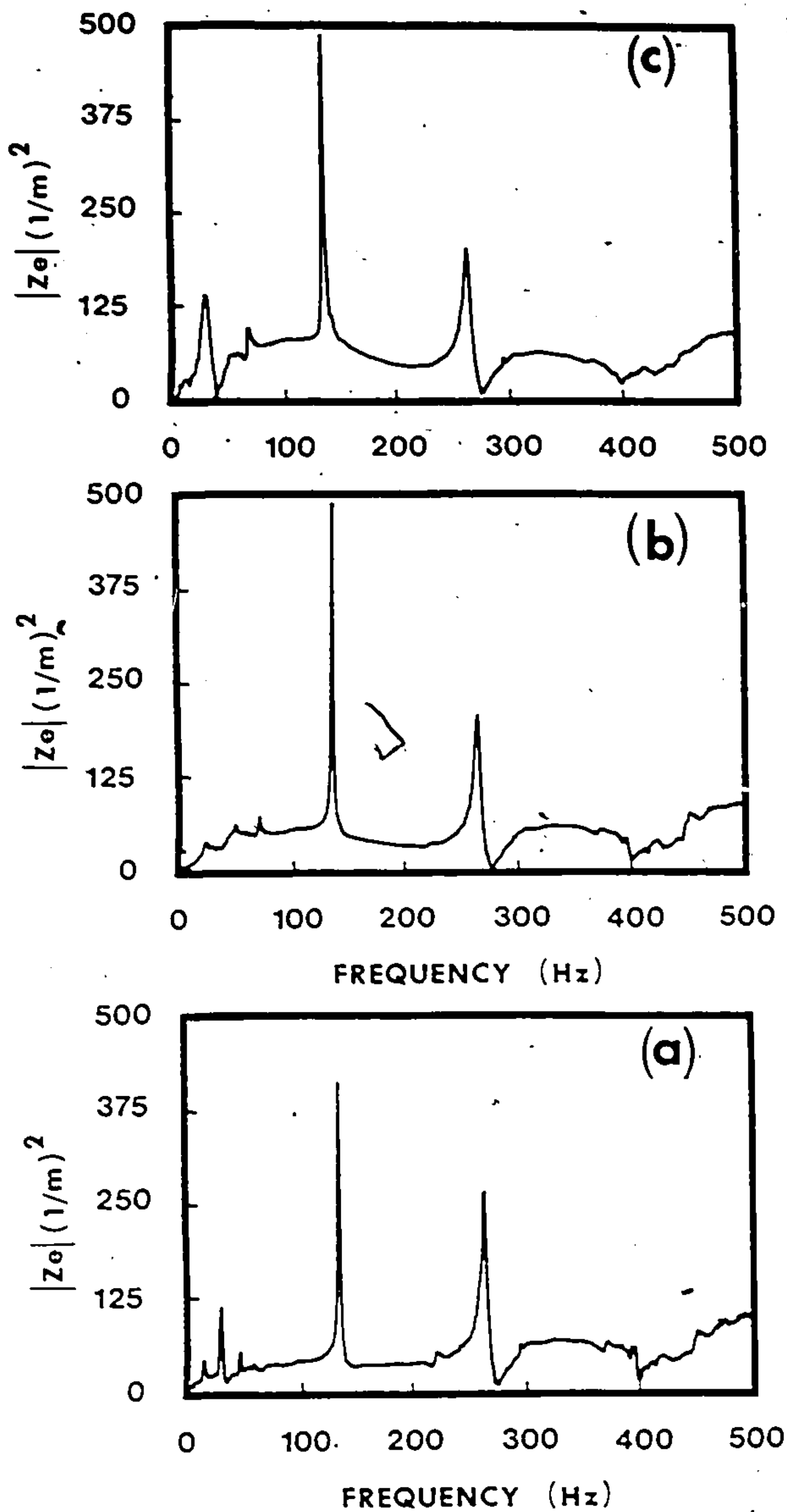

Figure 4.13 : Sequence of exit impedance functions determined using measured transfer function and 4 pole model.
[a: Vp= 2.3 m/s, b: Vp=2.9 m/s, c: Vp=3.8 m/s]

Figures 4.14 presents 3 spectra measured at the downstream microphone location taken from the sequence of spectra in the source identification. Several features, illustrating the characteristics of this type source are evident. In figure 4.14a the primary resonating frequency is 126 Hz. However, there is significant sound production (much more than usual) at what appears to be harmonics of this frequency. As the velocity is increased, the primary resonating frequency jumps to 250 Hz, with minor sound production at nominally 125 Hz and 375 Hz. At higher velocities the primary resonating frequency is 375 Hz. Thus the high production at the harmonics of 125 Hz in figure 4.13a is attributed to the fact that the harmonic frequencies are stable resonating frequencies of the acoustic source. Table 4.2 summarizes the results of source identification using the modified rig.

frequency Hz	Vp (m/s)	St	Gdp(St)
126.	1.52	6.25 (n=2,1)	0.11
250.	2.13	8.80 (n=2)	0.18
286.	2.69	8.11 (n=2)	0.05
342.	3.34	7.29 (n=2)	0.15
376.	3.87	7.63 (n=2)	0.10

Table 4.2 : Peak sounding data (orifice in exit plane).

Modification of the acoustic environment significantly altered the fluid mechanics of the oscillating shear layer in that it was now operating with two vortices between the orifice plates. Not only is this evident in the Strouhal data, it was confirmed using the flow visualization method presented in chapter 2. Division of the Strouhal number for the frequencies operating in the n=2 mode, produces a dependency of Strouhal number on velocity (Mach No.) consistent with the data presented in chapter 2.

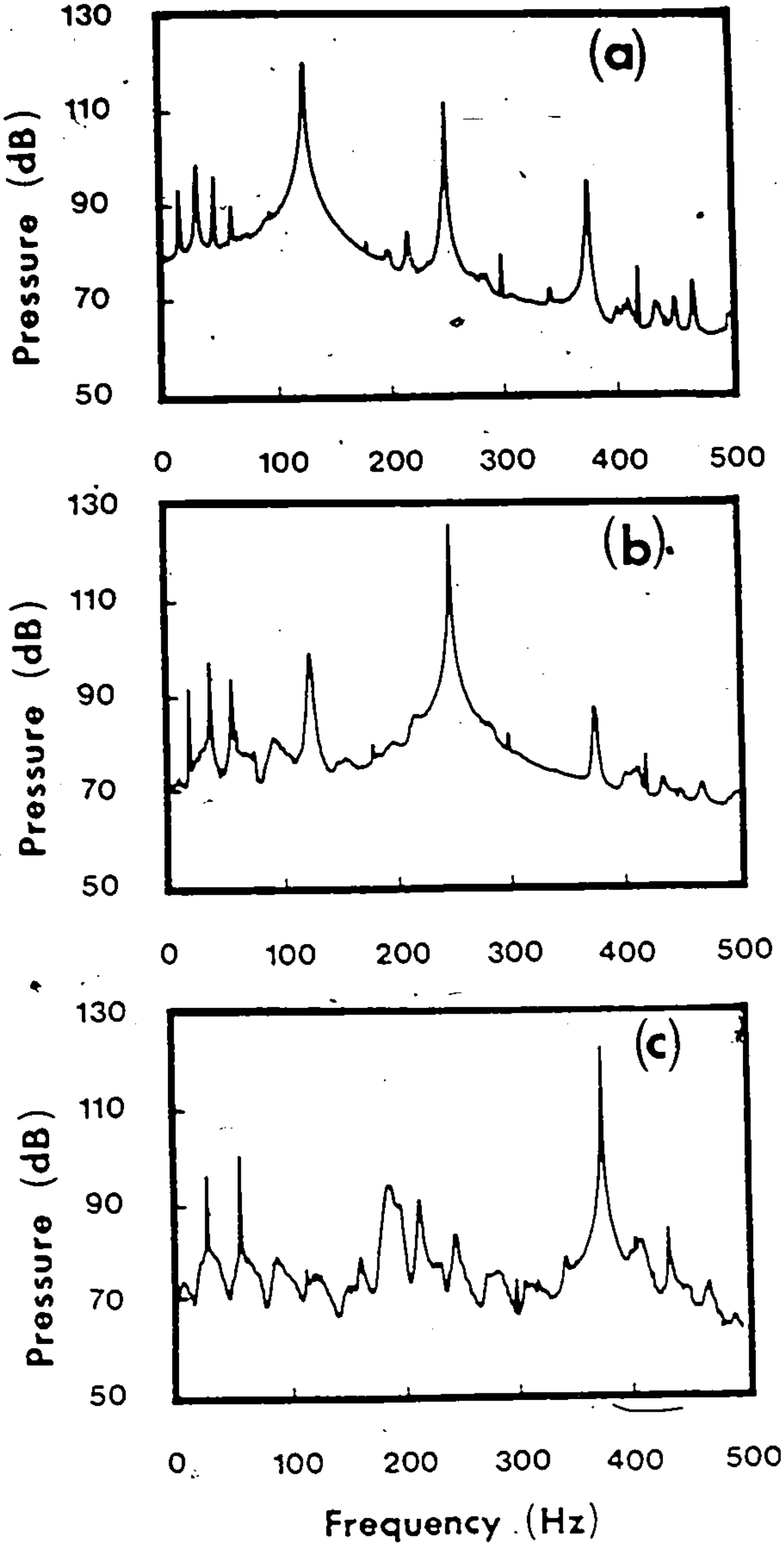

Figure 4.14 : Sequence of microphone spectra, downstream orifice plate in place. [a: Vp =1.5 m/s, b: Vp=2.13 m/s, c: Vp=3.9 m/s

4.5 Discussion

An acoustic model of the experimental facility has been developed which utilized the 4 pole approach in conjunction with experimentally measured entrance and exit impedance estimates. The validity of using a quasi static estimate for the change in impedance resulting from the pressure drop across the impedance location was investigated. The results indicate that this assumption is valid, although a slight over estimation of the resulting impedance occurred. Impedance estimation techniques which utilized the 4 pole model directly, reproduced (as they must) the predicted amplitude ratios at the measurement points. However, the end impedance estimates contained obvious errors related to the frequency resolution and microphone separation which may go unnoticed since the accurate prediction of the pressure ratios at the measurement points is assured. This method of impedance estimation is very efficient, and can be used in conjunction with the coherent power analysis procedures outlined in chapter 3 to measure the source impedance during sound production.

The application of the equivalent source identification procedure to the cavity resonator did not collapse the peak sounding data. The basic fluid mechanics of the process, and the resulting sound production are strongly sensitive to the acoustic environment. This is clearly indicated by the change in the shear layer oscillation to the n=2 mode with the change in the rig acoustic characteristics. Given this significant change in the fundamental source mechanism it is not surprising that a modelled change in the impulse response functions (Hpa,Hpc) did not account for the change in acoustic output. Within each set of data (table 4.1 and 4.2) however, the peak production level was reasonably well collapsed.

The identification of narrow band sources in resonant environments demands accurate damping estimates of the dynamic system. For broader band sources, off resonant response can be used to estimate the source strength, thus providing more data for the identification. The accuracy requirements necessary in the impulse response functions which permit an assessment of this approach to pure tones may be greater than can be achieved given the sensitivity of the results to the system impedance estimates.

CHAPTER 5

THEORETICAL MODEL DEVELOPMENT

5.0 Introduction

In this chapter a theoretical model is developed which provides further insight into the coupled fluid/acoustic phenomenon described in chapter 2. This model of the combined fluid/acoustic system incorporates the acoustic 4 pole model of the experimental piping system developed and tested in the previous chapter. A successful model, leading to improved experimental design must predict the main features of the acoustic production. These include the strong lock-in with the acoustic modes locating a velocity anti-node at or near the cavity resonator, as well as the frequency jumping and step like velocity/frequency plots typical of these oscillators.

5.1 Theoretical Model Overview

The conceptual framework of the oscillator model is based on a positive feedback, closed loop control theory type analysis. It does not examine the local interaction of small scale vorticity as in [2.7], or perform a detailed momentum balance throughout the cavity as in [2.16]. It does, however, look at the fluid/acoustic system using published characteristics of separated flows, and combines this with the 4 pole model of the piping acoustics developed in the previous chapter. In this sense it follows closely many of the predictor models of cavity resonance outlined in chapter 2 [2.6,2.10,2.11,2.13]. It is important to recognize the distinction between the acoustic production modelled as a resonance response phenomenon, and the coupled fluid/acoustic oscillations resulting from the instability of a self-excited system. It is this latter mechanism which is being modelled in this chapter.

5.2 Acoustic feedback loop

The double orifice resonator interacts primarily with those acoustic modes locating a velocity anti-node at or near the cavity location. In this context, it appears to the piping system as a dipole type source, allowing determination of potential resonating frequencies given a source location. However, it does not quantify the effect of acoustic damping or the proximity of the antinode to the exact cavity location on the mode selection and the potential for acoustic resonance. The developed software package outlined in chapter 4 allows simulation of either a Dp (dipole) or Du (monopole) type source at any location in the system, and calculation of either acoustic pressure or acoustic particle velocity at any location in the system. In figure 5.1 the magnitude of the steady state acoustic velocity response at the upstream orifice location per unit Pascal of dipole sound applied at the downstream orifice plate is predicted using the acoustic model. The upstream orifice plate location, cavity separation and pipe length correspond to the experimental geometry producing the measured frequency/velocity plot of figure 2.3. Also labeled are the nominal values of the resonating frequencies in the experimental data. The small discrepancy (not exceeding 2 percent) between the measured frequencies of peak acoustic output, and the frequency of the peaks in the computed function are due to inaccuracies in the acoustic model. The height, width and location of the peaks in this spectrum quantify the effects of the cavity location, orifice plate separation, system impedance values and total pipe length. Positioning the resonator near the centre of the piping system locates the source at either a pressure node or antinode for all plane wave acoustic modes and accounts for the large peaks at the even valued modes of the system. As the frequency increases, the distance of the resonator from the exact centre of the piping system becomes larger in comparison to the acoustic wavelength. This explains the steady increase in peak height seen at the frequencies of the odd valued mode numbers of the

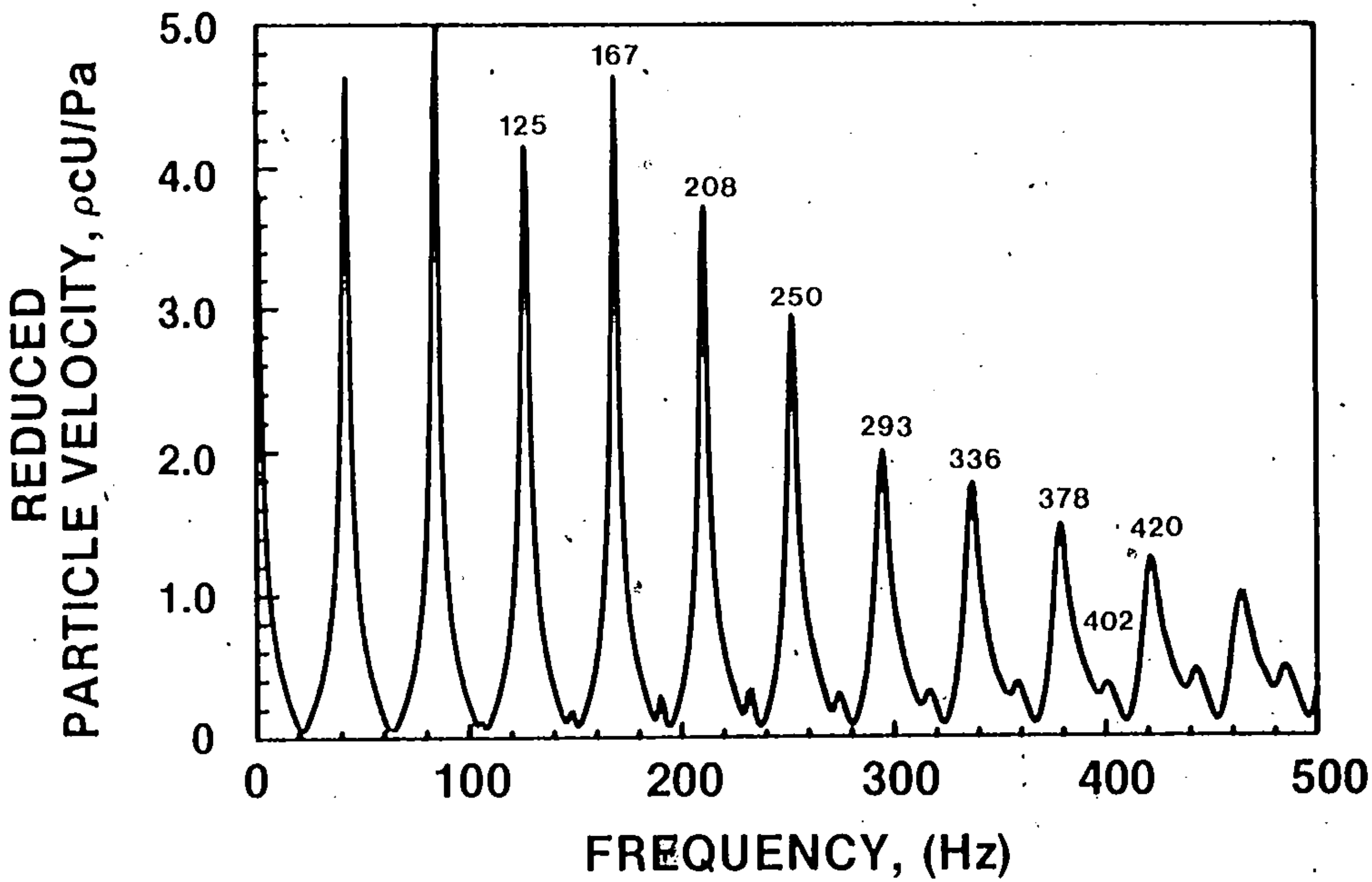

Figure 5.1 : Reduced acoustic particle velocity per unit dipole sound versus frequency. [Ls=4.06m, Lc=4.32cm, Lp=8.04m]

transfer function. At 402 Hz the first odd valued mode sounds. Based on the proposed model, this corresponds to sufficient acoustic gain in the feedback loop of the model to sustain the oscillation for the given flow velocity.

In figure 5.2a the reduced particle velocity transfer function (computed using the same procedure as that producing figure 5.1) is evaluated using the rig geometry producing the experimental frequency velocity plot of figure 2.4a. The nominal values of the experimental resonating frequencies are labeled at the corresponding peaks in the computed transfer function. Again the measured sounding frequencies align closely with the frequencies of the largest peaks in the computed function.

Figure 5.2b presents the computed transfer function using the experimental rig geometry producing the measured data of figure 2.4b. The measured frequencies of the experimental data are also labeled at the corresponding peaks in the computed transfer function. There is a clear coincidence with the frequencies of maximum amplitude in the transfer function and the measured resonating frequencies.

Evaluation of the reduced acoustic particle velocity per unit of dipole sound is an improvement in estimating likely oscillating frequencies of the cavity/acoustic system. However, the absence of sound production at intermediate frequencies whose peaks exceed the value at 402 hz in figure 5.1, as well as the absence of measured sound below 125 hz illustrate the limitations in using the computed transfer function by itself in predicting the possible frequencies of acoustic production. Questions also arise regarding the limits of stability of individual acoustic modes in the system, and the possibility of avoiding resonance completely for a particular geometric arrangement and limited velocity range.

The steady state acoustic particle displacement at the separation plane (upstream orifice plate) per unit of dipole sound generated at the downstream orifice plate is the feedback transfer function in the model and is given by:

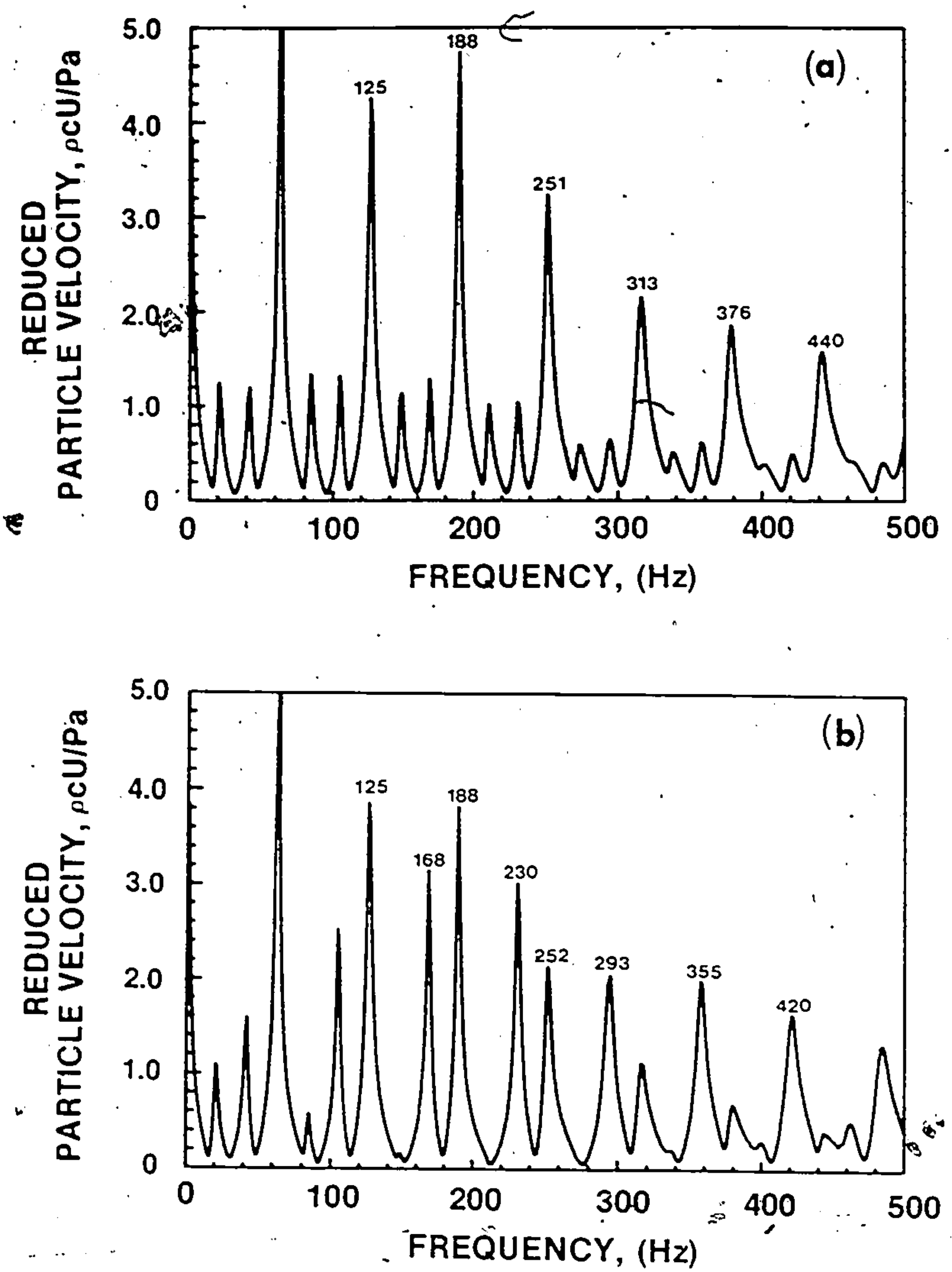

Figure 5.2 : Reduced acoustic particle velocity per unit dipole sound versus frequency. [a: Ls=5.33m, Lc=4.32cm, Lp=8.04m, b: Ls=2.78m, Lc=4.32cm, Lp=8.04m]

$$G(f) = 1/j\omega * [\rho cU/dP] \quad [5.1]$$

where:

$\rho cU/dp$ is the transfer function computed by the software package and:

ρc = characteristic impedance

U = acoustic particle velocity at upstream orifice location.

dP = unit of pressure applied at the downstream orifice.

5.3 Forward loop development

The forward loop of the oscillator model is dominated by the stability characteristics of the separated shear layer. The oscillating shear layer produces a dynamic cavity volume, which in turn results in velocity fluctuations across the cavity necessary to satisfy continuity conditions. The final stage of the forward loop analysis is the expansion and dynamic pressure recovery of the expanding jet into the downstream pipe.

Elder [5.1] examined the potential mechanisms of exciting organ pipe resonance by an oscillating jet flow. The Fourier components of a dynamic momentum balance across the jet indicated 3 separable components of the total fluctuating pressure. These include:

1. Direct acoustic condensation of the jet velocity ($P = Z*\bar{U}$). This mechanism would be most efficient at pressure anti-nodes.
2. A purely hydrodynamic pressure gradient responding to the fluctuating shear caused by the jet. This mechanism would be most efficient at a pressure node.
3. A purely non-linear component containing all higher order terms which disappear for sinusoidal jet modulation.

The first mechanism is not dominant for the source under study. Clearly the impedance at the source location (which closely resembles the reciprocal of the computed reduced acoustic particle velocity transfer function) is small. It is the second mechanism which is being modelled as the sole contributor to the acoustic production. This is reflected not only in the forward loop development, but is seen as the use of a single feedback transfer function in the feedback loop, ie. the acoustic velocities at the upstream orifice due to the fluctuating velocity at the downstream orifice plate are neglected.

5.3.1 Shear layer stability characteristics

The fluid mechanics of the coupled fluid/acoustic system can be characterized by the oscillation of the unstable shear layer downstream of the separation point and subsequent roll up and propagation downstream. The stability characteristics of axisymmetric inviscid jets have been investigated by Plaschko [2.22]. However the reference does not provide readily usable data for computing the axisymmetric modes of the shear layer motion. A more tractable solution provided by Michalke [2.12] for the growth characteristics of a two dimensional inviscid shear layer is easily incorporated into the model. The data of Michalke is used in the same fashion as Elder [2.11]. That is:

$U_c = C_r * U_m$ (wave convection speed)

$\delta = U_m / [2dU/dy]_o$ (characteristic dimension)

$\beta = \omega \delta / U_m$

$k = \alpha_r / \delta$

$\alpha = \alpha_i / \delta$

The wave growth is developed from the conservation of total vorticity in a separated shear layer subject to an initial perturbation. The solution of the propagating wave motion is given by:

$$\zeta(x,y,t) = A\,\lambda(y)\,e^{(\alpha x)}\,e^{j(\omega t - kx)}. \quad [5.2]$$

The exponential growth predicted in the inviscid solution is not exhibited in practice beyond the initial stages of the wave development. From the sequence of flow visualization pictures presented in chapter 2, it is seen that the scale of the rolled up vortex is not increased beyond roughly 3/4 of the mean path to the downstream orifice plate. This represents a distance of 9 cm for that particular cavity. The values of (α) and (k) of equation 5.2 are frequency dependent, and have been interpolated from the data of Michalke using a spline fit. In the model development, it is the acoustic field which provides the displacement perturbation at the separation point. Matching the acoustic perturbation displacement at the separation plane allows the shear layer motion to be described by:

$$\zeta(x,y,t) = G(f)\, e^{(\alpha x)}\, e^{j(\omega t - kx)} \qquad [5.3]$$

The two dimensional description of the shear layer motion is converted to an axisymmetric set of coordinates using:

$$D(x,t) = D_o - 2\,x \sin(\theta_o) + 2\,\zeta(x,y,t) \qquad [5.4]$$

where:

$D(x,t)$ = effective cavity diameter

D_o = entrance orifice diameter

θ_o = initial fluid separation angle

5.3.2 Dynamic cavity volume estimation

The bulk of the mean flow passing through the cavity is bounded by the radial position of the shear layer. The effect of the oscillating shear layer is to produce a time varying cavity volume between the two orifice plates. Continuity requirements force velocity fluctuations to occur at the cavity boundaries (inlet or exit orifice) as measured using the hotwire. An estimate of the dynamic cavity volume was made from the sequence of still photographs of chapter 2. Fifteen points along the upper edge of the "smoke" trace were spline fit and integrated over the length of the cavity to produce the axisymmetric swept volume. Figure 5.3 presents 4 of the traces obtained from the flow visualization photographs.

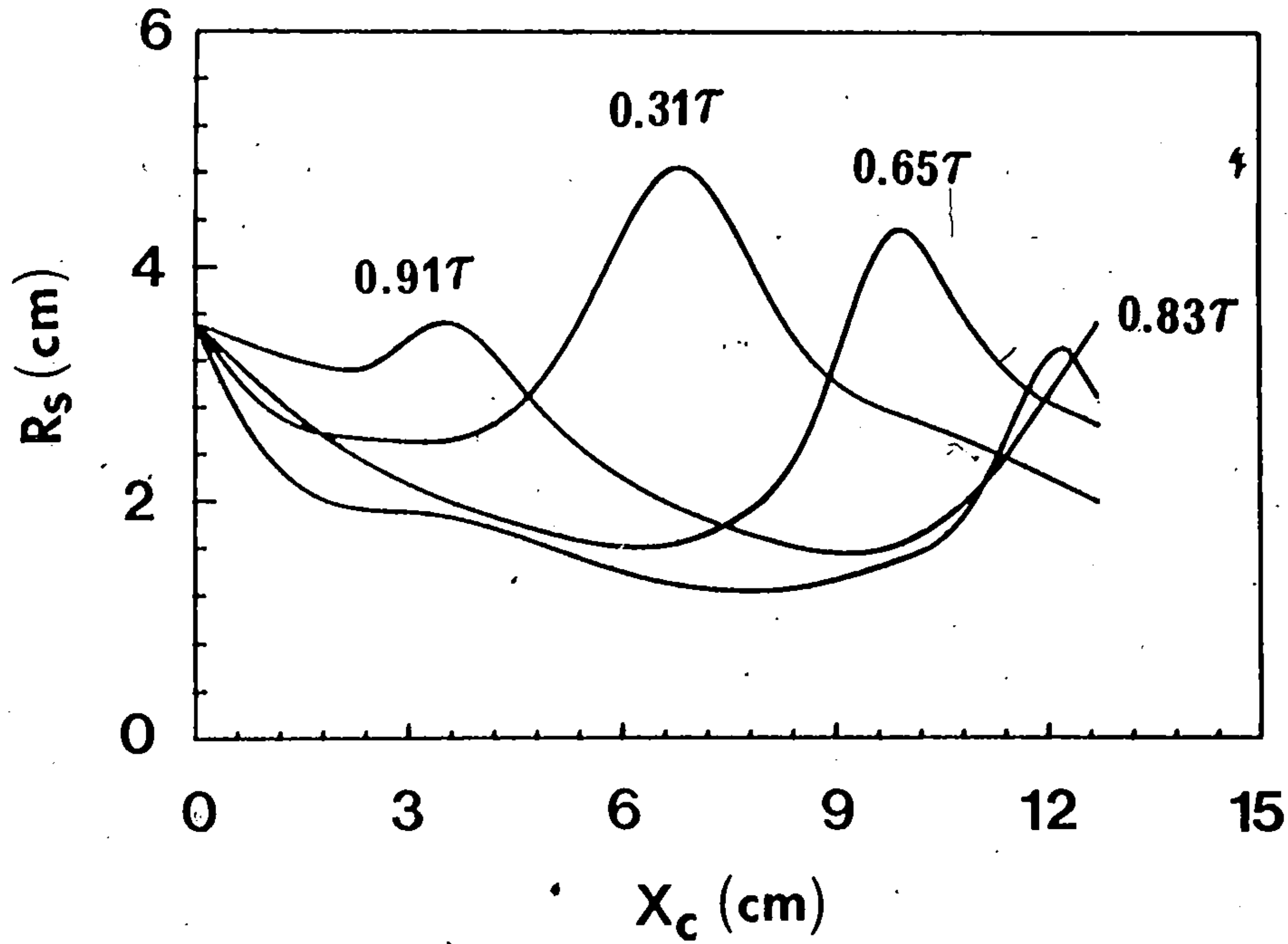

Figure 5.3 : Estimated boundaries of mean flow through double orifice cavity from flow visualization photographs. [Vm=18.5 m/s,Lc=12.9cm,fr=181 hz]

The vertical exaggeration seen in the data arises from the relative scales on the axes which were chosen to delineate the results at the different locations in the acoustic cycle. The data was forced through the separation point (upstream orifice edge) at $x=0$. which accounts for the exaggeration in the slope of the trace at $x=0$. Table 5.1 summarizes the calculated volume for these 4 traces. It is interesting to note that the reduction in effective exit area at the downstream orifice plate is associated with an increase in the cavity volume.

Time	Volume ($m^3 \times 10^4$)
T+0.31t	3.75
T+0.65t	2.85
T+0.83t	1.55
T+0.91t	2.77

Table 5.1 Calculated dynamic cavity volumes from flow visualization photographs

5.3.3 Velocity Fluctuation Estimation

The rate of volume addition to the volume bounded by the shear layer and the planes defined by the upstream and downstream orifice plates is given by:

$$-\,dQ/dt = V_e(t)\,A_e(t) - V_i(t)\,A_i(t) \qquad [5.5]$$

where:

$A_e(t)$ = effective exit area at downstream orifice

$A_i(t)$ = effective inlet area at upstream orifice

$V_i(t)$ = inlet velocity at upstream orifice

$V_e(t)$ = exit velocity at downstream orifice

The exit velocity fluctuations can be easily calculated if the inlet conditions are assumed constant and not time varying. Although the hotwire measurements indicate that velocity fluctuations do exist across the upstream orifice plate, this assumption should not qualitatively change the nature of the results. Rearranging equations 5.5 gives the exit velocity in terms of the volume fluctuations and the exit area.

$$V_e(t) = V_i / A_r(t) - (dQ/dt) / A_e(t) \tag{5.6}$$

where:

V_i = mean upstream orifice velocity

$A_r(t) = A_e(t) / A_i$ (exit area ratio)

The effective exit area is taken from the shear layer location at the downstream orifice plate, that is using equation 5.4 with $x = Lc$. The rms velocity fluctuations at the exit plane of the cavity are calculated from equation 5.6 using:

$$(Ve)_{rms} = \sqrt{1/T \int (V_e(t) - V_{em})^2 dt} \tag{5.7}$$

where:

$(Ve)_{rms}$ = exit rms velocity fluctuations

V_{em} = mean exit velocity

For a given frequency, upstream velocity and geometric layout, equations 5.3 through equations 5.6 are used to estimate the exit velocity. Ten integration points over the acoustic cycle are used to calculate the mean and rms velocity values.

The main characteristics of the forward portion of the control type model are illustrated in figure 5.4. Here the computed rms exit velocities assuming a constant acoustic perturbation displacement (0.01 mm) for various mean flow velocities are plotted against frequency. This figure indicates several important features typical of separated flows. These include the existence of a peak in the response spectra (in this case the computed velocity fluctuations) which increases linearly with velocity (exhibiting a Strouhal type relationship). As well, the spectra broaden with increasing velocity. This indicates the tendency of separated flows to amplify fluid disturbances over a wider frequency range at higher flow

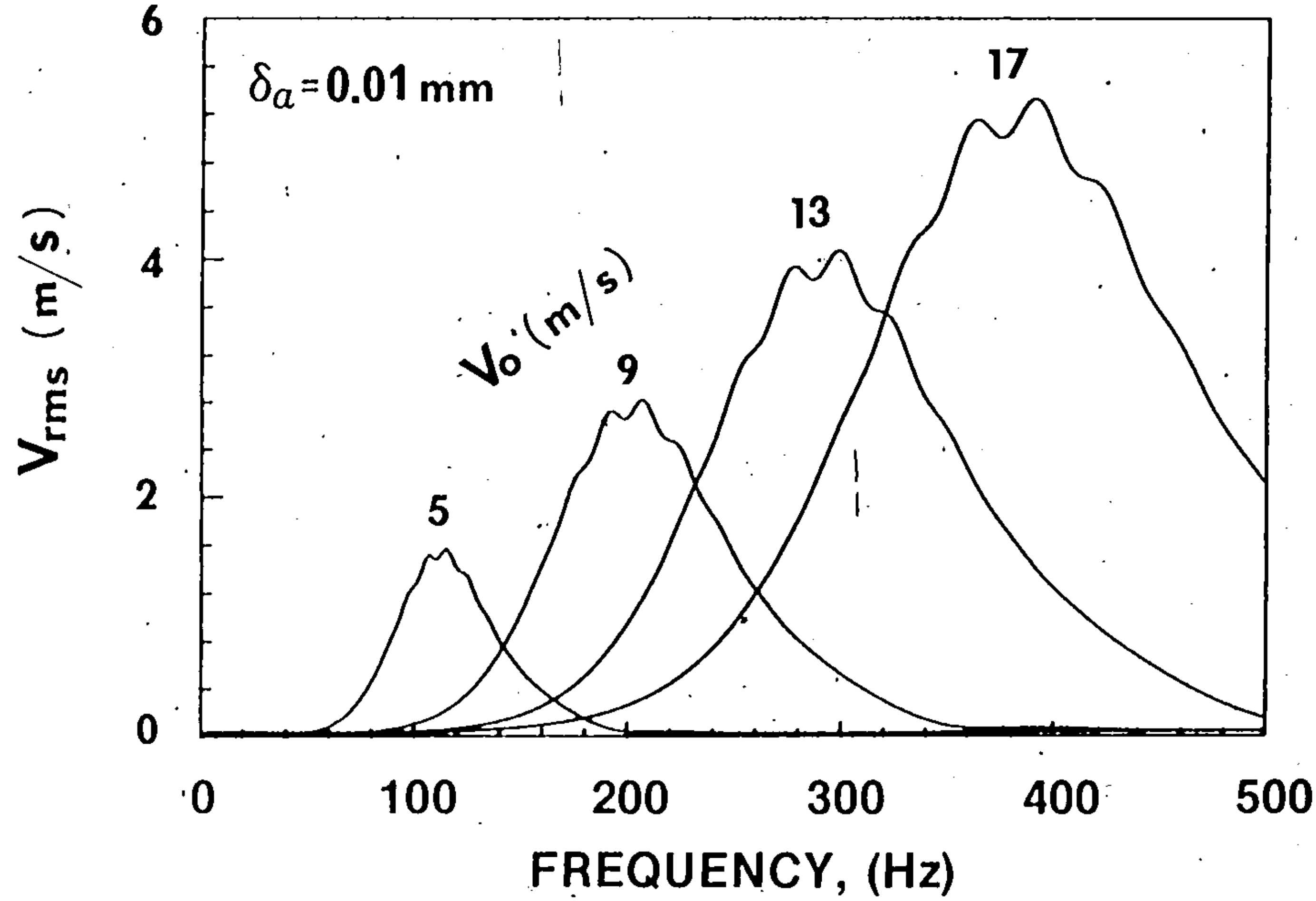

Figure 5.4 : RMS exit velocities computed using constant acoustic perturbation displacement of 0.01mm. [Lc=4.32cm, d=1.5mm, thetao=5]

velocities than at lower flow velocities. The peaks in the rms velocity calculations increase linearly with frequency as anticipated from equation 5.6. The value of the shear dimension (δ) in the analysis (which unfortunately is not known for the experimental data) influences strongly the maximum value in the spectra, as well as the frequency of maximum gain for a given flow velocity and cavity separation.

The non-linearity in the forward loop was investigated by varying the assumed acoustic displacement at the separation point. Figure 5.5 illustrates the change in the peak rms velocity values as a function of the perturbation displacement. The function is reasonably linear up to approximately 1.5×10^{-2} mm. At 500 Hz this yields 120 dB (re 20×10^{-6} Pa) assuming a constant characteristic impedance of ρc. If a severe non-linearity exists in the model, a small change in the perturbation displacement may change the assessment of stability or instability of the system.

5.3.4 Dynamic Pressure Recovery

The expansion of the jet flow into the downstream portion of the pipe is associated with a partial pressure recovery. For steady flow, this pressure recovery can be estimated assuming the expansion occurs across a sudden enlargement. That is:

$$P_r = 1/2\,\rho\,V_j^2(1 - 1/A_r) \qquad [5.8]$$

where:

P_r = mean pressure recovery

V_j = mean jet velocity

A_r = pipe to orifice area ratio.

The jet velocity is fluctuating, and can be described as a sum of the steady state term plus the calculated rms value. That is:

$$V_j(t) = V_{em} + V_{rms} \qquad [5.9]$$

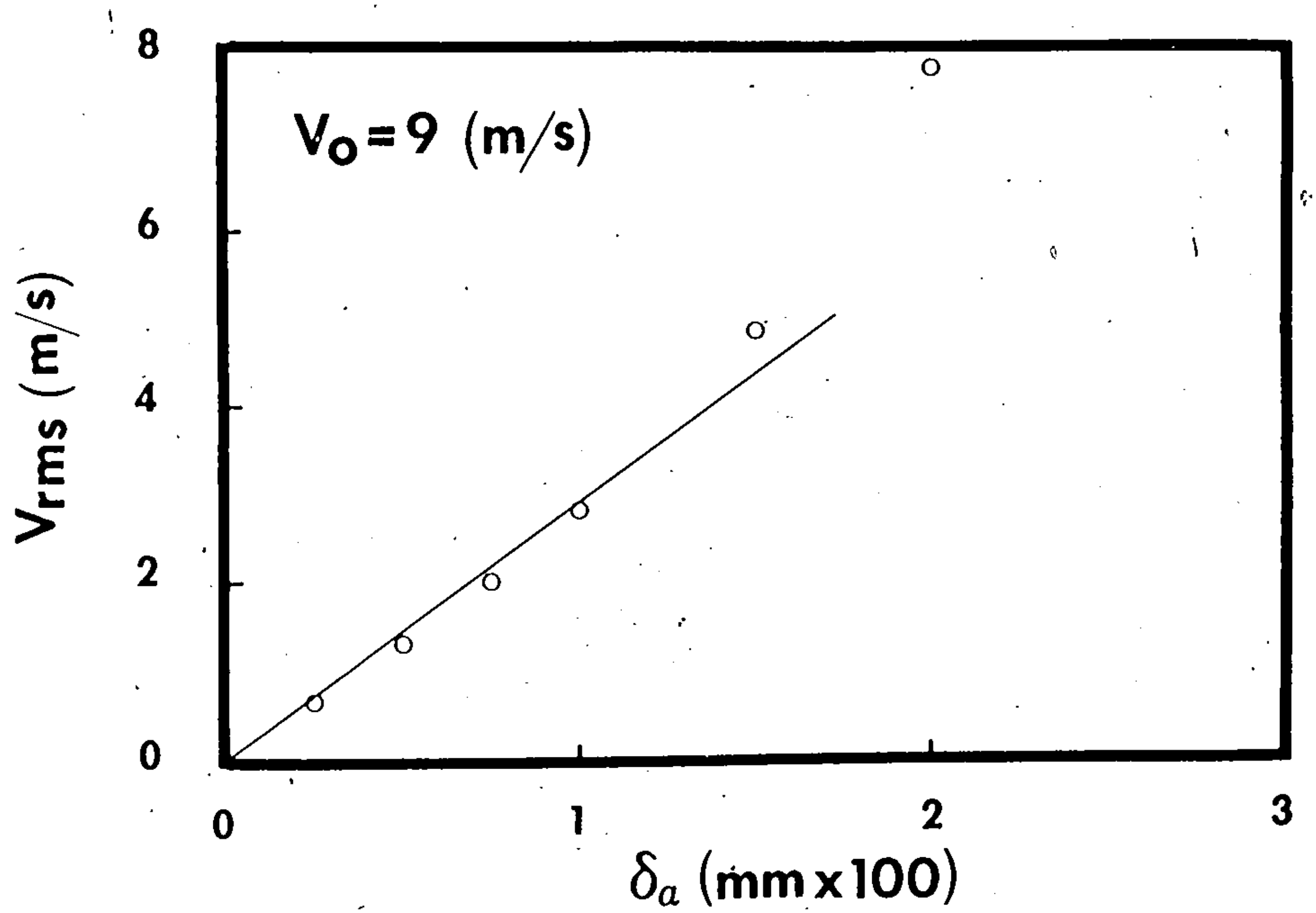

Figure 5.5 : Effect of perturbation displacement on predicted peak RMS velocities. [Lc=4.32cm,d=1.5mm,thetao=5]

Substitution of 5.9 into equation 5.8 and subtraction of the steady state term gives the dynamic pressure component as:

$$dP = 1/2\,\rho\,(1 - 1/A_r)\,(V^2_{rms} + 2\,V_{em}\,V_{rms}) \qquad [5.10]$$

5.4 Stability Analysis

Using a closed loop transfer function type model for the analysis gives the open loop transfer (OTF) function as:

$$OTF = H(f)^{*}\,G(f) \qquad [5.11]$$

where:

H(f) = forward loop transfer function

G(f) = feedback transfer function

In the present analysis the units of H(f) are Pascals/mm while the feedback transfer function has the units mm/Pascal. For a self excited system, a simplified stability criteria used in chatter analysis can be easily applied [5.2]. That is:

$$-1 < \text{real}\,/OTF/ < 1 \quad \text{stable} \qquad [5.12]$$

When multiple modes exceed the stability criteria, the frequency of maximum real/OTF/ is selected. Oscillations may also occur at several frequencies when the real/OTF/ for each of the modes are equal.

The sequence of numerical calculations used to assess the stability and sounding frequencies in the system is given by:

1. For the given geometric set (pipe length, upstream orifice location, cavity length, orifice diameter), and flow velocity evaluate G(f) the feedback transfer function (equation 5.1)
2. For the given frequency range, evaluate the fluctuating pressure at the exit plane of the cavity (equations 5.2 through 5.10) using 10 points over the acoustic cycle.

3. Using 5.12 assess the stability of the pipe acoustic modes. When multiple frequencies are potentially sounding, select the frequency with the maximum real /OTF/.

5.5 Model Predictions

The fundamental shear dimension (δ) is not known. This parameter would depend in part on the orifice geometry, and would also vary slightly with velocity. As discussed earlier, this dimension determines the frequency of maximum gain in the forward loop transfer function for a given flow velocity and cavity length. The value of (δ) was obtained by matching the minimum velocity necessary for sustained oscillation predicted by the model in the sixth mode (nominally 125 hz) with the first measured data point of figure 2.3. In this fashion, the model is forced to predict the occurrence of the coupled fluid/acoustic oscillations in the first sounding mode of the experimental data (nominally 125 Hz) at the lowest velocity used in the tests. It is possible to use the velocities of frequency jumping at higher frequencies/velocities in the experimental data to determine (δ). Using this approach would tend to reduce the errors in the predicted velocities for frequency jumping over the velocity range of interest. However, using the approach chosen will tend to amplify any errors in the model predictions, especially in the upper end of the velocities used in the study. The value of (δ) determined was 1.6mm and was kept constant throughout the rest of the model predictions.

Figure 5.6, 5.7a and 5.7b present the sequence of predicted sounding frequencies for an increasing velocity, the regions of predicted instability, and the experimentally measured data points. The experimental data for the three cases are reproduced from figures 2.3, 2.4a, and 2.4b. The feedback transfer functions used in the three cases correspond to those shown

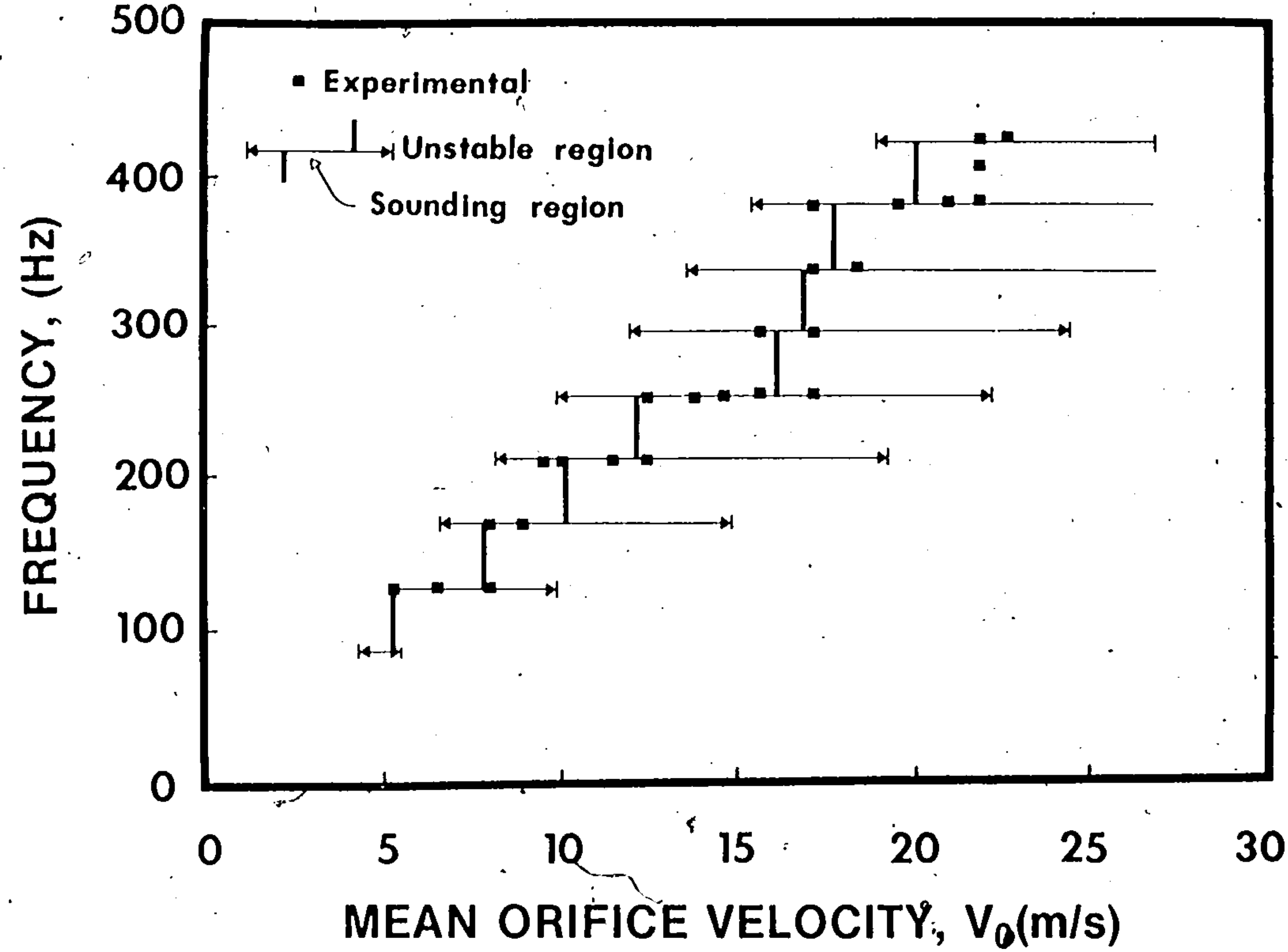

Figure 5.6 : Predicted stability regions, sounding frequencies and experimental data. [Ls=4.06m,Lc=4.32cm,Lp=8.04m]

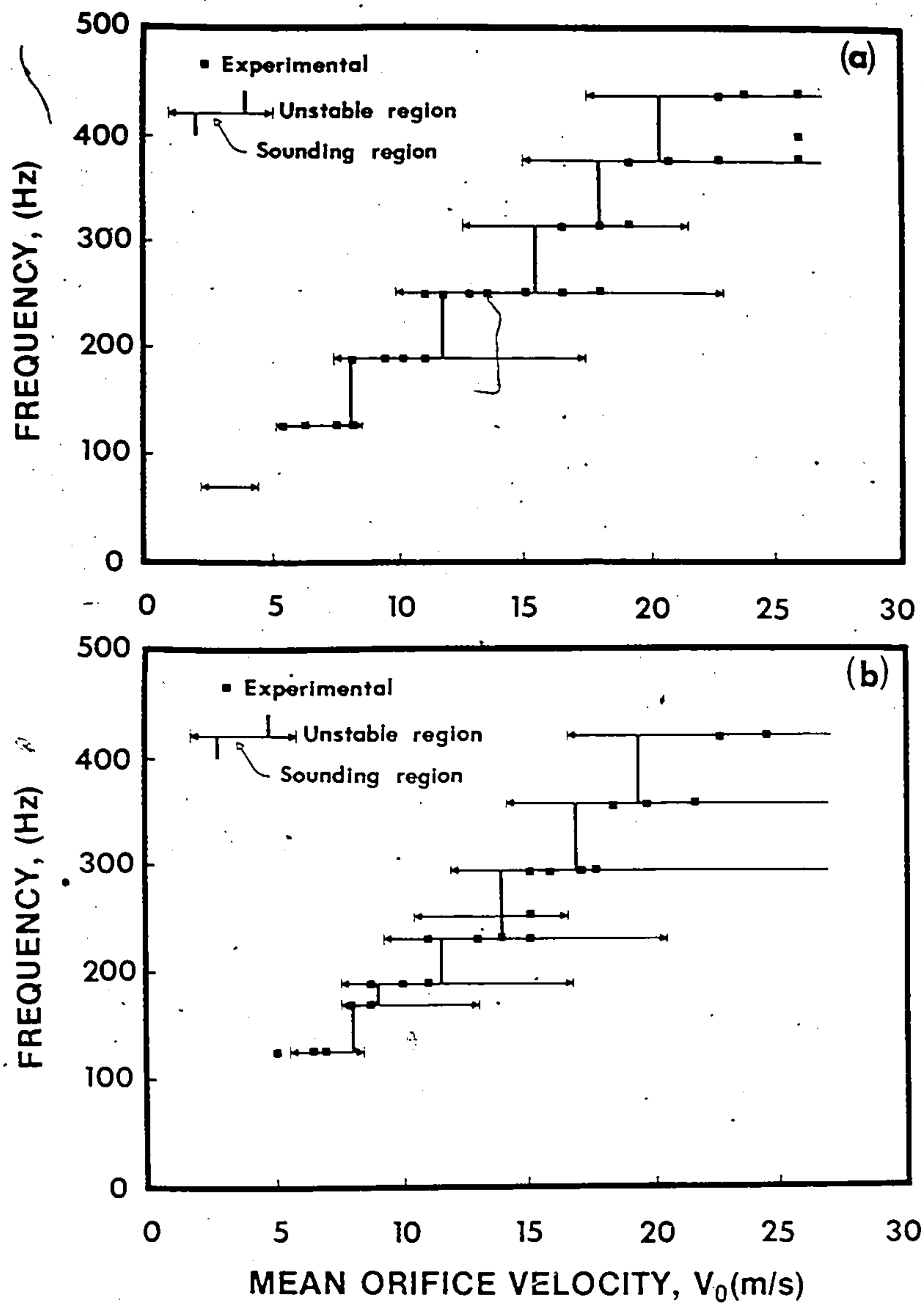

Figure 5.7 : Predicted stability regions, sounding frequencies and experimental data. [a:Ls=5.33m,Lc=4.32cm,Lp=8.04m, b:Ls=2.78m,Lc=4.32cm,Lp=8.04m]

in figures 5.1,5.2a and 5.2b. The maximum velocity used in the calculation was 25 m/s, thus restricting the prediction of the upper limits of stability in the higher frequencies.

There is generally good agreement between the predicted sounding frequencies and the velocities at which they occur, and the measured values. The model predicts a stair case type plot resulting from the lock-in phenomenon as seen in the experimental data. Although difficult to see in the experimental data, this lock-in is often associated with a small rise in frequency from the point of first occurrence until the jump to the next frequency takes place. At the velocities of frequency jumping, there is on occasion a reduction in frequency back to the frequency of maximum acoustic output. These characteristics of the lock-in are also predicted in the model results. However, only the frequency of maximum real OTF in each of the modes has been plotted. The velocities of frequency jumping are generally not associated with the maximum velocity for stability, or the velocity of maximum gain in the open loop transfer function. It occurs when the next sounding frequency exceeds the previous sounding frequency in open loop gain and is strongly determined by the maximum value and shape of G(f). This jump in frequency, dependent on the relative gains in the open loop transfer function, provides an explanation for the large scatter and lack of collapse in the Strouhal number calculation based on the frequency and velocity of first occurrence as plotted in figure 2.8.

It is important to note that the errors in predicting the frequencies of acoustic production arise from the limitation of the 4 pole model. However, the variation in the predicted velocities of frequency jumping with the measured values will depend on both G(f) and the modelling assumptions used in the forward loop of the analysis.

Several important observations regarding the main characteristic of the model prediction can be made from figure 5.6. The model predicts a minimum flow velocity for which no acoustic or fluid oscillations occur. The existence of fluid/acoustic oscillation below the first measured data point is predicted by the model. There also exists in the model predictions a velocity region above the minimum threshold velocity (approx. 2 m/s) for which no fluid/acoustic oscillation will occur. While these predictions require further experimental work to validate, they seem intuitively correct. Unfortunately, the first measured data point was obtained rather arbitrarily, using the experimentalist's ear to assess the existence of the sounding frequencies. In retrospect, it is clear that the A weighting characteristic of the human ear, resulting in significant attenuation at the frequencies involved, combined with attenuation loss of the sound transmitted to the surroundings make this a poor measuring instrument in this case. The flow visualization apparatus, the use of microphones or hotwire anemometry is a far better method for determining the existence of fluid/acoustic oscillations in this frequency/velocity range. Although the model does not predict any oscillations at 402 Hz, the criteria for instability in this mode was within 10% of being met. It is felt that the acoustic model at these higher frequencies is slightly over estimating the effective damping, and accounts for the absence of a clear peak in the feedback transfer function at 402 Hz of figure 5.1.

The predictions of figure 5.7a also indicate the possibility of fluid/acoustic oscillations below the first measured data point. However, as discussed previously, it is felt that this is a limitation in the experimental data, and not an erroneous prediction. The predicted region of stability (no fluid/acoustic oscillations) is wider in this instance, and results from the larger frequency separation between high amplitude peaks in G(f). This is seen in figure 5.2a as a clear separation between 65 Hz and 127 Hz.

The low frequency, low velocity considerations of the previous two cases also apply to the theoretical predictions of figure 5.7b. Of particular interest in these results are the absence of single frequency oscillations occurring at 252 Hz despite the potential for oscillations. This absence of single frequency oscillation is also seen in the measured data.

5.6 Critical Gain Estimates

The developed theoretical model can be used to estimate the minimum acoustic gains necessary to sustain the coupled fluid/acoustic oscillations. A variable gain control block was placed in series with the acoustic feedback transfer function of figure 5.1. The attenuation necessary to just satisfy the stability criterion was determined in each of the sounding modes. Table 5.2 summarizes the results of the calculations where the Strouhal number is based on the cavity separation ($lc = 4.32$ cm) and the velocity corresponds to the point of peak open loop gain for the given frequency. Acoustic perturbation displacements which might be a more important parameter in estimating potentially oscillating situations are easily calculated from the values provided.

Frequency (Hz)	Velocity (m/s)	St	(ρcU/dp) min
42.5	2.05	0.89	2.8
85.0	4.2	0.87	2.5
126.25	7.2	0.76	2.0
168.25	8.2	0.88	1.6
252.5	14.8	0.73	1.1
337.5	19.6	0.75	0.85
420.0	24.4	0.74	0.72

Table 5.2 Critical gain estimates

It has been demonstrated that the acoustic feedback transfer function (G(f)) of the model, can be used to identify possible sounding modes in the acoustic system. However, it has also been shown that this function by itself will identify more sounding frequencies than were determined experimentally for a given rig geometry. In the next two subsections of this thesis, two separate sets of experiments will be examined. The results of these experiments when used in conjunction with the evaluation of G(f) illustrate the possible use of this function in identifying potential sounding frequencies, as well as some of the limitations of the developed theoretical model.

5.6.1 Case Problem 1

The source identification experiments of the previous chapter can be used to illustrate the use of the minimum gain values in estimating the potential for acoustic/fluid oscillations. The effect of the exit orifice plate on the piping acoustics is significant, and is a result of the strong velocity dependent change in the exit impedance. As discussed in chapter 4, the change in the exit impedance with flow occurs primarily in the lower frequency range and can be efficiently modelled using a quasi static estimate of the impedance from the steady state pressure drop across the exit plane.

Figure 5.8a presents the predicted particle velocity transfer function, computed using the geometry present during the source identifications experiments with the exit orifice plate in place. No account was made in the acoustic model for the presence of the orifice plate at the plenum entrance. Figure 5.8b presents the function computed using the equivalent length data of [4.24] to model the exit orifice plate. The experimental sounding frequencies are labeled on both figures. There is improvement in the alignment of the peaks in figure 5.8b, and the labeled sounding frequencies. There is also an improvement in the coincidence of the measured sounding frequencies and the frequency of the largest peaks in the computed function. This gives confidence in the acoustic model as well as the use of this function to determine the likely frequencies of acoustic production. There is, however, no indication in

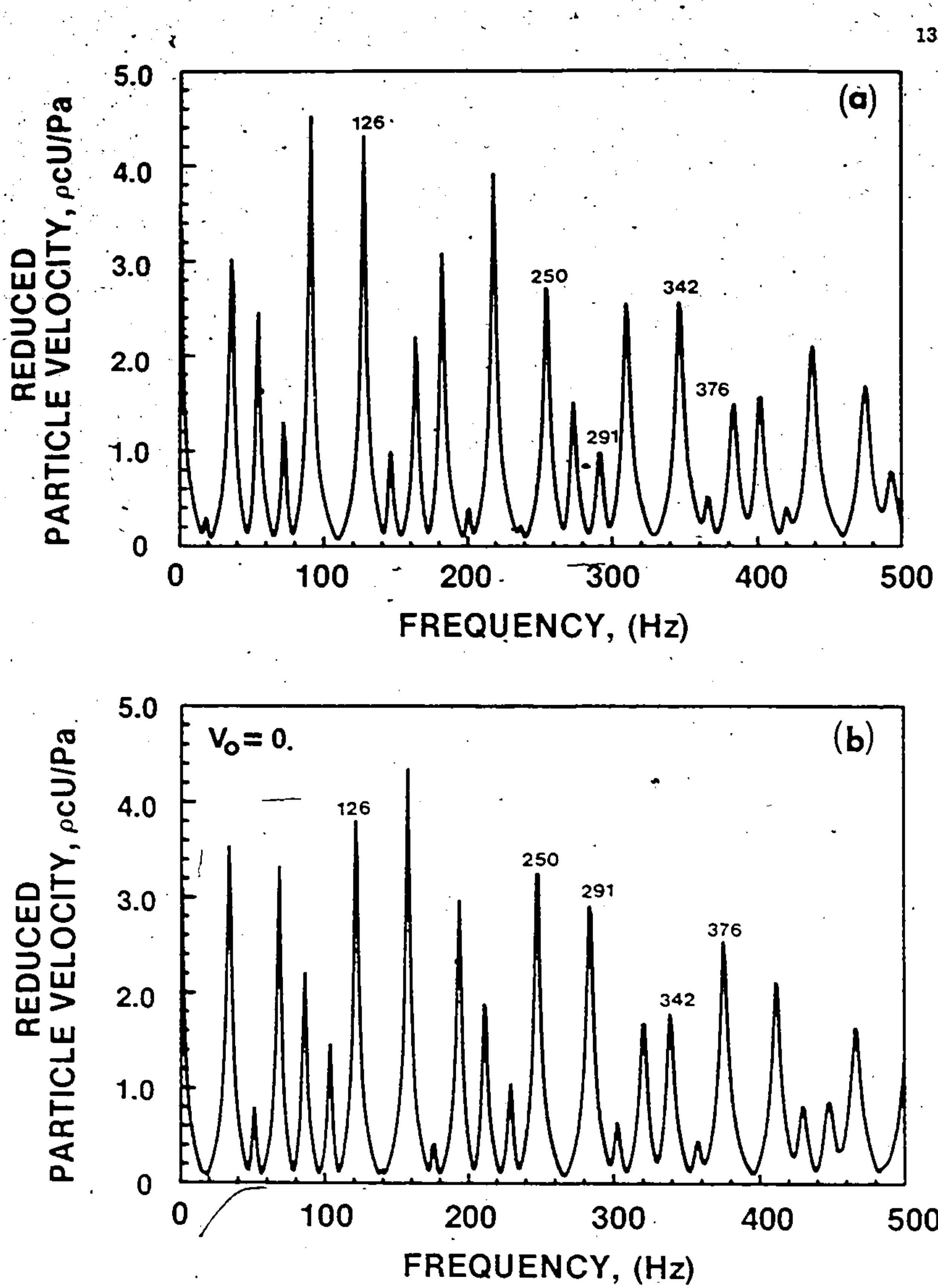

Figure 5.8 : Reduced acoustic particle velocity per unit dipole sound. [Ls=5.4m,Lc=9.0cm,Lp=9.29m] [a:exit impedance=0., b: orifice modeled using equivalent approach,c-g same as b with quasi static estimate of exit impedance.]

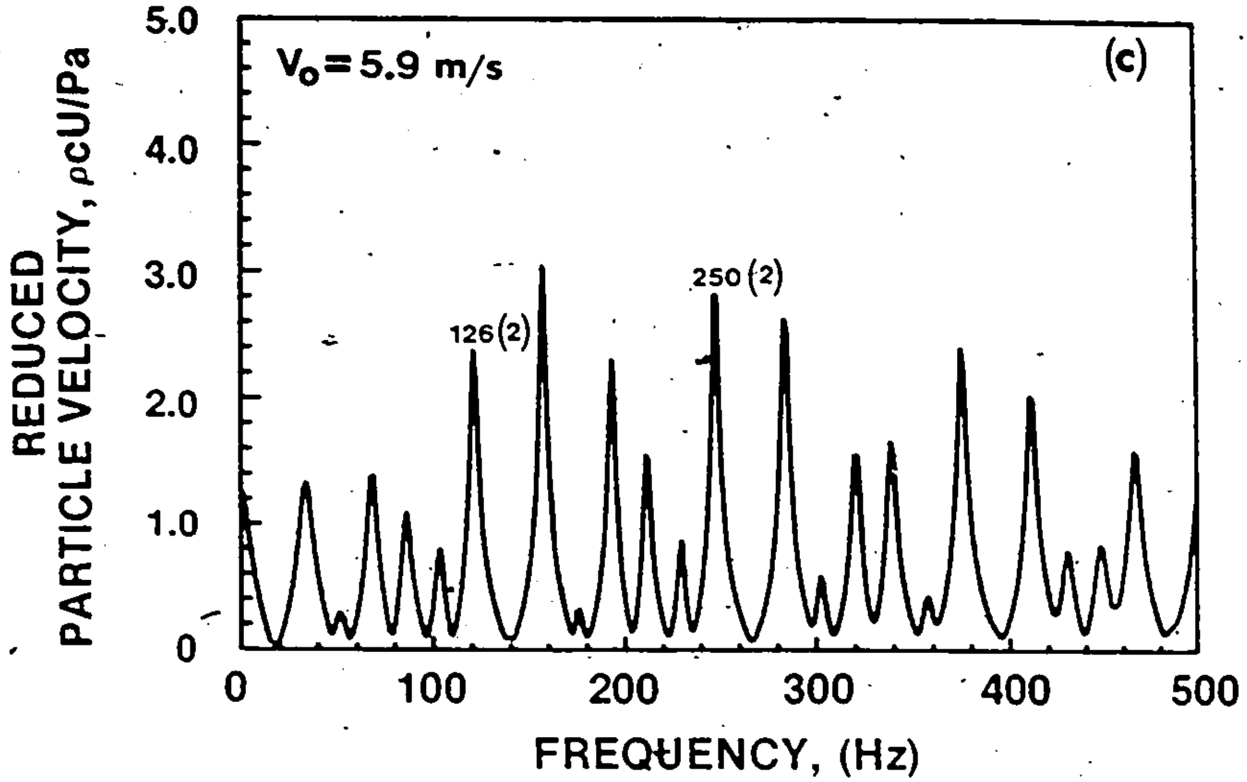

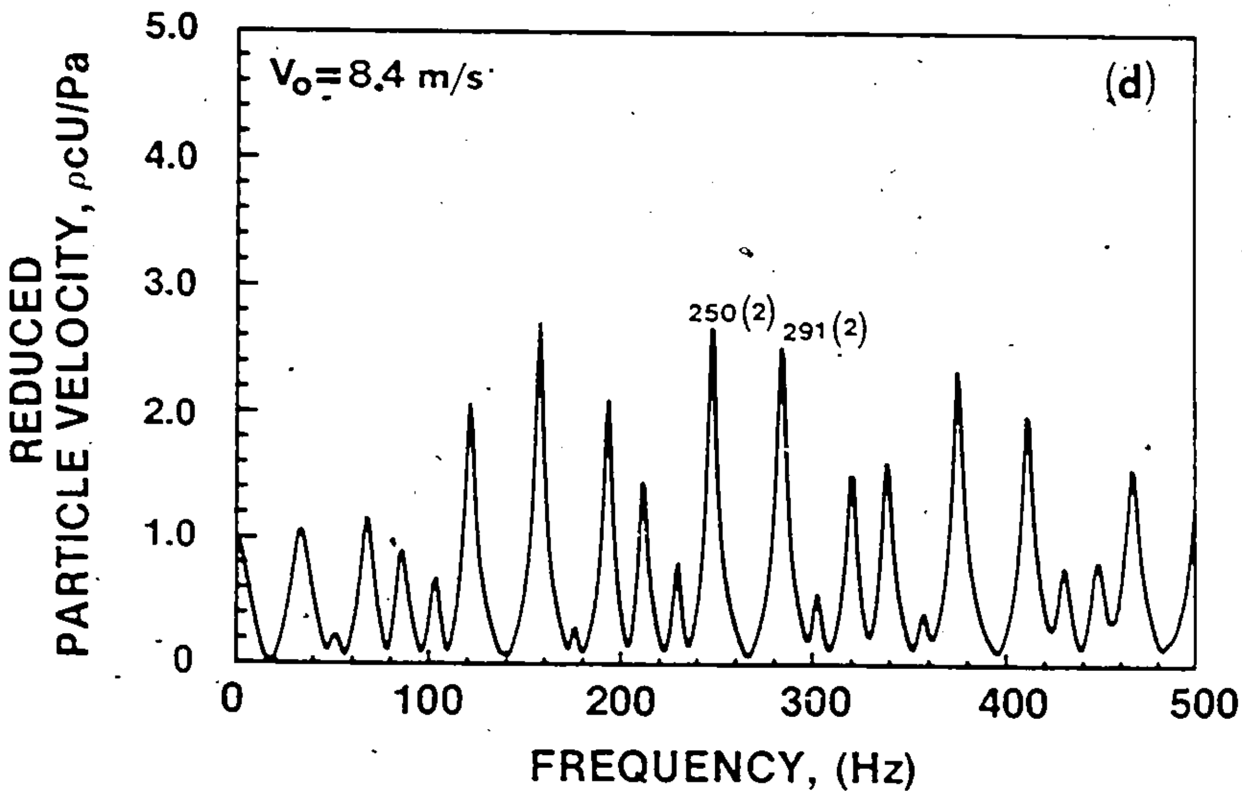

Figure 5.8 continued

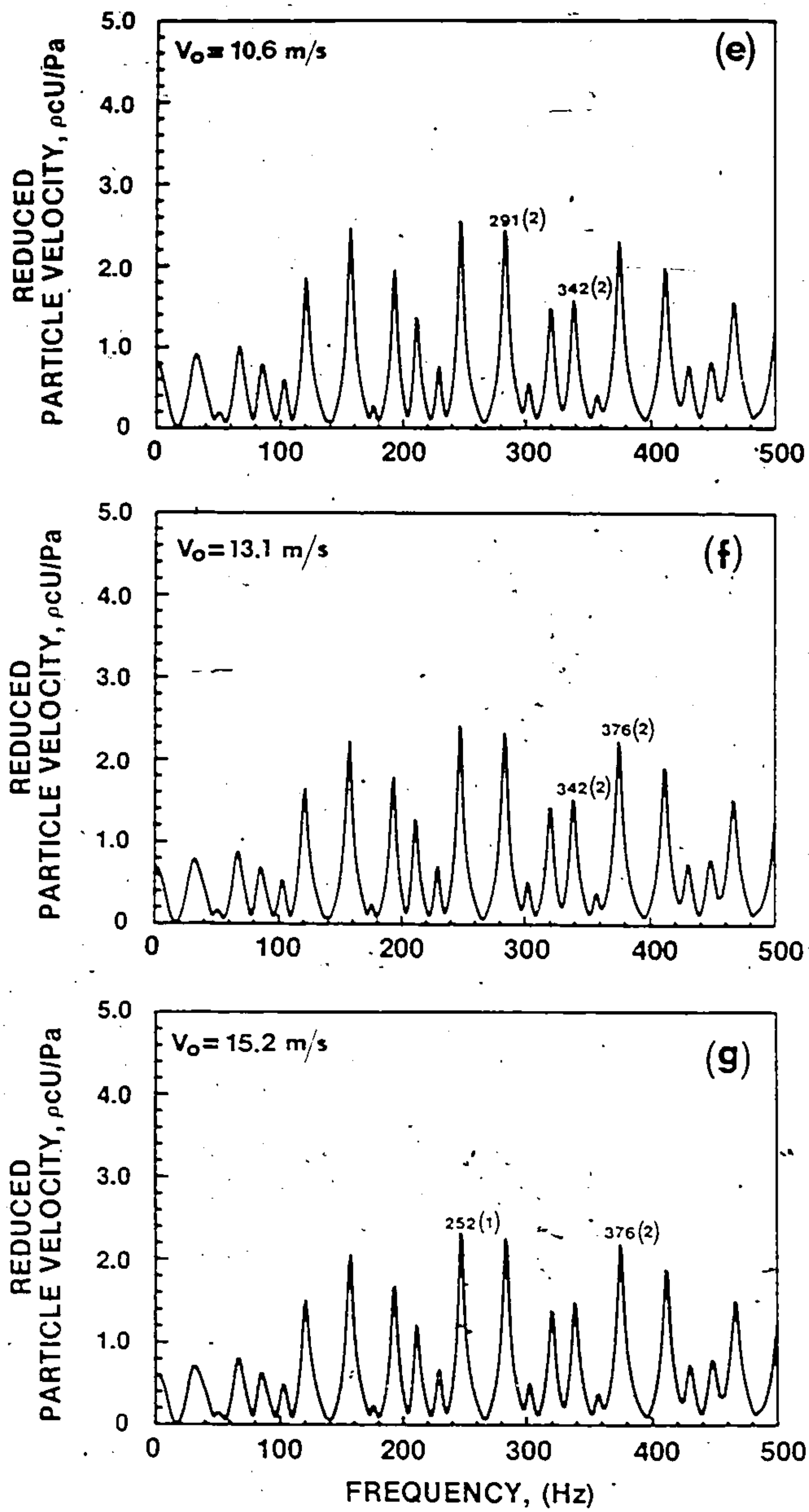

Figure 5.8 continued

the shape or appearance of the predicted function (computed for zero flow velocity) that might explain the jump in the shear layer oscillation to the n = 2 mode.

Figures 5.8c through 5.8g present the calculated particle velocity transfer function at the flow velocities of peak acoustic production. Also labelled are the sounding frequency, the "next" sounding frequency and the mode of the shear layer oscillation determined using the flow visualization apparatus. The acoustic model utilizes the equivalent length model of the orifice plate, as well as the quasi-static estimate of the exit impedance using the measured static pressure drop across the piping exit plane. There is a significant attenuation in the predicted peak values of the transfer function, primarily at the lower frequencies. There is also a small improvement in the alignment of the labelled sounding frequencies and the location of the peaks in the transfer function. In figure 5.8g the jump down in frequency with an increase in velocity is associated with the change in the mode of oscillation. The first measured sounding frequency is 126Hz (n=2). Using table 5.2, the n=1 mode at this flow velocity would require a minimum ρc*U/dp of roughly 2.4. This is significantly greater than the calculated value at 63 Hz of figure 5.8c. At higher flow velocities there is sufficient acoustic feedback to support oscillations in the n=1 mode, however, the experimental data indicates oscillation in the n=2 mode until a flow velocity of 16.1 m/s. Based on these observations it appears that there is a "lock-in" on the mode of shear layer oscillation as well as the well known lock in on frequency.

The results of this case study illustrate the strength of the four pole modelling procedures, and their use in evaluating ~~GFI~~. The results also validate in part the use of the minimum gain criterion in determining the potential of fluid/acoustic oscillation in the fundamental shear layer mode (a single vortex in the cavity). However, limitations in the present model were are also revealed in that the jump to higher shear layer modes of oscillation which occurred in the experimental results could not be predicted.

5.6.2 Case Problem 2

The data of a brief experiment conducted early in the experimental program are presented in figure 5.9. During a period of partial rig dismantlement, the cavity resonator was mounted to the first acrylic pipe section (closest to the plenum), without further upstream sections attached. The velocity was measured using a hotwire positioned on the centerline of the pipe at the plane of the downstream face of the upstream orifice plate. The resulting frequency/velocity plot is substantially different than previously presented graphs. There is a region of apparent lock in centered about 120 Hz, however, there is a substantial rise in frequency with velocity through this range. A jump in frequency from 126Hz to 207 Hz occurs, followed by second region of lock in which also displays a large frequency rise. There is a jump down in frequency with a increase in velocity from 261 to 257 Hz. This is followed by a velocity region of unsteady broader band noise production. It was not possible to detect any periodic fluid oscillation using the flow visualization apparatus in this velocity region. Pure tone acoustic production is reinstated at a flow velocity of 42 m/s at a frequency of 357 Hz. The upper frequency velocity data exhibit a uniform increase in frequency with velocity. The straight line through the data was chosen to best fit the last three data points. The Strouhal number provided on this graph is based on the slope of the line and the cavity length ($lc = 8.4$ cm). Figure 5.10 presents the reduced acoustic velocity transfer function, computed using the geometric data producing the data set of figure 5.9. The maximum values in the computed function are clipped in the plot allowing the results to be presented using the vertical scale of previously presented calculations. The peak height at 121.5 Hz is 13.4, the peak height at 233.75 Hz is 14.7. Also shown in figure 5.10 is an estimate of the minimum acoustic gain in the computed function required to support the acoustic/fluid oscillation in the $n = 1$ mode. This curve was estimated from the data in table 5.2 and a Strouhal number of 0.61. Due to the

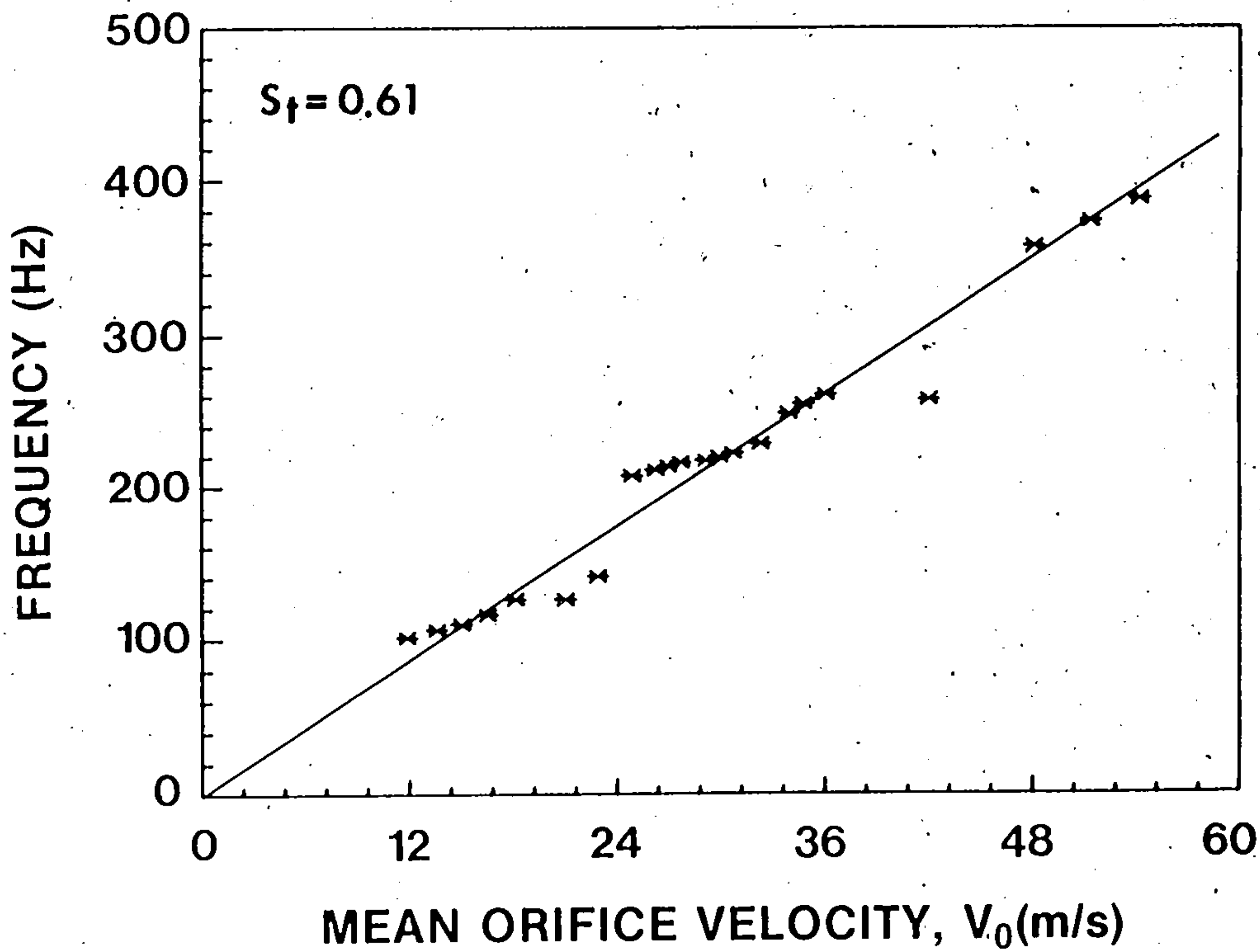

Figure 5.9 : Frequency of acoustic production versus mean orifice velocity, cavity mounted on first pipe section. [Lt=1.36m, Lc=8.4cm]

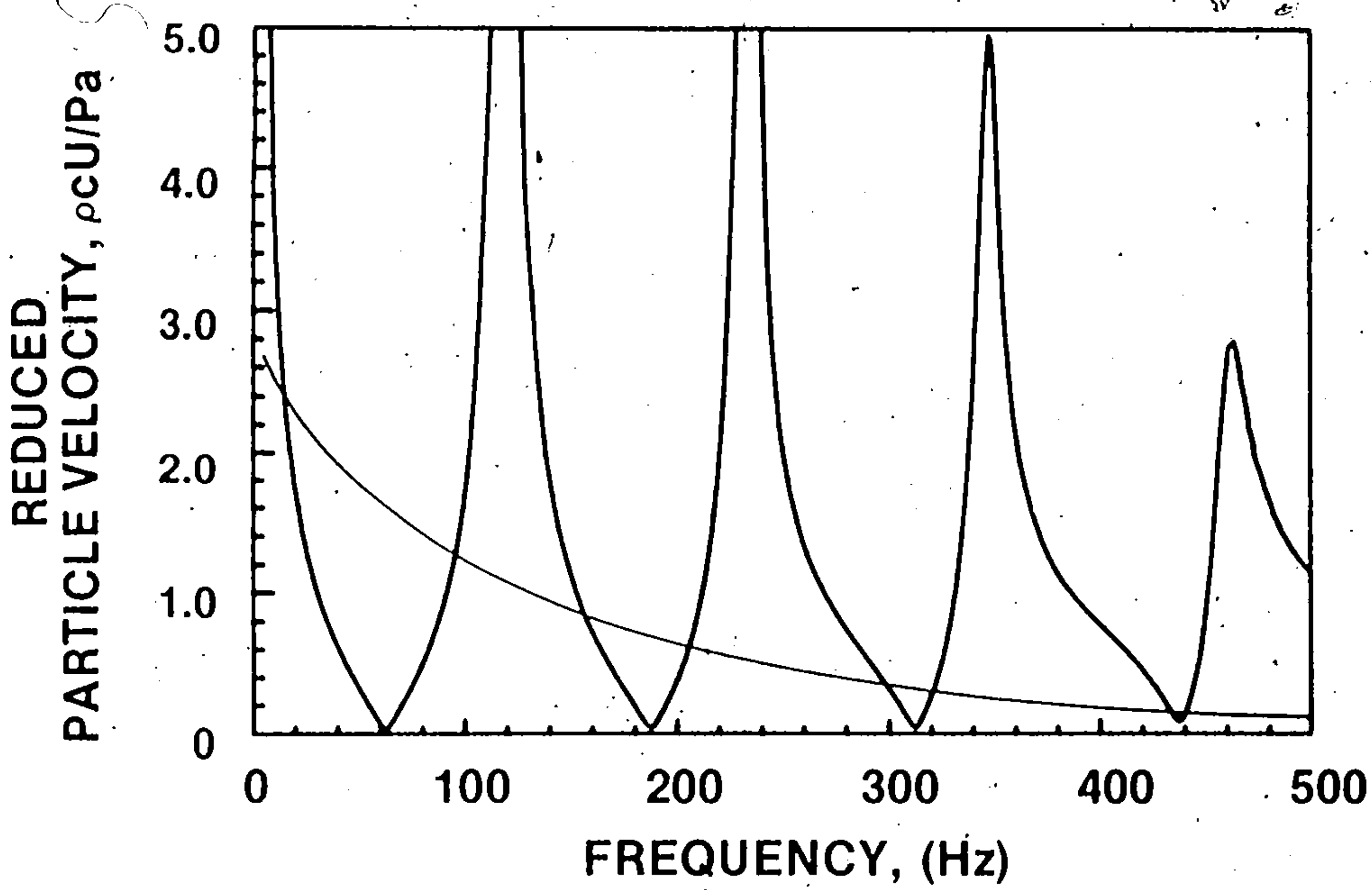

Figure 5.10 : Reduced acoustic particle velocity versus frequency. [Lt=1.36m, Ls=8.4cm]

limitation in the upper velocity values of table 5.2, the curve above 200 Hz is extrapolated from the curve below 200 Hz. The acoustic model used in the calculation incorporates the previously measured exit impedance value, without modelling the acoustic interaction between the short pipe and the plenum. The entrance impedance as seen from inside the pipe was set to zero. Despite limitations in the calculations, general observations can be made. There is an increase in the frequency region of intersection between successive peaks in the transfer function and the estimated required minimum value. At higher flow velocities, virtually all frequencies (related through the Strouhal number) satisfy the minimum gain requirement. As well, at higher frequencies there is significant peak height attenuation. Both of these conditions suggest the frequency velocity plot displayed in figure 5.9. The loss of pure tone production and clearly identifiable periodic fluid oscillation at 257 Hz occurs before the predicted narrow region at 300Hz. There is, however, reason to suspect the acoustic model used in the analysis given the very short pipe used in the experiments. Also, there may be a difference between the centerline and shear velocity given the absence of any piping sections and flow conditioners preceding the upstream orifice plate.

The experimental data presented in this second case study highlight an aspect of the fluid/acoustic phenomenon investigated in this thesis. That is, the tendency for a reduced lock in effect when there is sufficient amplification over a wide frequency range to support the oscillation, and, when there is no dominant frequency to control the fluid/acoustic system. When this situation occurs, a frequency/velocity plot is obtained which possesses less of a step like appearance, and a more readily identifiable Strouhal characteristic.

5.7 Summary

A transfer function, control theory type analysis of the fluid/acoustic oscillator was developed. The acoustic feedback portion incorporates a 4 pole model of the piping system.

This is combined with published shear layer growth characteristics for a 2 dimensional inviscid shear layer. The critical model parameter (δ) for the shear layer was determined by matching the predicted minimum velocity necessary for sustained oscillation at 125 Hz, with the lowest measured velocity in the experimental data where sound production at 125 hz was detected. The model predicts the velocity of frequency jumping reasonably well when this value is used over a wide frequency/velocity range. The use of a constant, velocity independent characteristic shear dimension (δ) will account for some of the increase in the error in the predicted data at the higher velocities.

The model predictions suggest that the measured velocity of frequency jumping does not define the stability limits of the oscillation for a given acoustic mode. The existence of stable regions (no acoustic production in $n=1$ mode) for particular velocity/frequency values predicted using the developed model could not be verified with the present experimental data. The reduced acoustic particle velocity for the experimental conditions incorporating the exit orifice plate was calculated for the flow velocities of maximum acoustic production. Application of the minimum gain criteria predicted that there would not be $n=1$ shear layer mode oscillation in the first likely sounding piping acoustic mode (63 Hz). This was supported from the experimental data. However, the experimental results reveal a jump to the $n=2$ mode (126 Hz) which cannot be predicted using the present model.

The results of the theoretical model raise many questions which can best be answered through further experimental work. Experimental design recommendations which are based on the results and trends predicted by the model will be discussed in the next chapter.

CHAPTER 6

SUMMARY AND CONCLUSIONS

6.0 Introduction

A variety of topics which deal with the problem of acoustic resonance in pipelines have been investigated in this thesis. The areas of study include: detailed measurements of a pure tone noise source, development and testing of a fundamental acoustic measurement technique, the generation and testing of an acoustic model of the piping system, application of a general noise source characterization method to the source identified in chapter 2, and finally the development of a theoretical model explaining many of the characteristics displayed by the cavity resonator. A chapter by chapter summary of the major results and contributions of the work presented in this thesis is provided in section 6.2. Also included in this chapter is a general discussion of the phenomenon, conclusion regarding the applicability of the results, and proposals for future work, particularly related to improved experimental design.

6.1 Chapter Summary

6.1.1 Chapter 2

A literature review examining recent experimental work, and theoretical model developments pertaining to the generation of acoustic resonance in ducts and pipes was presented. A flow arrangement, and resulting acoustic source was identified which was capable of low frequency acoustic production. Previous researchers identified the strong dependence of the acoustic production and coupled fluid dynamics on the Q factor (damping) in the excited mode. It was also demonstrated by earlier researchers that the acoustic production of this flow arrangement was dependent not only on the damping, but was influenced strongly by the position of the source within the piping (ducting) system. The experimental program outlined in chapter 2 was undertaken in order to identify more clearly the acoustic mode selection characteristics of this type of resonator. As well, the influence of the cavity geometry on the frequency/ velocity relationship was investigated. The possibility of eliminating completely the periodic fluid oscillations and coupled sound production by the introduction of high turbulence levels was investigated. This approach has been applied by previous researchers to eliminate the vortex shedding process and coupled sound production generated by cylinders subject to cross flow, but has never been investigated ~~in~~ relation to cavity oscillators in pipelines.

The experimental program utilized a facility designed and built for the work presented in this thesis. The acoustic source was generated by placing two standard geometry orifice plates in the flow. The orifice plate separation distance was small (< 2%) in comparison to the acoustic wave length of the lowest frequency excited. It was determined that the source interacted with those acoustic plane wave modes possessing a pressure node (velocity anti node) at or near the cavity location. The Strouhal number based on mean orifice velocity and orifice plate separation ranged from 0.5 to 1.0 and was sensitive to both cavity diameter and velocity. The sensitivity of Strouhal number to cavity diameter decreased with increasing diameter. The sensitivity to velocity is in part due to the lack of flow conditioners immediately upstream of the separation point. An estimate of the peak modal pressures in the sounding modes indicated an insensitivity in acoustic production to velocity. This can be explained by an early saturation in the ability to extract acoustic energy from the flow. A flow visualization study showed the presence of an oscillating shear layer near the upstream orifice plate, and subsequent roll up and propagation of a large scale vortex. Hotwire anemometry measurements at the downstream orifice plate indicated strong axial velocity fluctuations. The RMS velocity was a maximum at the pipe centerline when the shear layer (located using the flow visualization method) was at a minimum radial position. It was demonstrated that the periodic fluid oscillation and acoustic production could be eliminated if sufficient random turbulence was present at the shear point. The scale of the turbulent velocity fluctuations which destroyed the periodic oscillation was estimated to equal the acoustic velocity amplitudes during acoustic production before the introduction of the turbulence generators.

6.1.2 Chapter 3

In this chapter a literature review of basic acoustic measurement techniques related to the identification of impedance values in piping systems was presented. A method suitable for in situ determination of passive, non radiating components was selected and tested. Also examined was the two microphone method for acoustic intensity calculations. It is recommended that this approach be used in future work to characterize the acoustic output and flow energy extraction ability of the source. An acoustic model of the piping system is not required to utilize the intensity analysis, decreasing significantly the potential for inaccuracies in the results.

A novel measurement technique utilizing coherent spectral analysis methods was developed to allow impedance estimation in the presence of a contaminating noise source. This two microphone method is easily extended to acoustic intensity measurements, as well as the 4 pole acoustic impedance measurement approach examined in chapter 4. It was proposed in the open literature that a multi-pass data acquisition could be used in performing selective acoustic intensity measurements. The feasibility of using a multi-pass data acquisition with the developed impedance measurement approach was investigated in detail. It was demonstrated that two passes of data acquisition can introduce errors (attributed to bias errors) which are amplified through the matrix inversion implicit in the impedance calculation. However, utilization of the 4 pole method of impedance estimation in conjunction with the coherent cross spectral measurements will provide a viable method for estimating source impedance during sound production.

6.1.3 Chapter 4

In this chapter the 4 pole method was used to develop an acoustic model of the piping system. The acoustic model incorporated impedance functions obtained using the procedures outline in chapter 3. Detailed testing of both the model's predictive ability, as well as the experimental procedures necessary for accurate model construction was undertaken. It was demonstrated that impedance estimation using measured acoustic pressure ratios and the 4 pole model directly can introduce significant errors into the calculations which can easily go unnoticed. These errors arise from frequency resolution limitations which must be present when using a discrete Fourier transform.

A general source characterization method using the 4 pole model was applied to the double orifice resonator investigated in chapter 2. This approach, which has been applied by earlier researchers to broad band acoustic source was unable to generate a unique characterization of the acoustic production.

6.1.4 Chapter 5

In this chapter, the acoustic production and coupled fluid oscillations generating by the double orifice flow geometry was modelled as the instability of a self excited system. The analysis combined the acoustic model developed in chapter 4 with published growth characteristics of separated flows. It was demonstrated that calculation of the reduced acoustic particle velocity at the upstream orifice plate per unit of dipole sound at the downstream orifice identified the likely frequencies of acoustic production. This transfer function, which is closely related to the reciprocal of the impedance at the source location quantifies the effects of cavity location, cavity geometry, net system acoustic damping and can be used to locate potential troublesome source positions in a piping system.

A fundamental model parameter was obtained by matching results predicted by the theoretical model with a single experimental data point. Using this approach, the model is likely to incur larger errors in the higher velocity ranges of the study. The model was able to predict reasonably well the sequence of measured sounding frequencies. The model predicts stable regions where no acoustic production is expected. Using the developed model, minimum acoustic gain values were estimated which are required to support the coupled fluid/acoustic oscillation. Experimental data was obtained which suggested the tendency of the system to oscillate at higher shear layer modes when this criterion was not met.

6.2 General discussion

The self excited model of the acoustic/fluid phenomenon does not include any incompressible effects which influence the separation, growth, and roll up of the shear layer. In this sense the model only accounts for the effect of the acoustic environment on the ability to support the resulting oscillations. It is well known that the basic phenomenon of cavity oscillations can exist in the absence of acoustic reinforcement. The photograph of figure 6.1 was taken using the flow visualization technique outline in chapter 2. It shows the flow pattern through the test section of a scale model of an hydraulic leaf gate. Air bubbles injected upstream of the upstream gate were used to seed the flow. The roll up and propagation of the large scale vortex is virtually identical to that shown in the sequence of photographs of chapter 2. Significant structural vibration involving the test section, feed and discharge pipes existed, with many frequencies in the structural response spectrum. The

Figure 6.1 : Still photograph of flow between gates in hydraulic gate model, (gates fixed).

phenomenon depicted in figure 6.1 was very unsteady with the frequency of oscillation varying between the frequencies seen in the structural response spectra. In an earlier dynamic model study of the leaf gate, it was found that the flexible mounting of the upstream gate, resulted in significant gate vibration and a very steady phenomenon. In the context of the self excited model developed in chapter 5, the gate vibration replaces the acoustic response in supplying a steady perturbation displacement at the separation point.

The regions of stability predicted using the theoretical model arise because of the exclusion of the incompressible effects which support the oscillation. These incompressible effects include the frequency independent, instantaneous interaction of the small scale vorticity present in the separated flow. From an designer's perspective trying to avoid acoustic resonances in a pipeline, it may be sufficient to ignore these effects altogether. However, from a hydraulic engineering perspective, ignoring the incompressible effects may lead to disaster. It was not possible to identify large scale periodic fluid oscillation in the pipeline with out significant acoustic production. Similarly it was not possible to observe large scale periodic fluid oscillation in the gate test section without structural motion. When the structural motion was small (fixed gates) the fluid oscillations were unsteady. These observations suggest that the incompressible effects are only important when the elastic response (either acoustic or structural) is small.

The role of mean turbulence level at the separation point on the phenomenon has not been investigated in significant detail. The developed theoretical model neglects turbulence at the separation point altogether. However, it was demonstrated clearly in chapter 2 that turbulence could eliminate completely the oscillations. The effect of turbulence in the theoretical model might be accounted for by using the difference between the available acoustic perturbation displacement (calculated from G(f)) and the random turbulent displacements at the separation point as the feedback portion of the analysis.

Using this approach, the degree of turbulence, and its effect will vary with velocity and the acoustic environment.

6.3 Conclusions

Acoustic resonance generation by a cavity in a pipeline was studied experimentally. A simple model of the phenomenon was also developed. Despite its simplicity, the predictive ability of this model, both qualitatively and quantitatively, was good. This theoretical model incorporated published characteristics of separated inviscid sheared flows, with a model of the acoustic system utilizing measured impedance functions. It is important to recognize that the measured impedance functions are in fact derived quantities. In chapters 3 and 4 of this thesis it was demonstrated that determination of the system impedance functions are strongly influenced by the discretization error which must be present when using a discrete Fourier transform. The height and width of the peaks in the feedback portion of the theoretical model are directly affected by these "measured" impedance functions. This, in turn, influences the regions of predicted fluid/acoustic oscillations, the predicted sequence of sounding modes, and the lower limiting velocities necessary for fluid/acoustic oscillations to occur. Thus, one is forced to conclude that the theoretical predictions are as sensitive (and possibly more sensitive) to the acoustic model (which for such a simple experimental system would appear easy to obtain), as they are to the significant simplifying assumptions used to model the fluid mechanics. Given the complexity of industrial ducting and piping systems, resonance avoidance at the design stage utilizing the minimum gain approach (outlined in chapter 5), rather than modification and attention to detail in the flow control device would be the wrong approach. However, given an existing system, the results of the work presented in this thesis may be used to identify likely source locations. Computation of the feedback transfer function G(f), using best estimates of the system impedance parameters for potential source locations (ie.,valves), may locate quickly the source. The results of this thesis confirm that separated regions, with sharp re-attachment points are to be avoided. However, the results also indicate that a successful modification to eliminate the acoustic production may be the generation of significant turbulence at the separation point.

6.4 Proposals for future work

The effect of mean turbulence on the performance of the cavity resonator, and its relative scale to the acoustic particle velocity should be investigated further. The relationship between the cavity resonator's ability to extract energy from the flow as function of flow velocity should also be examined in more detail. This is best achieved utilizing the intensity measurements outlined in chapter 3. A flow conditioner located upstream of the cavity should be utilized to reduce some of the variation in shear velocity and shear angle with velocity.

The model predicts regions of velocity where acoustic/fluid oscillations are not expected. The characteristics of the cavity resonator in these predicted stable regions, and the effect of the piping acoustics (cavity location and net acoustic damping) on the resulting fluid/acoustic oscillation (if any) should be investigated in detail. By using a short pipe, the frequencies of potential fluid/acoustic oscillation will be well separated. Combining this with a reduced orifice plate separation will produce predicted velocity regions where no acoustic production is expected. For a fixed source location, the effect of net acoustic damping can be investigated by modifying (by dissipative damping) the exit conditions of the piping system. Alternatively if higher frequencies are used then reactive resonance suppression is possible. Figure 6.2 presents the computed velocity transfer function utilizing the geometry which may best separate potential sounding modes, as well as offer the potential for reactive suppression

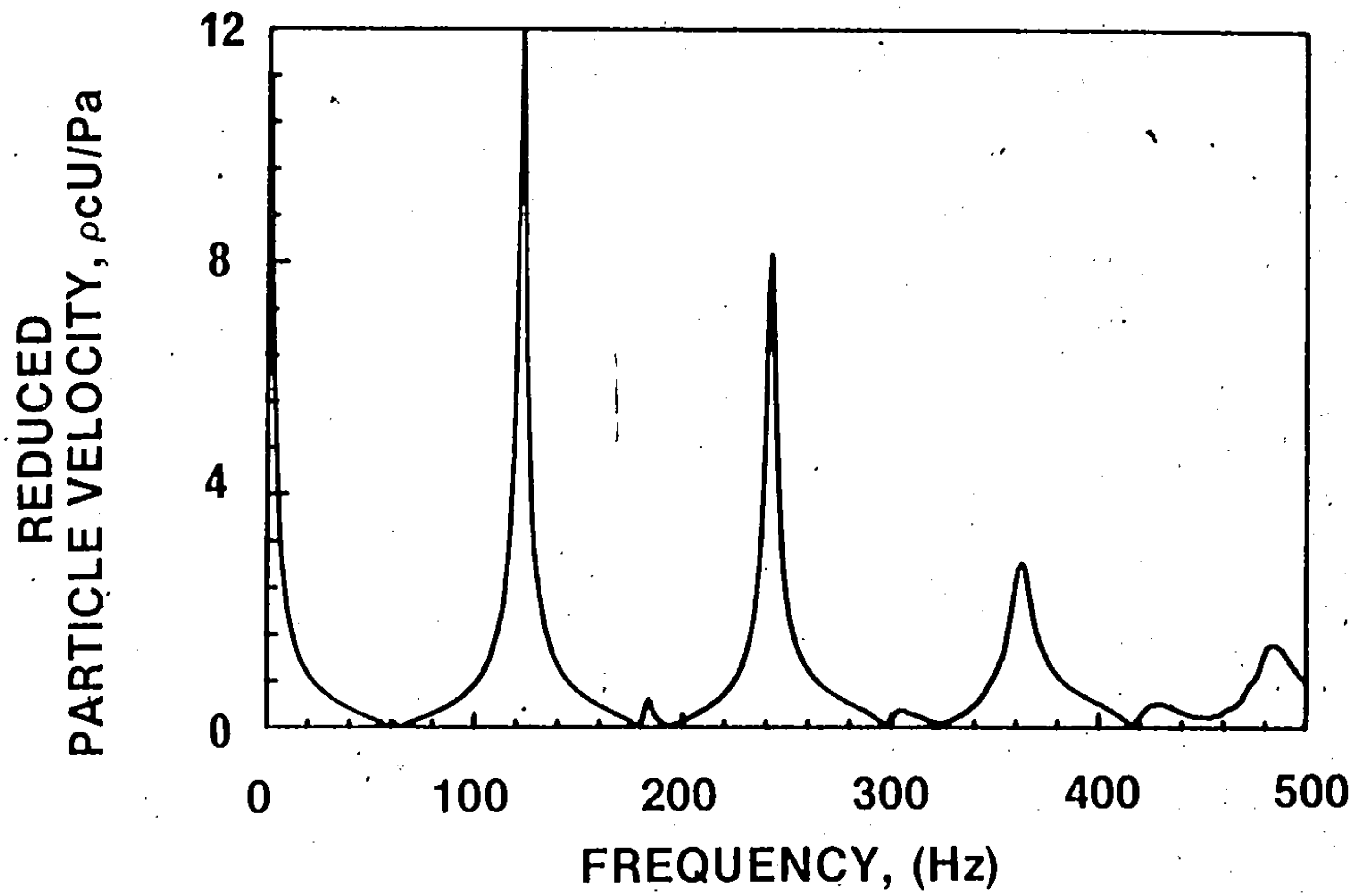

[6.2] Reduced acoustic particle velocity per unit dipole sound.
[Ls=1.3m, Lc=4.3cm, Lp=2.77m]

using physically realizable sized side branch resonators. The length of the available upstream acrylic section with the attached bellmouth as well as the last section attached to the plenum was used in the calculation. By locating the source near the centre of the pipe, the potential sounding frequencies are well separated. Using a side branch piping section to suppress the peak at 125 hz will require a resonator pipe length of less than 1.5 m. By making this variable in length, the 250 hz mode can also be suppressed. The challenge will be to design sufficient bandwidth into the side branch resonator to allow control of the degree of suppression in the selected frequency.

REFERENCES

[1.1] "Flow Induced Structural Vibrations", IUTAM-IAHR Symposium Karlsruhe 1972, Editor: Eduard Naudascher, Springer-Verlag.

[1.2] "Practical Experiences with flow-induced vibrations", IAHR/IUTAM Symposium, Karlsruhe 1979, Editors: E. Naudascher, D. Rockwell, Springer-Verlag.

[1.3] International Conference on Flow Induced Vibrations, Bowness-on- Windermere, England, 1987.

[2.1] "Main steam piping vibration driven by flow-acoustic excitation", R.T. Hartlen, W. Jaster, Practical Experiences with Flow-Induced Vibrations, IAHR/IUTM Symposium Karlsruhe, Springer-Verlag Berlin Heidelberg New York.

[2.2] "Resonance effects in wake shedding from parallel plates; some experimental observations", R. Parker, J. Sound Vib., 1966, 4, 62-72.

[2.3] "Resonance effects in wake shedding from parallel plates; calculation of resonant frequencies", R. Parker, J. Sound Vib., 1967, 5, 330-343.

[2.4] "Low frequency resonance effects in wake shedding from parallel plates", R. Parker, W.M. Griffiths, J. Sound Vib., 1968, 7, 371-379

[2.5] "The excitation of acoustic resonance by vortex shedding", N.A. Cumpsty, D.S. Whitehead, J. Sound Vib., 1971, 18(3), 353-369

[2.6] "Self-excitation of an acoustic resonance by vortex shedding", F.S. Archibald, J. Sound Vib., 1975, 38(1), 81-103

[2.7] "Flow-resonant sound interaction in a duct containing a plate, Part I: semi-circular leading edge", M.C. Welsh, A.N. Stokes, J. Sound Vib., 1984, 95(3), 305-323

[2.8] "The dissipation of sound at an edge", M.S. Howe, J. Sound Vib., 1980, 70, 407-411

[2.9] "Wind tunnel experiments in the flow over rectangular cavities at subsonic and transonic speeds", J.E. Rossiter, Areo. Res. Counc. Britain, R. @ M., No. 3438, 1966.

[2.10] "Estimation of possible excitation frequencies for shallow rectangular cavities", A.J.Bilanin, E.E.Covert, AIAA Journal, Vol. 11, No. 3, March 1973, 347-351.

[2.11] "Self-excited depth-mode resonance for a wall-mounted cavity in turbulent flow", S.A. Elder, J. Acoust. Soc. Am., Vol. 64, No. 3, Sept. 1978, 877-890.

[2.12] "On spatially growing disturbances in an inviscid shear layer", A. Michalke, J. Fluid Mech., Vol. 23, part 3, 1965, 521-544.

[2.13] "On the tones and pressure oscillations induced by flow over rectangular cavities", C.K.W. Tam, P.J.W. Block, J. Fluid Mech. (1978), Vol. 89, part 2, 373-399

[2.14] "Flow-excited resonances in covered cavities", J.J. Keller, M.P. Escudier, J. Sound Vib., 1983, 86(2), 199-226.

[2.15] "Fluid dynamics of a flow excited resonance, Part I: Experiment", P.A. Nelson, N.A. Halliwell, P.E. Doak, J. Sound Vib., 1981, 78(1), 15-38

[2.16] "Fluid dynamics of a flow excited resonance, Part II: Flow acoustic interaction", P.A. Nelson, N.A. Halliwell, P.E. Doak, J. Sound Vib., 1983, 91(3), 375-402

[2.17] "Oscillations of Impinging Shear Layers", D. Rockwell, AIAA Journal, Vol. 21, No. 5, May 1983, 645-663.

[2.18] "Review-Self-sustaining oscillations of flow past cavities", J. Fluids Eng., D. Rockwell, E. Naudascher, Vol. 100, June 1978, 152-165

[2.19] "Self-generation of organized waves in an impinging turbulent jet at low Mach number", D. Rockwell, A. Schachenmann, J. Fluid Mech. (1982), vol. 117, 425-441

[2.20] "The organized shear layer due to oscillations of a turbulent jet through an axisymmetric cavity", D. Rockwell, A. Schachenmann, J. Sound Vib. 1982, 85(3), 371-382

[2.21] "Self-sustained oscillations of turbulent pipe flow terminated by an axisymetric cavity", A. Schachenmann, D. Rockwell, J. Sound Vib., 1980, 73(1), 61-72

[2.22] "Helical instabilities of slowly divergent jets", P. Plaschko, J. Fluid Mech., 1979, 92, 209-215.

[2.23] "An experimental investigation of pure tone generation by vortex shedding in a duct", H. Nomoto, F.E.C. Culick, J. Sound. Vib., 1982, 84(2), 247-252.

[2.24] Rayeigh, "Theory of Sound", (two volumes), 1877, New York: Dover Publications, second edition, 1945 re-issue.

[2.25] "Improvements to a smoke generator for use in wind tunnels", R.W. Basset, H.S. Fowler, 1971, N.R.C. Report 12288.

[2.26] "The effect of sound on vortex shedding from cylinders", R.D. Blevins, J. Fluid Mech., 1985, vol. 161, 217-237

[3.1] ASTM C384-58, 1972, Standard method of test for impedance and absorbtion of acoustical materials by the tube method.

[3.2] "Acurate method for the experimental evaluation of the acoustical impedance of a black box", M.L. Kathuriya, M.L. Munjal, J. Acoust. Soc. Am., Vol 58, 1975, 451-454

[3.3] "Methods for evaluating the performance of small acoustic filters", W.S. Gately, R. Cohen, J. Acoust. Soc. Am., Vol 46, 1969, 6-16.

[3.4] "Method for evaluation of the acoustical impedance of a black box, with or without mean flow, measuring pressures at fixed positions", M.L. Kathuriya, M.L. Munjal, J. Acoust. Soc. Am., Vol. 62, No. 3, September 1977.

[3.5] "Impedance tube technology for flow acoustics", V.B. Panicker, M.L. Munjal, J. Sound Vib., 1981, 77(4), 573-577.

[3.6] "Experimental determination of acoustic properties using a two- microphone random-excitation technique", A.F. Seybert, D.F. Ross, J. Acoust. Soc Am., Vol 61, No. 5, May 1977

[3.7] "The application of cepstral techniques to the measurement of transfer functions and acoustical reflection coefficients", J.S. Bolton, E. Gold, J. Sound Vib., 1984,

[3.8] Engineering applications of correlation and Spectral analysis, J.S. Bendat, A.G. Piersol, New York, John Wiley, 1980.

[3.9] Sound Intensity (Theory), Technical Review, Bruel and Kjaer, No.3, 1982.

[3.10] "Measurement of acoustic intensity using the cross-spectral density of two microphone signals", F.J. Fahy, J. Acoust. Soc. Am., Vol. 62, No. 4, October 1977.

[3.11] "A measuring method of acoustic intensities of forward and backward propagating waves", S. Takagi, T. Nakamura, Y. Irie, Presented at the ASME Eng. Division conference, Cincinnati, Ohio, Sept., 1985.

[3.12] "Finite difference approximation errors in acoustic intensity measurements", J.K. Thompson, D.R. Tree, J. Sound Vib., 1981, 75(2), 229-238.

[3.13] "Errors in acoustic intensity measurements", S.J. Elliott, J. Sound Vib., 1981, 78(3), 439-445.

[3.14] "The practical assessment of errors in sound intensity measurement", S. Watkinson, J. Sound Vib., 1986, 105(2), 255-263.

[3.15] "Characteristics of microphone arrangements for sound intensity measurement", P.S. Watkinson, F.J. Fathy, J. Sound Vib., 1984, 94(2), 299-306.

[3.16] "A selective two microphone acoustic intensity method", J.Bucheger, W. Trethewey, H.A. Evensen, J. Sound Vib., 1983, 90(1), 93-101.

[3.17] "The measurement of acoustic intensity by selective two microphone techniques with a dual channel analyser", P.R.Wagstaff, J.C.Henrio, J. Sound Vib., 1984, 94(1), 156-159.

[3.18] "Cross-spectral method of measuring acoustic intensity by correcting phase and gain mismatch errors by microphone calibration", G. Krishnappa, J. Acoust. Soc. Am., 69(1), Jan. 1981.

[3.19] "Errors in two channel acoustic intensity analysis", R.E. Harris, J.A. Fitzpatrick, J. Sound Vib., 1986, 106(2), 347-352.

[4.1] "Velocity ratio-cum-transfer matrix method for the evaluation of a muffler with mean flow", M.L. Munjal, J. Sound Vib., 1975, 39(1), 105-119.

[4.2] "A note on various formulations for four-pole parameters of a pipe with mean flow", C.W.S. To, J. Sound Vib., 1983, 88(2), 207-211.

[4.3] "On the transfer matrix for a uniform tube with a moving medium", M.L. Munjal, P.T. Thawani, J. Sound Vib., 1983, 91(4), 597-600.

[4.4] "A note on propagation of acoustic plane waves in a uniform pipe with mean flow", M.G. Prasad, M.J. Crocker, J. Sound Vib., 1984, 95(2), 284-290.

[4.5] "Acoustic interactions in pump and pipework systems", D.H. Wilkinson, A. Marshall, D. Hoadley, Central Electricity Generating Board, Marchwood Engineering Laboratories, Job No. TF366, Nov. 1976.

[4.6] "ACOUST: A program to calculate one-dimensional acoustic wave behaviour in pump/pipe circuits of arbitrary connection geometry", A. Marshall, C.E.G.B., MKarchwood Engineering Laboratories, Job No. TF366, 1978.

[4.7] "Acoustic transmission matrix of a variable area duct or nozzle carrying a compressible subsonic flow", J.H. Miles, JASA, Vol. 69, No. 6, June 1981, 1577-1586.

[4.8] "The acoustic simulation and analysis of complicated reciprocating compresssor piping systems, I: Analysis technique and parameter matrices of acoustic elements", C.W.S. To, J. Sound Vib., 1984, 96(2), 175-194.

[4.9] "The acoustic simulation and analysis of complicated reciprocating compresssor piping systems, II: Program structure and applications", C.W.S. To, J. Sound Vib., 1984, 96(2), 175-194.

[4.10] "A transient testing technique for the determination of matrix parameters of acoustic systems I: Theory and Principles", C.W.S To, A.G. Doige, J. Sound Vib., 1979, 62(2), 207-222

[4.11] "The application of a transient testing method to the determination of acoustic properties of unknown systems", C.W.S. To, A.G. Doige, J. Sound Vib., 71(4), 1980, 545-554

[4.12] "A time-averaging transiant testing method for acoustic properties of piping systems and mufflers with flow", T. Y. Lung, A.G. Doige, JASA 73 (3), 1983, 867-876.

[4.13] "Experimental evaluation of the areoacoustic characteristics of a source of pulsating gas flow", M.L. Kathuriya, M.L. Munjal, J. Acoust. Soc. Am, 65(1), 1979, 240-248.

[4.14] "Acoustical source characterization studies on a multi-cylinder engine exhaust system", M.G. Prasad, M.J. Crocker, J. Sound Vib., 90(4), 1983, 479-490.

[4.15] "Modelling the exhaust noise radiated from reciprocating internal combustion engines - A literature review.", A.D. Jones, NCE, 23(1), 1984, 12-31

[4.16] "Experimental characterization of noise sources for duct acoustics", A.G. Doige, H.S. Alves, ASME 86-WA/NCA-15

[4.17] "Source identification testing for flow-generated noise", A.G. Doige, H.G Alves, Noise-Con 85, 71-76.

[4.18] "Evaluation of the acoustical source impedance in a duct using a four load method", M.G. Prasad, 12th International Congress in Acoustics, Toronto, July 1986, Paper No. M3-6

[4.19] "On the application of the four load method to determining acoustic properties in a duct", M.G. Prasad, ASME, 86-WA/NCA-16

[4.20] "The effects of flow on the performance of a reactive acoustic attenuator", C.R. Fuller, D.A. Bias, J. Sound Vib., 1979, 62(1), 73-92

[4.21] "Computation of flow-induced vibrations in piping systems", R.J. Gibert, Advanced Structural Dynamics, ed. J. Donea, Applied Science, 1980, 315-336.

[4.22] "Experimental study of two singular points of a circuit", R.J Gibert, CEA-N-1735

[4.23] "Turbulent field and acoustic source properties of governor valves", J. Chadha, CEGB, MM/MECH/TF130, Feb. 1979.

[4.24] "Pressure pulsations at orifice plates and general pipeline flow- Acoustic simulation", K.K. Botros, W.M. Jungowski, W.Studzinski, J.L. Szabo, V. Kulle, 1986 Internation Gas research Conference, Toronto, 243-256.

[4.25] "Acoustics-An Introduction to its Physical Principles and Applications", A.D. Pierce, McGraw-Hill series in Mechanical Engineering

[5.1] "On the mechanism of sound production in organ pipes", S.A. Elder, J. Acoust. Soc. Am., Vol. 54, No. 6, 1973, 1554-1564

[5.2] Machine tool structures, F. Koenigsberger, J. Tlusty, Pergamon Press, Oxford; New York, 1969.

APPENDIX I

Hotwire Calibration Data

Wire No. P. 14

R20 = 3.3 Ω

RL = 0.6 Ω

Temp. 20°C

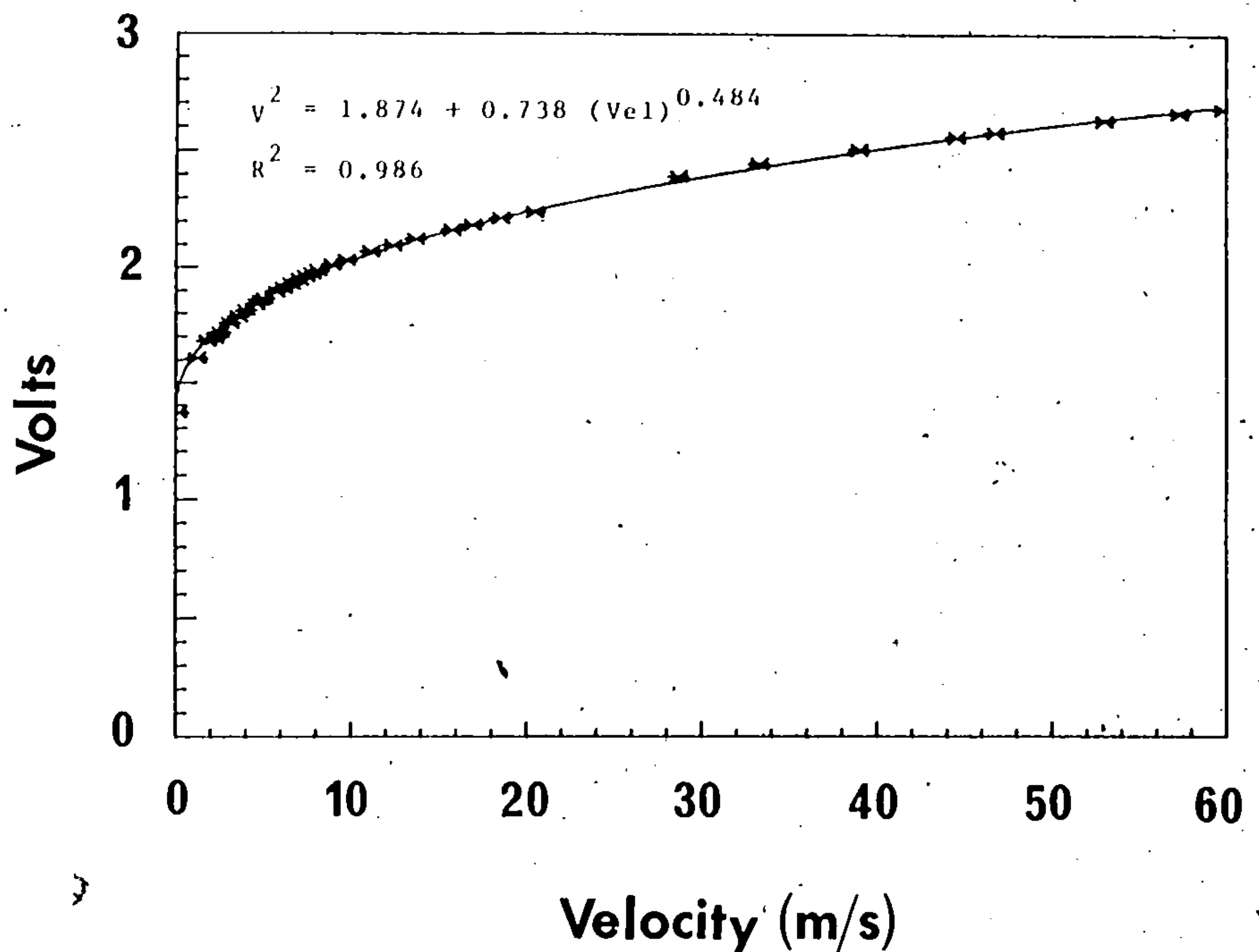

Figure AI.1 : Hotwire calibration curve.